AD-A175 082 CALCULATION OF CUMULATIVE DISTRIBUTIONS AND DETECTION PROBABILITIES IN CO..(U) CALIFORNIA UNIV SAN DIEGO LA JOLLA DEPT OF ELECTRICAL ENGINEE.. C W HELSTROM 1/2

UNCLASSIFIED 31 MAR 86 AFOSR-TR-86-2103 AFOSR-82-0343 F/G 9/4 NL

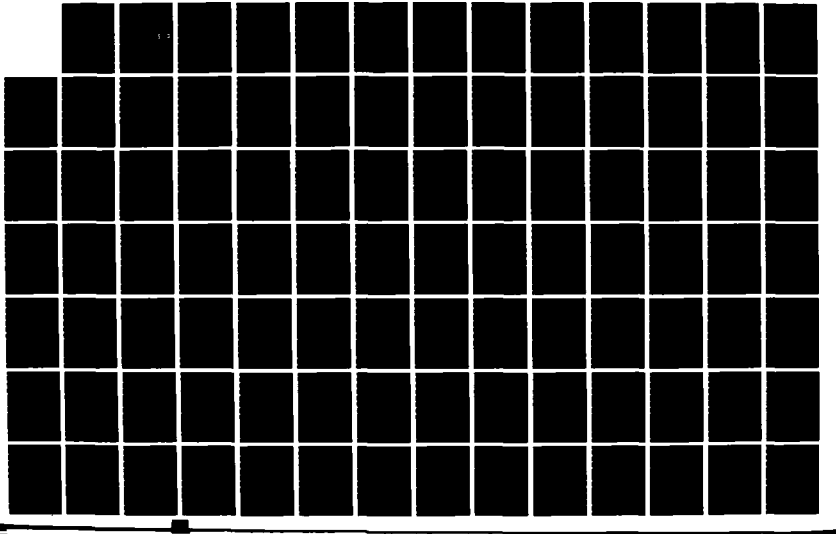

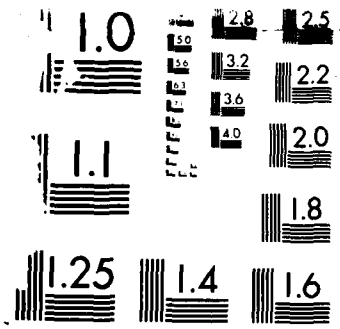


RESOLUTION TEST CHART

(2)

AFOSR-TR- 86-2188

AD-A175 082

# Calculation of Cumulative Distributions and Detection Probabilities in Communications and Optics

Final Report

AFOSR Grant 82-0343



Carl W. Helstrom

Department of Electrical Engineering and Computer Sciences

University of California, San Diego

La Jolla, CA 92093



March 1986

## Abstract

This report treats the numerical computation of cumulative distributions of random variables occurring primarily in communications, radar, and optics when their moment-generating or probability-generating functions are known. The cumulative distribution of a continuous random variable is expressed as a Laplace inversion integral of its moment-generating function, that of an integer-valued random variable as a contour integral that arises from Cauchy's theorem and whose integrand involves the probability-generating function. These integrals are evaluated by numerical quadrature along contours in the complex plane chosen for efficiency and convenience. Applications include radar detection probabilities with fading and unfading signals and fixed-threshold and constant-false-alarm-rate receivers; the distributions of the integrated output of a linear rectifier and of the filtered output of a quadratic rectifier; the error probability in a binary symmetric communication channel with intersymbol and cochannel interference; the distribution of shot noise; the distributions of the numbers of electrons emerging from photoelectric detectors, photomultipliers, and avalanche diodes; and significance probabilities in statistical rank tests.

Table of Contents

# I. Distributions of Continuous Random Variables

## 1. Computing Cumulative Distributions from Moments and Moment-Generating Functions

A receiver that is to detect a particular type of signal, as in radar and communications, processes its input in such a way as to generate a random variable that we shall denote by v. If v exceeds a decision level V, the receiver decides that the signal is present. The efficacy of the receiver is measured by its probability of detection, which is the probability

$$q^+(V) = \Pr\ (v > V) = \int_V^\infty p(v)\ dv \tag{1.1}$$

that it makes an affirmative decision when its input consists of the signal in the presence of random noise of a specified character. Here p(v) is the probability density function (p.d.f.) of the random variable v, and $q^+(V)$ is the complementary cumulative distribution function (c.c.d.f.). The probability $q^+(V)$ may be needed as a function of the input signal-to-noise ratio. Also relevant is the false-alarm probability that $v > V$ when only noise is present.

Depending on the nature of the signal and the noise and on the structure of the receiver, probabilities such as $q^+(V)$ may be very difficult to calculate. In many situations, however, it is not so difficult to determine the moment-generating function (m.g.f.) h(z) of the random variable v, which is the Laplace transform of its p.d.f. p(v),

$$h(z) = E(e^{-zv}) = \int_{-\infty}^\infty p(v)e^{-zv}\ dv. \tag{1.2}$$

In other problems, although a closed form for the m.g.f. h(z) may be unknown, one can determine the moments

$$\mu_n = E(v^n) = \int_{-\infty}^{\infty} v^n \, p(v)dv, \qquad n = 1, 2, \ldots, \tag{1.3}$$

of the random variable v, which are the coefficients of the power series

$$h(z) = 1 + \sum_{n=1}^{\infty} \mu_n (-z)^n/n! = 1 + \sum_{n=1}^{\infty} a_n (-z)^n \tag{1.4}$$

representing the m.g.f. in the neighborhood of the origin. The principal topic of this first part of our report is the determination of the c.c.d.f. $q^+(V)$ from the m.g.f. $h(z)$.

Detectors of light signals, as in optical communications and radar, often base their decisions about the presence or absence of a signal on the number k of photoelectrons counted at the output of a device such as a photoelectric cell, a photomultiplier, or an avalanche diode. The probability

$$Q_n^+ = \Pr(k \geq n) = \sum_{k=n}^{\infty} p_k \tag{1.5}$$

that this number k exceeds an integer-valued decision level n is useful for characterizing the performance of the detector. Here $p_k$ is the probability that exactly k electrons are counted. Although it may not be known for all values of k, it is possible in many problems to determine the probability generating function (p.g.f.) $h(z)$ of the random variable k, defined as

$$h(z) = \sum_{k=0}^{\infty} p_k z^k. \tag{1.6}$$

Our research has dealt primarily with numerical methods for calculating probabilities such as those in (1.1) and (1.5) from the generating functions $h(z)$. Part I of this report treats the distributions of continuous random

variables such as v; Part II treats the distributions of integer-valued random variables such as k.

(a) The Inversion Integrals

It is assumed that the m.g.f. h(z) is regular at least in a vertical convergence strip parallel to and containing the Im z-axis of the complex plane. The inverse transform to (1.2) is

$$p(v) = \int_{c-i\infty}^{c+i\infty} h(z)e^{vz}\, dz/2\pi i, \tag{1.7}$$

where c lies in the convergence strip and on the Re z-axis. The cumulative distribution function (c.d.f.)

$$q^{-}(V) = Pr\ (v < V) = \int_{-\infty}^{V} p(v)\, dv \tag{1.8}$$

can be obtained by integrating (1.7), provided that c is positive,

$$q^{-}(V) = \int_{c-i\infty}^{c+i\infty} z^{-1}\, h(z)e^{Vz}\, dz/2\pi i, \qquad c > 0. \tag{1.9}$$

Its complement, which we have called the c.c.d.f. or the probability of detection, is by (1.1)

$$q^{+}(V) = 1 - q^{-}(V) = -\int_{c-i\infty}^{c+i\infty} z^{-1}\, h(z)e^{Vz}\, dz/2\pi i, \qquad c < 0. \tag{1.10}$$

These integrals cannot often be expressed in closed form, and one must resort to numerical methods for evaluating the cumulative distribution and its complement.

The most common procedure utilizes the Edgeworth series. One defines the cumulant expansion by

$$\ln h(z) = \sum_{n=1}^{\infty} b_n (-z)^n = -\bar{V}z + \tfrac{1}{2}\sigma^2 z^2 + r(z),$$

$$r(z) = \sum_{n=3}^{\infty} \kappa_n (-z)^n / n!, \qquad (1.11)$$

where $\bar{V} = E(v)$, $\sigma^2 = \mathrm{Var}\ v$, and $\kappa_n = n! b_n$ is the n-th cumulant of v. When the m.g.f. h(z) is not given in closed form, the coefficients $b_n = \kappa_n / n!$ of this series can be obtained from the coefficients $a_n = \mu_n / n!$ of (1.4) by the recurrent relations

$$b_{n+1} = a_{n+1} - \frac{1}{n+1} \sum_{r=1}^{n} r b_r a_{n+1-r}, \qquad n > 1, \qquad (1.12)$$

starting with $b_1 = a_1 = \bar{V}$.

One then expands the m.g.f. from (1.11) as

$$h(z) = \exp\left(-\bar{V}z + \tfrac{1}{2}\sigma^2 z^2\right)\left\{1 + \sum_{k=1}^{\infty} \frac{[r(z)]^k}{k!}\right\}, \qquad (1.13)$$

writes out the terms in the brackets as a series in powers of (-z), substitutes it into (1.7), and integrates term by term to obtain a series for the probability density function p(v). This series is in turn integrated term by term to produce, after appropriate rearrangement, the well-known Edgeworth series for the c.d.f. $q^-(V)$. It is an asymptotic series in the sense that although its terms at first decrease in magnitude, the series diverges when carried beyond a certain point. Those terms, proportional to derivatives of the error function, are oscillatory functions of their argument $(V-\bar{V})/\sigma$, and the terms of high order attain large positive and negative values. Computation with the series is difficult to manage, therefore, and the results are unreliable in the tails of

the distribution where $|V - \bar{V}| >> \sigma$.

(b) The Path of Steepest Descent

In our approach one avoids the expansion in (1.13), which is the cause of all the trouble, and simply integrates (1.9) or (1.10) numerically. The numerical quadrature formulas we have used divide the integration variable into equal intervals or steps and approximate the integral as a weighted sum of the values of the integrand at the ends of those intervals. Once the value of the integrand has decreased below a certain limit, one halts the summation.

For efficiency one would like to minimize the number of such steps required for a given accuracy, and one therefore desires the absolute value of the integrand to drop off to zero as rapidly as possible along the contour of integration. The contour along which the absolute value of the integrand decreases most rapidly to zero is called its path of steepest descent [1]. This path crosses the Re z-axis at a saddlepoint $x_0$ of the integrand, which is a root of the equation

$$\Psi'(z) = \frac{d\Psi(z)}{dz} = \frac{d}{dz} \ln h(z) + V - z^{-1} = 0, \qquad (1.14)$$

where

$$\Psi(z) = \ln h(z) + Vz - \ln (\pm z) \qquad (1.15)$$

is the "phase" of the integrand in (1.9) or (1.10). [$(\pm z) = +z$ for $q^-(V)$ in (1.9); $(\pm z) = -z$ for $q^+(V)$ in (1.10).] Viewed as a function of $x = \mathrm{Re}\ z$, $\Psi(z)$ is minimum at the saddlepoint $z = x_0$. Along the path of steepest descent, which may have several branches, Im $\Psi(z)$ is constant. On the principal branch crossing the Re z-axis at $z = x_0$, Im $\Psi(z) = 0$. In many problems this is the only branch.

Because computing the path of steepest descent during the numerical integration would be cumbersome, one prefers to approximate it, if possible, by a

simple curve that lies close enough to it that the integrand will decrease almost as rapidly. In seeking such a curve, it is helpful to plot paths of steepest descent for a few typical values of the parameters of the distribution. One must first determine the saddlepoint $x_0$ where the path crosses the Re z-axis by solving (1.14). One can often do so most expeditiously by Newton's method, which replaces a trial value of $x_0$ at each stage by

$$x_0 \leftarrow x_0 - \frac{\Psi'(x_0)}{\Psi''(x_0)}, \tag{1.16}$$

primes indicating differentiation. Because of the convexity $\cup$ of the phase $\Psi(z)$ for $z = x$ on the Re z-axis, this method converges rapidly. The root $x_0$ of (1.14) is sought in $0 < x < \gamma_+$ for (1.9) and in $\gamma_- < x < 0$ for (1.10), where $\gamma_-$ is the rightmost singularity of $h(z)$ on the negative real axis and $\gamma_+$ is the leftmost singularity of $h(z)$ -- if any -- on the positive real axis. If it is inconvenient to calculate the second derivative $\Psi''(z)$, the secant method can be used instead. If even the first derivative $\Psi'(z)$ is difficult to calculate, one can solve the equation

$$\text{Im } \Psi(x_0 + i\varepsilon) = 0 \tag{1.17}$$

by the secant method for a sufficiently small positive value of $\varepsilon$, or one can minimize $\Psi(z)$ in the region $\gamma_- < x < 0$ or $0 < x < \gamma_+$ by, for instance, the golden-section algorithm [2].

One traces an approximate path of steepest descent by starting at a point $z_1 = x_0 + i\delta$ a small distance $\delta$ above the saddlepoint. Given the k-th point $z_k$ on the approximate path, one calculates the segment $\Delta z$ to the next point $z_{k+1} = z_k + \Delta z$ by the formula [3]

$$z_{k+1} - z_k = \Delta z = -\delta \frac{\Psi'^*(z_k)}{|\Psi'(z_k)|}, \tag{1.18}$$

checking the value of Im $\Psi(z_K)$ occasionally to see whether it remains close to the constant value C for the path. When it begins to deviate unduly, one returns to the exact path by solving the equation

$$\text{Im } \Psi(x+iy) = C$$

by Newton's method or the secant method, searching in x when the slope $|\tan (\arg \Delta z)|$ exceeds 1 and in y when it is less than 1. (On the main branch, C = 0.) It is instructive also to calculate the magnitude exp [Re $\Psi(z)$] of the integrand to see whether it is decreasing with satisfactory rapidity along this path.

If the main branch of the path of steepest descent heads toward infinity in such a direction that the originally vertical contour in (1.9) or (1.10) can be deformed into it without crossing any singularities of the integrand, even at infinity, all is well, and this is the only significant branch. In some problems, however, the path along which Im $\Psi(z) = 0$ may become parallel to the Re z-axis or even approach it asymptotically. Such a behavior indicates that singularities of the integrand may lie at infinity and that the path of steepest descent possesses several or even an infinite number of branches. These come in from infinity, turn around, and pass back out to infinity. On each such branch lies a saddlepoint of the integrand, and in order to trace it, one must first locate its saddlepoint. Again one solves the equation $\Psi'(z) = 0$ for what is now a complex root z. Newton's method (1.16) can be used, with $x_0$ replaced by complex trial values $z_0$, but the selection of the initial trial value generally requires preliminary analysis of the function $\Psi(z)$ in the complex plane. If one starts too far away, Newton's method will go awry.

The path of steepest descent passes through each saddlepoint $z_0$ in a direction specified by that of the complex number $i\Psi''(z_0)$. By starting at points

$$z_0 \pm i\delta\Psi''(z_0)/|\Psi''(z_0)|$$

at a small distance $\delta$ on each side of the saddlepoint $z_0$, one can trace that branch of the path of steepest descent by the method just described. Along it, Im $\Psi(z)$ is constant,

$$\text{Im } \Psi(z) \equiv \text{Im } \Psi(z_0) = C,$$

but it is not necessarily zero.

If the m.g.f. $h(z)$ possesses zeros above and below the Re z-axis, the path of steepest descent through the saddlepoint $x_0$ may pass through all or some of them as it goes off to infinity. Between each pair of zeros lies another saddlepoint of the integrand. Even more complicated configurations of saddlepoints and path segments may occur, as illustrated by Rice [3], and finding a suitable contour of integration may be most difficult. One may then resort to the original straight vertical contour in (1.9) and (1.10). In some problems the value of the integrand along this straight path may oscillate and decrease so slowly that other methods of inverting the m.g.f. must be sought. Rice [4] has shown how in certain instances one can make the integral converge more rapidly by subtracting out terms whose integrals along the contour are known exactly.

It may happen that one knows the moments $\mu_n$ of the random variable v, but not the analytical form of the m.g.f. $h(z)$. One can then express the phase $\Psi(z)$ as

$$\Psi(z) = \sum_{n=1}^{\infty} b_n(-z)^n + Vz - \ln(\pm z), \qquad (1.19)$$

whose coefficients $b_n = \kappa_n/n!$ can be determined from the quantities $a_n = \mu_n/n!$ by the recurrence in (1.12). One stops the summation in (1.19) when the term

$b_n(-z)^n$ becomes sufficiently small. Alternatively one can take

$$\Psi(z) = \ln h(z) + Vz - \ln(\pm z)$$

and compute the m.g.f. $h(z)$ from the power series in (1.3). In many problems the magnitude of the integrand of (1.9) or (1.10) decreases to a level at which the integration can be terminated while the point $z = x + iy$ still lies within the domain of convergence of the series in (1.3) and (1.19).

(c) Parabolic Paths

When, as often, all the singularities of the m.g.f. lie on the negative Re z-axis, the path of steepest descent ultimately goes off to infinity along a path resembling a parabola, and the original vertical contour in (1.9) or (1.10) can be deformed into this path without crossing any singularities of the integrand. One can then take as the contour of integration a parabola passing through the saddlepoint, on which

$$z = x_0 + \tfrac{1}{2}\kappa y^2 + iy \tag{1.20}$$

with $\kappa$ the curvature at the saddlepoint. The integrals to be evaluated can be put into the form

$$q^{\pm}(V) = \mathrm{Re}\int_0^{\infty} e^{\Psi(z)}(1-i\kappa y)\,dy/\pi, \tag{1.21}$$

with $\Psi(z)$ given by (1.15). For $V >> E(v)$ it is most accurate to compute $q^+(V)$, and for that integration $\gamma_- < x_0 < 0$; for $V << E(v)$ one computes $q^-(V)$, for which $0 < x_0 < \gamma_+$. For V near $E(v)$ it does not much matter which saddlepoint one chooses.

Designating the dominant terms in the phase $\Psi(z)$ far from the saddlepoint by

$\tilde{\Psi}(z)$, one calculates the curvature $\kappa$ of the approximating parabola at $y = 0$ by [5]

$$\kappa = \frac{\tilde{\Psi}'''(x_0)}{3\tilde{\Psi}''(x_0)}, \tag{1.22}$$

and in most problems it suffices to take

$$\tilde{\Psi}(z) = \ln h(z) + Vz. \tag{1.23}$$

The curvature $\kappa$ is not needed to great accuracy.

The numerical integration is carried out by the trapezoidal rule, which Schwartz [6] and Rice [3] have shown to be superior for infinite integrals of analytic functions. The step size $\Delta y$ in the integration variable $y$ can be taken initially as

$$\Delta y = [\gamma\Psi''(x_0)]^{-1/2}, \tag{1.24}$$

which with $\gamma$ of the order of 1 or 2 roughly measures the width of the integrand of (1.21) in the neighborhood of the saddlepoint. One then successively halves the step size $\Delta y$ until the values of the integral cease changing in the number of figures desired. In many problems the number of significant figures roughly doubles each time one divides $\Delta y$ by 2 [6]. The numerical integration is conveniently terminated when the absolute value $\exp [\mathrm{Re}\ \Psi(z)]$ of the last term added to the trapezoidal sum falls below $\varepsilon\Delta y$ times the absolute value of the sum itself, with $\varepsilon$ some suitably small number depending on the number of significant figures desired. We found $\varepsilon = 10^{-6}$ adequate for most purposes.

(d) Integration Along a Path of Steepest Descent

When the parabola is not a sufficiently close approximation to the path of steepest descent, it may be possible to find some other simple curve along which to integrate; an example will be given in Section 8. If the path of steepest

descent has many branches, as discussed in part (b), one may decide to integrate instead along a close approximation to each branch plotted by the method described there.

That approximate path consists of short, straight segments $\Delta z$ of length $\delta$ connecting a sequence of points $z_0$, $z_1$, $z_2$, ..., with $\Delta z$ given by (1.18). One way of approximating the integral along any given semibranch starting at $z_0$,

$$Q = \mathrm{Re} \sum_{k=0}^{\infty} \int_{z_k}^{z_{k+1}} e^{\Psi(z)}\, dz/2\pi i, \tag{1.25}$$

is to replace each term by what corresponds to the trapezoidal approximation,

$$\mathrm{Re} \int_{z_k}^{z_{k+1}} f(z)dz/2\pi i = \mathrm{Re}\, \{[f(z_k) + f(z_{k+1})]\, \Delta z/4\pi i\},$$

$$f(z) = \exp\,[\Psi(z)]. \tag{1.26}$$

By a semibranch we mean any portion of the path beginning at a saddlepoint $z_0$ and extending to infinity; the branches of the path of steepest descent above the real axis consist of two semibranches, one entering $z_0$ from infinity, the other leaving it in the opposite direction. The contribution of the entering branch is equal to the negative of the sum in (1.25).

The advantages of the trapezoidal rule demonstrated by Schwartz [6] and Rice [3] for integrals of analytic functions seem not to carry over to this situation. Experience has shown that as the step size $\delta = |\Delta z|$ is halved, the values of the trapezoidal sum do not converge with the rapidity observed when applying the trapezoidal rule, for instance, to an integral such as (1.21). We have found superior convergence when instead we used the five-point formula of Birkhoff and Young [7]:

$$\mathrm{Re}\int_{z_k}^{z_{k+1}} f(z)\,dz/2\pi i = \mathrm{Re}\,\{\frac{\Delta z}{60\pi i}\,\{24f(\bar{z}_k) + 4[f(z_k) + f(z_{k+1})]$$

$$- [f(\bar{z}_k + \frac{i\Delta z}{2}) + f(\bar{z}_k - \frac{i\Delta z}{2})]\}\}, \tag{1.27}$$

where

$$\bar{z}_k = (z_k + z_{k+1})/2. \tag{1.28}$$

The error is of the order of $\delta^7$, but for each segment of the contour one must compute four times as many values of the integrand $f(z) = \exp[\Psi(z)]$ as for (1.26). It is not difficult to program this numerical quadrature in connection with the procedure embodied in (1.18) for tracing the approximating path of steepest descent.

The contribution of each branch of the path of steepest descent can be roughly estimated by the saddlepoint approximation [3, 8]

$$Q \tilde{=} \mathrm{Re}\,\{[2\pi\Psi''(z_0)]^{-\frac{1}{2}} \exp\,\Psi(z_0)\}, \tag{1.29}$$

where $z_0$ is the saddlepoint on the branch. By means of this formula one can decide whether it is necessary to carry out the numerical integration on the branch.

## 2. Quadratic Detection of Radar Signals.

### (a) Signals of Fixed or Random Strength

The input to a radar receiver is passed through a filter matched to the shape of the expected echo signal, and the output of the filter is applied to a quadratic rectifier. The noise in the input is white and Gaussian; echoes from a target may also be present. The sampled outputs of the rectifier in a particular range bin are summed in M successive interpulse intervals to produce a detection statistic of the form

$$Z = \tfrac{1}{2} \sum_{j=1}^{M} r_j^2, \tag{2.1}$$

where $r_j^2$ is the output of the rectifier in the j-th interval. When suitably normalized, Z has a chi-squared distribution with 2M degrees of freedom under hypothesis $H_0$ that no signal is present; its moment generating function (m.g.f.) is

$$h_0(u) = E(e^{-uZ} \mid H_0) = (1 + u)^{-M}. \tag{2.2}$$

Under hypothesis $H_1$ that a target is present, an echo is received in the j-th interval with energy $E_j$ and signal-to-noise ratio $d_j^2 = 2E_j/N$, $1 \le j \le M$, where N is the unilateral spectral density of the white-noise background. Then the m.g.f. of Z is

$$h_1(u) = E(e^{-uZ} \mid H_1) = (1 + u)^{-M} \exp\left(-\frac{Su}{1 + u}\right),$$
$$S = \tfrac{1}{2} D^2 = \tfrac{1}{2} \sum_{k=1}^{M} d_k^2 = E_T/N, \tag{2.3}$$

where $E_T$ is the total received energy. The probability $Q_d$ of detection is given by the M-th order Q-function,

$$Q_d = \Pr(Z > Z_0 \mid H_1) = Q_M(D, \sqrt{2Z_0}), \tag{2.4}$$

where $Z_0$ is the decision level with which the statistic Z is compared [9, pp. 215-219]. The false-alarm probability

$$Q_0 = Q_M(0, \sqrt{2Z_0}) \tag{2.5}$$

can be expressed in terms of the incomplete gamma function. A saddlepoint approximation was applied in [8] to the calculation of the decision level $Z_0$ and the probability $Q_d$ of detection for large numbers M of pulses integrated; typical results are tabulated there and compared with the exact probabilities.

When the radar echoes fade, the distribution of the statistic Z must be averaged with respect to the distribution of signal amplitudes. It is simplest to average the m.g.f. in (2.3) and invert it to calculate the cumulative distribution of Z and thence the average probability of detection. Four typical distributions of the fading amplitudes were enounced by Swerling [10], and we list them here with the resulting m.g.f.'s of Z:

Case I: $D = AD_0$, where A has a Rayleigh distribution,

$$p(A) = (A/A_0^2) \exp(-A^2/2A_0^2), \qquad A > 0, \tag{2.6}$$

yields the m.g.f.

$$\begin{aligned} h_1(u) &= (1 + u)^{-(M-1)}[1 + (B_1 + 1)u]^{-1} \\ B_1 &= \tfrac{1}{2}\langle D^2\rangle = \langle E_T\rangle/N, \end{aligned} \tag{2.7}$$

$\langle\cdot\rangle$ indicating an average with respect to the distribution of signal amplitudes.

Case II: $d_j = A_j d_0$, $\forall j$, where the $A_j$ are statistically independent and have Rayleigh distributions like that in (2.6), yields the m.g.f.

$$h_2(u) = [1 + (1 + B_2)u]^{-M},$$
$$B_2 = \tfrac{1}{2}\langle d_j^2\rangle = \langle E_j\rangle/N = B_1/M. \tag{2.8}$$

The distribution of the statistic Z is a scaled chi-squared distribution with 2M degrees of freedom.

Case III: $D = AD_0$, where A has the density function

$$p(A) = (A^3/2A_0^2)\exp(-A^2/2A_0^2), \qquad A > 0, \tag{2.9}$$

yields the m.g.f.

$$h_3(u) = (1 + u)^{-(M-2)}[1 + (1 + B_3)u]^{-2},$$
$$B_3 = \tfrac{1}{4}\langle D^2\rangle = \langle E_T\rangle/2N. \tag{2.10}$$

Case IV: $d_j = A_j d_0$, $\forall j$, where the $A_j$ are statistically independent and have the distribution of Case III, yields the m.g.f.

$$h_4(u) = (1 + u)^{M}[1 + (1 + B_4)u]^{-2M},$$
$$B_4 = \tfrac{1}{4}\langle d_j^2\rangle = \langle E_j\rangle/2N = B_3/M. \tag{2.11}$$

The distributions of the sum Z arising from these "Swerling cases" are given by di Franco and Rubin [11, ch. 11]. For cases III and IV the cumulative distributions are quite complicated, involving hypergeometric functions of orders depending on M. For case IV, for instance, calculating the detection probability $Q_d$ requires summing M terms, each containing an incomplete gamma-function of order $M + k - 1$, $0 < k \leq M$.

In general, if

$$G(u) = E(e^{-Su}) = \int_0^\infty p(S)\, e^{-uS}\, dS \qquad (2.12)$$

is the m.g.f. of the positive-valued random variable S, representing the total strength of the fading echoes, the m.g.f. of the random variable Z in (2.1) is, by (2.3),

$$h(u) = (1 + u)^{-M}\, G\left(\frac{u}{1 + u}\right) . \qquad (2.13)$$

Its singularities will always lie in the left halfplane. In particular, if the signal strength has a gamma distribution, of which Swerling's cases I - IV are special instances,

$$p(S) = [\Gamma(k)]^{-1}\, (k/\bar{S})^k\, S^{k-1}\, e^{-kS/\bar{S}}, \qquad (2.14)$$

where $\bar{S}$ is the mean total signal-to-noise ratio, then

$$G(u) = \left(1 + \frac{\bar{S}u}{k}\right)^{-k} \qquad (2.15)$$

and the m.g.f. of Z is

$$h(u) = (1 + u)^{k-M}\, (1 + bu)^{-k}, \qquad b = 1 + \bar{S}/k. \qquad (2.16)$$

For cases I - IV, k = 1, M, 2, 2M respectively.

The method of integration along a parabolic contour, as in (1.21), has been successfully applied to evaluating the tail probabilities for both unfading signals and signals having random strengths described by distributions p(S) of the form in (2.14). A bound has been derived for the truncation error incurred by cutting off the integration in (1.21) at a finite value of y [12]. In most instances it suffices to stop the numerical integration when the absolute value of the integrand falls below a fraction $\varepsilon$ of the accumulated sum times the step size $\Delta y$, whereupon the relative truncation error will be less than $\varepsilon$. The number

of steps of numerical integration required to attain a certain accuracy is more or less independent of the number M of signals processed by the radar receiver.

(b) Detection in Noise of Unknown Level

When the radar is being jammed by a transmitter of Gaussian noise spread over a frequency band much wider than that of the target echoes, the receiver is faced with the problem of detecting them in noise of unknown and random spectral density. A stratagem that is often adopted utilizes K samples $r_j'^2$ of the quadratically rectified output of a narrowband pass filter tuned to the same frequency as that of the echoes, or to a nearby frequency; these samples are taken at times when no signals are expected to be present, and it is presumed that they have the same probability distribution as the noise components of the terms $r_j^2$ in (2.1). The strength of that noise is then, within an inessential constant of proportionality, estimated by the value of the statistic

$$Z' = \tfrac{1}{2} \sum_{j=1}^{K} r_j'^2. \tag{2.17}$$

When these samples $r_j'^2$ indeed represent noise alone, the statistic Z' has a scaled chi-squared distribution with 2K degrees of freedom and is independent of Z in (2.1). The decision level with which the statistic Z is compared in order to decide whether any radar echo is present is made proportional to Z', or equivalently, the receiver forms the statistic

$$X = Z - \beta Z', \tag{2.18}$$

and it decides that a signal is present whenever $X > 0$. The constant $\beta$ is selected to achieve a pre-assigned false-alarm probability

$$Q_0(\beta) = \Pr\,(X > 0 \mid H_0), \tag{2.19}$$

and one wishes to calculate the probability

$$Q_d(\beta;\ S) = \Pr\ (X > 0 |\ H_1) \tag{2.20}$$

of detecting a sequence of M radar echoes of total signal-to-noise ratio S.

If the signal to be detected has a fixed, known strength, as in (2.3), the statistic X has the m.g.f.

$$\eta(u) = E(e^{-uX}) = (1 + u)^{-M}(1 - \beta u)^{-K} \exp\left(-\frac{Su}{1 + u}\right) \tag{2.21}$$

with S the signal-to-noise ratio defined in (2.3). The probability of detection is then given as in (1.10) by

$$Q_d(\beta;\ S) = -\int_{C_-} u^{-1}(1 + u)^{-M}(1 - \beta u)^{-K} \exp\left(-\frac{Su}{1 + u}\right) \frac{du}{2\pi i}, \tag{2.22}$$

where $C_-$ is a contour parallel to the imaginary u-axis and passing between the origin and the essential singularity of the integrand at $u = -1$. One evaluates (2.22) when the signal strength S is so small that the expected value of $X = Z - \beta Z'$ is negative; here

$$E(X) = S + M - \beta K. \tag{2.23}$$

When $E(X) > 0$, on the other hand, one evaluates

$$1 - Q_d(\beta;\ S) = \int_{C_+} u^{-1}(1+ u)^{-M}(1 - \beta u)^{-K} \exp\left(-\frac{Su}{1 + u}\right) \frac{du}{2\pi i} \tag{2.24}$$

along a contour lying in $0 < \mathrm{Re}\ u < 1/\beta$.

The prescription, "Choose the alternative hypothesis $H_1$ when $X = Z - \beta Z' > 0$," is equivalent to the F-test of the analysis of variance, and the F-statistic is

$$F = KZ/MZ'. \tag{2.25}$$

The false-alarm probability $Q_0(\beta)$ is related to the central F-distribution, and the detection probability $Q_d(\beta; S)$ to the noncentral F-distribution, the signal-to-noise ratio S playing the role of the noncentrality parameter. In [13] the computation of the noncentral F-distribution by integrating (2.22) or (2.24) numerically along a straight vertical contour was treated, and a bound on the error incurred by truncating the range of numerical integration was presented. It was shown that the simple rule that the summation be stopped when the absolute value of the integrand falls below a fraction $\varepsilon$ of the accumulated sum times the step size $\Delta y$ suffices to bound the relative error in the computed probability within that same fraction $\varepsilon$.

If the radar echoes are fading as described in part (a), the average detection probability is obtained by averaging the integrals in (2.22) and (2.24) with respect to S,

$$Q_d(\beta; \bar{S}) = -\int_{C_-} u^{-1}(1 + u)^{-M}(1 - \beta u)^{-K}\, G\left(\frac{u}{1 + u}\right) \frac{du}{2\pi i}, \tag{2.26}$$

$$1 - Q_d(\beta; \bar{S}) = \int_{C_+} u^{-1}(1 + u)^{-M}(1 - \beta u)^{-K}\, G\left(\frac{u}{1 + u}\right) \frac{du}{2\pi i}, \tag{2.30}$$

where $\bar{S}$ is the average total signal-to-noise ratio and G(u) is the m.g.f. of the distribution of the random signal-to-noise ratio S, as in (2.12). Again it is possible to evaluate these probabilities by numerical integration along a vertical straight line or other suitable contour. Bounds on the truncation error when the m.g.f. is given as in (2.15) have been determined [12].

## 3. Robust Radar Detectors (J. A. Ritcey)

Mean-level detectors (MLD) are commonly used in radar to maintain a constant false-alarm rate (CFAR) when the background noise level is unknown. In Section 2 we described the application of saddlepoint integration techniques to radar detection problems in which the test statistic is compared with either a fixed threshold or with an adaptive threshold composed of a weighted estimate of the mean level of the background noise, derived from a given reference channel [12]. The method was developed for an arbitrary number of pulses noncoherently integrated and for both a nonfluctuating and a chi-square fluctuating target. We have also considered a variant of the basic MLD that is more robust in the presence of interference in the reference channel, and we have obtained exact analytical results for the probabilities of detection and false alarm when the interference-to-noise ratio (INR) is nonzero. In practice, the interference could result either from returns from real objects such as other targets or clutter, or from pulsed-noise jamming. Here we consider only Swerling II target returns and only single-pulse processing (no noncoherent integration). The approach is to write the detection probability as a contour integral, which is evaluated by the method of residues. Variants of this system in which noncoherent integration is employed or other target models are considered would require numerical contour integrations. In the model we consider here, developing an analytical expression for the moment-generating function (m.g.f.) of the reference-channel estimate is the primary mathematical problem.

Radar detection of a known signal in additive white Gaussian noise of unknown variance is often accomplished by comparing the test statistic for a single range cell with an adaptive threshold equal to a scaled estimate of the unknown noise variance. For a system that quadratically rectifies the output of a matched filter to obtain the test statistic, the problem can be modeled by the

following hypothesis testing problem:

$$H_0: \quad v = \frac{1}{2}(x^2 + y^2)$$

$$H_1: \quad v = \frac{1}{2}\left((x+s)^2 + (y+t)^2\right); \ |d|^2 = s^2 + t^2. \tag{3.1}$$

The random variables x, y are independent Gaussian noise samples with zero mean and unit variance. The target echo provides a fixed signal-to-noise ratio (SNR) for a steady target, and the amplitude can be taken as a random variable when the echo fluctuates. The phase of the complex amplitude d = s + it is uniformly distributed over $(0, 2\pi)$, and the total SNR is

$$S = |d|^2/2. \tag{3.2}$$

Implementing the generalized likelihood ratio test, the system decides for hypothesis $H_0$ ("signal absent") or for hypothesis $H_1$ ("signal present") according to whether

$$v \underset{H_0}{\overset{H_1}{\gtrless}} ar \tag{3.3}$$

where r is an estimate of the noise variance and a is a positive thresnold parameter. Typically the radar uses the n range cells surrounding the cell under test to compute an estimate

$$r = \sum_{j=1}^{n} z_j \tag{3.4}$$

where

$$z_j = \frac{1}{2}(x_j^2 + y_j^2) \tag{3.5}$$

and the $x_j$, $y_j$, $j = 1,2, \ldots, n$, are independent and identically distributed

(i.i.d.) zero-mean Gaussian random variables; we have incorporated a scaling factor $n^{-1}$ into the threshold parameter a. In a locally homogeneous noise environment the $x_j$, $y_j$ all have common unit variance. The performance is completely specified by the false alarm and detection probabilities

$$Q_0 = \int_0^\infty f(r) \int_{ar}^\infty p_0(v)\, dv\, dr \tag{3.6}$$

$$Q_d = \int_0^\infty f(r) \int_{ar}^\infty p_1(v)\, dv\, dr \tag{3.7}$$

where f(r) is the probability density function (p.d.f.) of the estimate r and $p_i(v)$, i = 0, 1, is the p.d.f. of v under each hypothesis. An equivalent hypothesis test is

$$z = v - ar \underset{H_0}{\overset{H_1}{\gtrless}} 0 \tag{3.8}$$

where the random variable z has a p.d.f. $p_z(z)$ whose Laplace transform is given by

$$h_z(u) = \int_0^\infty e^{-uz}\, p_z(z)dz = \int_0^\infty e^{-uv}\, p(v)dv \int_0^\infty e^{aru}\, f(r)dr \tag{3.9}$$

or

$$h_z(u) = \langle e^{-uz} \rangle = \langle e^{-uv} \rangle \langle e^{uar} \rangle = h(u)\, d(-au) \tag{3.10}$$

where h(u), d(u) are the moment-generating functions (m.g.f.) of v and r respectively. If we specify a Swerling II target model, the m.g.f. is given by

$$h(u) = (1+bu)^{-1},\ b = 1 + \bar{S}, \tag{3.11}$$

and $\bar{S} = \frac{1}{2} \langle |d|^2 \rangle$ is the average SNR. The estimate r, in a homogeneous environment, has the m.g.f. d(u) given by

$$d(u) = (1+u)^{-1}, \tag{3.12}$$

The detection probability can be written as a contour integral involving these m.g.f.'s. Since $h_z(u)$ and $p_z(z)$ are related by an inverse Laplace transform, we find directly from (3.8) that

$$Q_d = Pr\,[z > 0 \mid H_1] = \int_0^\infty \int \frac{du}{2\pi i} e^{uz}\, h(u)\, d(-au)dz \tag{3.13}$$

or

$$Q_d = -\int_{C_-} \frac{du}{2\pi i} u^{-1}\, h(u)\, d(-au) \tag{3.14}$$

where the contour of integration $C_-$ consists of a vertical path in the complex u-plane crossing the negative real axis at $u = c_1, -b^{-1} < c_1 < 0$. The contour is closed in an infinite semi-circle in the left half-plane (LHP). Since d(u) is the m.g.f. of a positive random variable, the only singularities lie in the LHP. Therefore, d(-au) is analytic in the LHP and (3.14) can be immediately evaluated in terms of the residue at the simple pole, $u = -b^{-1}$. Thus, the detection probability is simply related to the m.g.f. of the estimate r by

$$Q_d = d(a/b);\ b = 1 + \bar{S}, \tag{3.15}$$

and the false-alarm probability is

$$Q_0 = d(a).$$

The key point of this result is that given a closed-form analytical expression for the m.g.f. d(u) we immediately have a result for the detection performance. We are encouraged, therefore, to investigate other systems that develop a

different estimate r, but one whose m.g.f. can still be obtained.

To reduce the degradation caused by interfering targets falling within the reference channel, Rickard and Dillard [14] proposed a class of detectors $\mathscr{D}_\ell$, $\ell = 0, 1, 2, \ldots, n-1$, where the $\ell$ largest range cells are censored from the noise-variance estimate. If the quadratically rectified output for the j-th range cell is denoted by $z_j$, the detector $\mathscr{D}_k$ uses the unscaled estimate

$$r = \sum_{j=1}^{k} z_{(j)} \tag{3.16}$$

where $k = n-1$ and $0 \leq z_{(1)} \leq z_{(2)} \leq \ldots \leq z_{(n)} \leq \infty$ are the order statistics of the sample $(z_1, z_2, \ldots, z_n)$. Since r is a biased estimator of the unknown noise variance we consider the more general statistic

$$r = \sum_{j=1}^{k-1} z_{(j)} + cz_{(k)} \tag{3.17}$$

for some constant $c > 0$. The contour integral (3.14) requires the m.g.f. of r, d(u).

For a homogeneous noise environment where the $z_j$'s are i.i.d. with p.d.f. $p(z) = e^{-z}$, $z \geq 0$, the m.g.f. of r can be shown to be given by

$$d(u) = \langle e^{-ur} \rangle = \sum_{j=1}^{k} \left[1 + \left(\frac{c+k-j}{n+1-j}\right) u\right]^{-1}. \tag{3.18}$$

From (3.18) we note that the noise-level estimate will be unbiased if we scale r by $k^{-1}$ and choose $c = n + 1 - k$. Then

$$\frac{r}{k} = \frac{1}{k}\left[\sum_{j=1}^{k-1} z_{(j)} + (n+1-k)z_{(k)}\right] \tag{3.19}$$

is an unbiased estimate of the unknown noise variance that is robust with respect to the presence of several large interference pulses in the reference samples $(z_1, \ldots, z_n)$.

The performance of the CMLD in a multiple-target environment can be obtained directly from (3.15), given the m.g.f. d(u). It can be shown that the joint m.g.f.

$$h_\ell(u,s) = \langle \exp[-u(z_{(1)} + \ldots + z_{(k-1)}) - sz_{(k)}] \rangle, \tag{3.20}$$

where $z_{(1)} \leq z_{(2)} \leq \ldots \leq z_{(k)} \leq \ldots \leq z_{(n)}$ are the order statistics drawn from an independent and exponentially distributed sample $(z_1, z_2, \ldots, z_\ell \ldots, z_n)$ and where

$$\langle z_i \rangle = \begin{cases} \alpha^{-1} & i = 1, \ldots, \ell, \\ 1 & i = \ell+1, \ldots, n, \end{cases}$$

$$\alpha^{-1} = 1 + INR, \tag{3.21}$$

is given by

$$h_\ell(u,s) = \binom{m}{\ell}^{-1} \sum_{i=0}^{\ell} \left\{ \binom{n-k}{i} \frac{\alpha^{\ell-1}}{(\ell-i)!} \right\}$$

$$\cdot \sum_{\substack{\ell_1=1 \\ \ell_1 \neq \ell_2 \neq \ldots \neq \ell_{\ell-i}}}^{k} \sum_{\ell_2=1}^{k} \cdots \sum_{\ell_{\ell-i}=1}^{k} \sum_{j=1}^{k} \left[ 1 + \frac{(\alpha-1)(i+r_j(i)) + \theta_j}{\psi_j} \right]^{-1} \tag{3.22}$$

where

$$\psi_j = n + 1 - j,$$

$$\theta_j = s + u(k - j),$$

and

$$r_j(i) = \begin{cases} \gamma_j(\ell_1) + \ldots + \gamma_j(\ell_{\ell-i}), & i = 1, \ldots, \ell-1, \\ 0, & i = \ell, \end{cases}$$

$$\gamma_j(\ell) = \begin{cases} 1, & j \leq \ell, \\ 0, & j > \ell. \end{cases}$$

The multiple sum in the second line of (3.22) is present only when $i < \ell$. The reason we have evaluated the joint m.g.f. $h_\ell(u,s)$ is twofold: First, the CMLD with arbitrary bias constant c has a reference channel m.g.f. given by $h_\ell(u,cu)$ when $\ell$ interferers are present. Second, we can evaluate the performance of the so-called Order Statistic Detector (OSD) described by Rohling [15], which was the estimate $r = z_{(k)}$, a single order statistic. This system may be considerably easier to implement than the CMLD.

As an example of a particular result, Figure 3.1 shows the additional SNR required (often called the CFAR loss) for the MLD, CMLD, and OSD in a multiple target environment to achieve a given $Q_d$ at fixed $Q_0$ over that required by the Neyman-Pearson detector, which is the optimal detector when the background noise level is known. Notice that although the CFAR loss increases with INR for the MLD, the CMLD and OSD have a bounded loss as the INR $\to \infty$. These results have been more fully reported in a paper to appear in the IEEE-AES [16] and in a Ph.D. thesis [17].

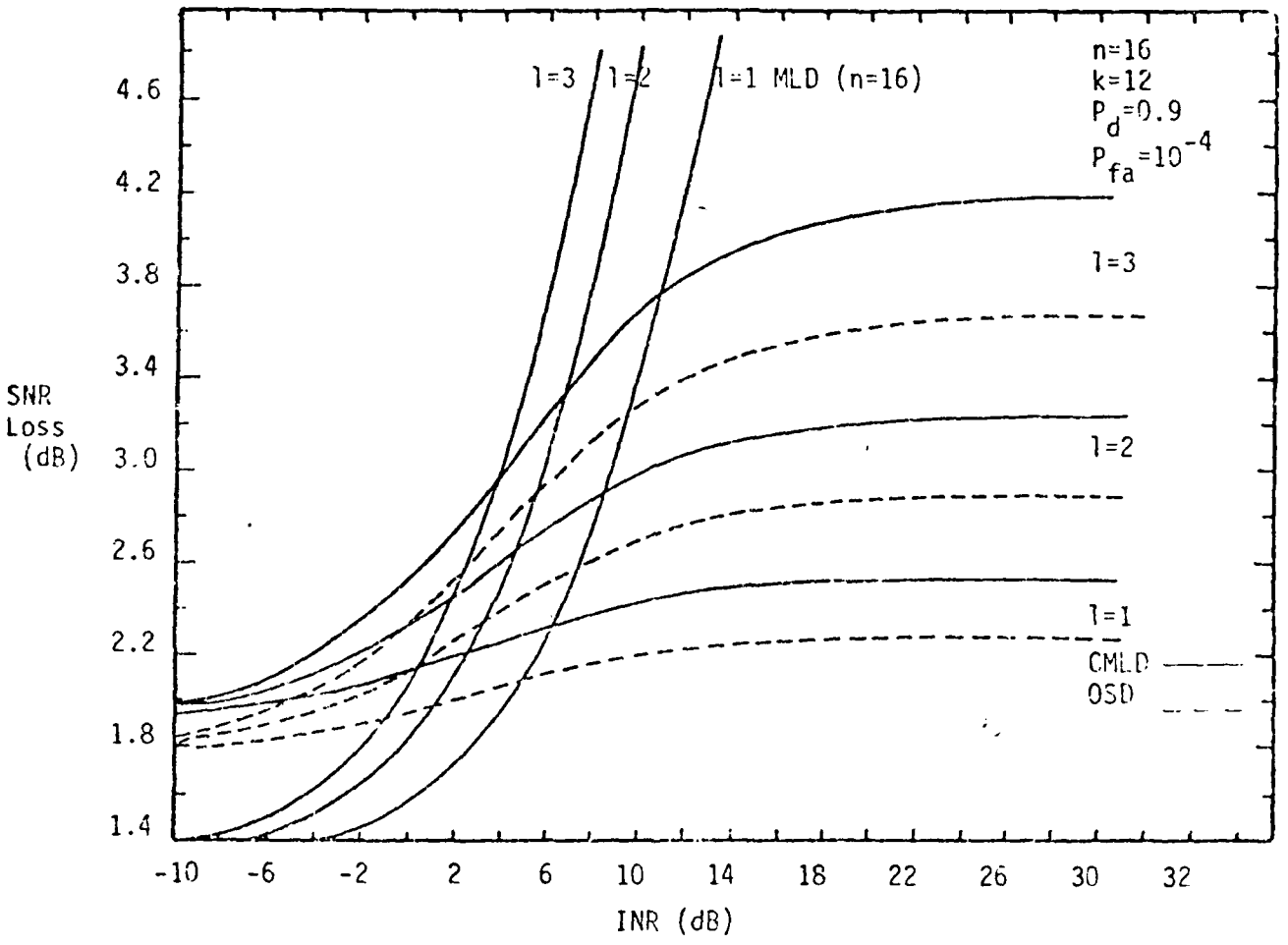


Figure 3.1 Comparison of the MLD, CMLD, and OSD in a multiple target environment.

## 4. The Integrated Output of a Linear Rectifier

In the receiver of a radar searching for a target at a particular range, the output of a narrowband filter matched to the echo signal is rectified and sampled at an appropriate time to provide a datum v. The data $v_1, v_2, \ldots, v_M$ acquired during M successive interpulse intervals are summed, or "integrated," to yield a statistic

$$V = v_1 + v_2 + \ldots + v_M, \tag{4.1}$$

and if this exceeds a certain decision level $V_0$, the radar decides that a target is present.

When the noise is Gaussian and the rectifier has a quadratic characteristic, the detection probability $q^+(V_0) = Pr\ (V > V_0)$ is given by the M-th-order Q-function [9, p. 219]. If the rectifier is linear, on the other hand, the distribution of V is not known in analytical form. Marcum [18] used the Edgeworth series to approximate the false-alarm and detection probabilities of a system integrating the outputs of a linear rectifier. This problem is conveniently handled by the method described in Section 1.

With appropriate normalization we can write

$$v_k = [(s_x + x_k)^2 + (s_y + y_k)^2]^{1/2} \tag{4.2}$$

where $x_k$ and $y_k$ are independent Gaussian random variables with mean zero and unit variance, and $S = \frac{1}{2}(s_x^2 + s_y^2)$ is the input signal-to-noise ratio, assumed the same for all k, $1 \leq k \leq M$. Then the probability density function of the $v_k$'s is

$$p(v) = v \exp(-\tfrac{1}{2} v^2 - S)\ I_0(\sqrt{2S}v), \qquad v > 0, \tag{4.3}$$

where $I_0(\cdot)$ is the modified Bessel function [9, p. 168]. The moments of $v_k$ were given by Rice [19, eq. (3.10-12), p. 107] as

$$\mu_n = E(v_k^n) = 2^{n/2}\Gamma(\tfrac{n}{2} + 1)\ {}_1F_1(-n/2,\ 1;\ -S) \tag{4.4}$$

in terms of the confluent hypergeometric function

$${}_1F_1(a,1;x) = 1 + \sum_{r=1}^{\infty} \frac{\Gamma(a+r)}{\Gamma(a)} \frac{x^r}{(r!)^2}. \tag{4.5}$$

When S = 0 the m.g.f. of $v_k$ is given in closed form by [19]

$$h_0(z) = E[\exp(-v_k z)] = 1 - (2\pi)^{1/2}\ z\ e^{z^2/2}\ \operatorname{erfc} z, \tag{4.6}$$

where

$$\operatorname{erfc} z = (2\pi)^{-1/2} \int_z^{\infty} e^{-u^2/2}\ du \tag{4.7}$$

is the error-function integral. The m.g.f. of V is then

$$h(z) = [h_0(z)]^M. \tag{4.8}$$

When n is large, the n-th moment $\mu_n$ is asymptotically

$$\mu_n \cong 2^{n/2}\Gamma(\tfrac{n}{2} + 1)e^{-S/2}\ I_0(\sqrt{2(n+1)S})$$

by eq. (13.5.13), p. 508 of Abramowitz and Stegun [20]. Using Stirling's formula for the factorial and the asymptotic formula for the modified Bessel function, we find for $n \gg 1$

$$a_n = \mu_n/n! \sim (8\pi nS)^{-1/2}\ n^{-n/2}\ \exp[\tfrac{n-S}{2} + (2nS)^{1/2}].$$

These coefficients decrease so rapidly with increasing n that the power series in (1.4) for the m.g.f. of the $v_k$ converges everywhere in the complex z-plane.

The first four coefficients of this series

$$h_0(z) = \sum_{k=0}^{\infty} a_k (-z)^k \tag{4.9}$$

are

$$a_0 = 1,\ a_1 = (\pi/2)^{1/2}\ {}_1F_1(-\tfrac{1}{2},1;-S)$$

$$a_2 = 1 + S,\ a_3 = (\pi/8)^{1/2}\ {}_1F_1(-3/2,1;-S). \tag{4.10}$$

The rest can be evaluated by the recurrence

$$a_{m+2} = \frac{2(m+1+S)(m-1)a_m - ma_{m-2}}{(m^2 - 1)(m + 2)} \tag{4.11}$$

so that the series in (4.5) needs to be summed only twice. One can then use the recurrence in (1.7) to determine the coefficients of the series

$$\ln h_0(z) = \sum_{k=0}^{\infty} b_k (-z)^k. \tag{4.12}$$

Multiplying these by M yields the terms in the expression (1.17) for the phase $\Psi(z)$ of the integrands of (1.9), (1.10), and (1.12).

The false-alarm probability $Q_0 = \Pr(V > V_0 |\ S = 0)$ can be computed by numerical quadrature of (1.21), using (4.6)-(4.8) to calculate $h(z)$ on the path of integration. The saddlepoint $x_0$ was calculated by Newton's method as in (1.16), and the curvature $\kappa$ of the parabolic path of integration was determined by (1.22). By combining this method with the secant method we were able to determine the decision level $V_0$ to attain a pre-assigned false-alarm probability $Q_0$. The detection probability $Q_d = \Pr(V > V_0 |\ S > 0)$ could then be calculated by (1.21), in which the m.g.f. $h(z)$ was computed as in (4.9)-(4.12), with (4.8). This method worked very efficiently and enabled us to compute the curves shown in Fig. 4.1, which supplement the one given by Marcum [18, p. 253]. These show the ratio in dB of the signal strength required when using a linear

rectifier to that required when using a quadratic rectifier to attain a given probability $Q_d$ of detection, for $Q_d$ = 0.5, 0.99, 0.999, 0.9999 and for various numbers M of pulses integrated. The false-alarm number

$$N_{fa} = (M \ln 2)/Q_0$$

was set at $10^6$.

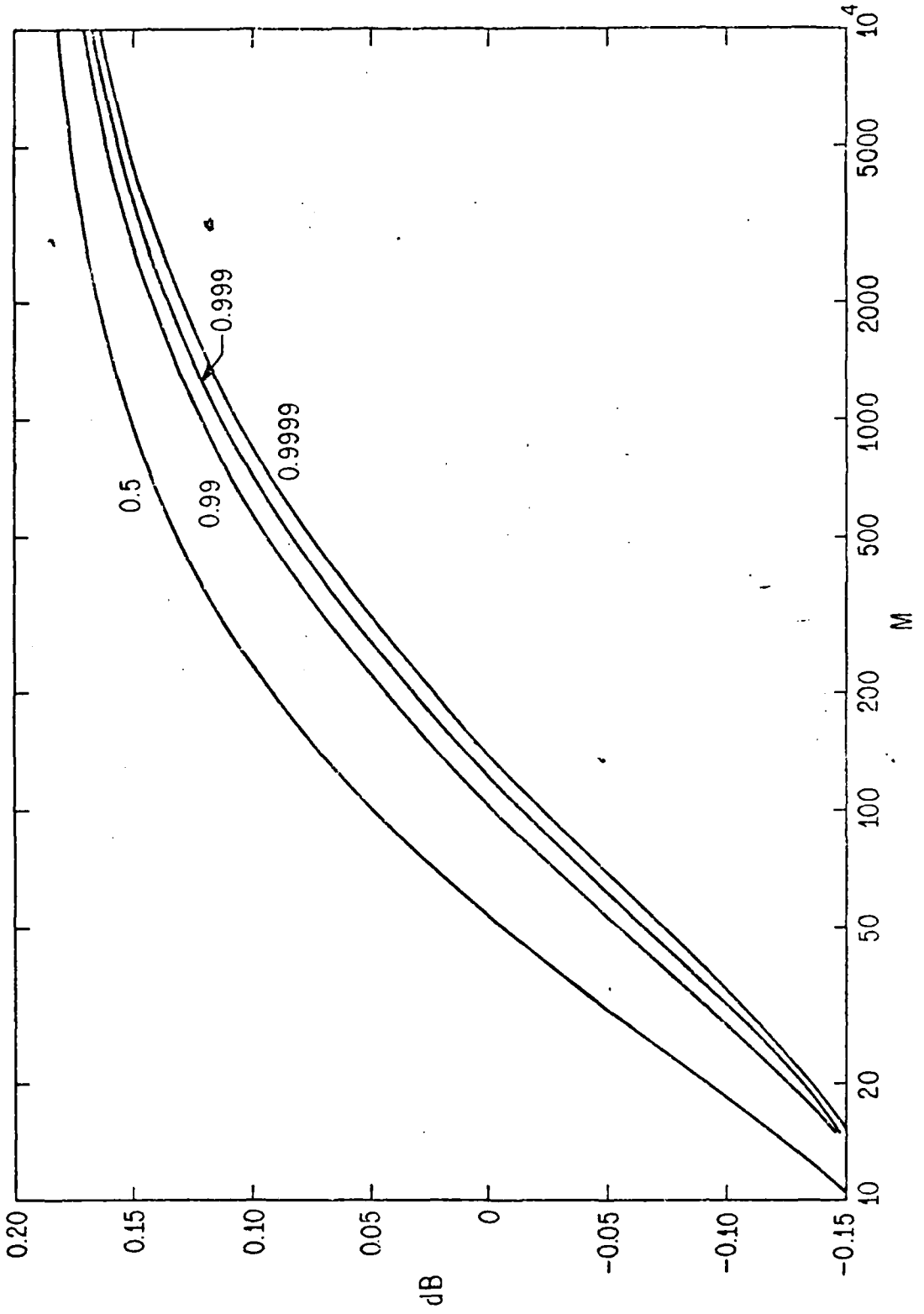


Fig. 4.1. Ratio in dB of SNR required by linear detector to that required by quadratic detector to attain detection probability $Q_d$, versus number M of pulses integrated. Curves are indexed with the values of $Q_d$. False-alarm number $N_{fa} = 10^6$.

## 5. Distribution of the Filtered Output of a Quadratic Rectifier

In a fundamental paper [21] Kac and Siegert showed how to calculate the moment-generating function (m.g.f.) of the filtered output of a quadratic rectifier whose input is Gaussian noise and, possibly, a coherent signal. Only in one very special case, however, did they invert the m.g.f. to obtain the probability distribution of the output. In general, numerical methods are necessary, and saddlepoint integration has proved to be a most efficient one.

Let the input to the rectifier be a narrowband Gaussian random process

$$v(t) = \mathrm{Re}\,[S_0(t) + N(t)]e^{i\Omega t} \tag{5.1}$$

with carrier frequency $\Omega$. Here $S_0(t)$ is the complex envelope of a coherent signal, and $N(t)$ is a stationary circular Gaussian random process with mean zero and complex autocovariance function

$$\phi(t_1-t_2) = \tfrac{1}{2}E[N(t_1)N^*(t_2)], \tag{5.2}$$

with $E[N(t_1)N(t_2)] = 0$. The output

$$\tfrac{1}{2}|S_0(t) + N(t)|^2$$

of the quadratic rectifier is applied to a filter with positive impulse response $K(\tau) > 0$. To be calculated is the distribution of the output w of that filter at time T,

$$w = \tfrac{1}{2}\int_0^T K(\tau)|S_0(T-\tau) + N(T-\tau)|^2\,d\tau. \tag{5.3}$$

The m.g.f. of the random variable w is [21]

$$h(z) = E(e^{-zW}) = [D(z)]^{-1} \exp\left[-\frac{z}{2}\sum_k \frac{|s_k|^2}{1 + \lambda_k z}\right], \tag{5.4}$$

where the $\lambda_k$ are the eigenvalues of the integral equation

$$\int_0^T \phi(u-v)\, K(v)\, g_k(v)\, dv = \lambda_k g_k(u), \qquad 0 < u < T, \tag{5.5}$$

whose eigenfunctions are $g_k(t)$, normalized so that

$$\int_0^T K(t)\, g_k^*(t)\, g_m(t)\, dt = \delta_{km}. \tag{5.6}$$

In (5.4)

$$D(z) = \prod_k (1 + \lambda_k z) \tag{5.7}$$

is the Fredholm determinant and

$$s_k = \int_0^T g_k^*(t)\, K(t)\, S_0^*(T-t)\, dt. \tag{5.8}$$

If the input is instead a lowpass Gaussian process $s_0(t) + n_0(t)$, where $n_0(t)$ is Gaussian noise with mean zero and autocovariance function $\phi(t_1-t_2)$, the m.g.f. is

$$h_1(z) = [D(z)]^{-1/2} \exp\left[-\frac{z}{2}\sum_k \frac{s_k^2}{1 + \lambda_k z}\right], \tag{5.9}$$

where the $s_k$ are defined as in (5.8) with $S_0^*(T-t)$ replaced by $s_0(T-t)$, and $D(z)$ is again the Fredholm determinant (5.7) associated with (5.5).

The m.g.f. $h(z)$ in (5.4) can be inverted by the residue theorem to give the probability density function $p(w)$ of the output $w$ when $S(t) = 0$, but when the

product $WT_{int}$ of the bandwidth W of the input noise and the integration time $T_{int}$ of the output filter is large, the resulting series is difficult to sum accurately because the leading terms are large and of alternating sign. When $S(t) \neq 0$, one might convolve the Rayleigh-Rice distributions that are the inverse transforms of the factors of (5.4), but it is difficult to do so accurately, particularly in the tails of the p.d.f. Numerical Fourier transformation of $h(-i\omega)$ is also inaccurate in the tails of the distribution.

Because of the square root in (5.9), the residue theorem cannot be applied to it. In determining the p.d.f. of the average power of a mean-zero random process, a special case of (5.9), Slepian [22] integrated the Laplace inversion integral with (5.9) numerically around cuts on the negative Re z-axis between the branch points $-1/\lambda_K$ of $[D(z)]^{1/2}$. The method of saddlepoint integration avoids difficulties such as these by taking the contour of integration in (1.9) or (1.10) along a contour close to the path of steepest descent of the integrand and far from its singularities on the negative Re z-axis.

When $S_0(t) = 0$ and the input noise has a Lorentz spectral density,

$$\Phi(\omega) = 2\mu(\omega^2 + \mu^2)^{-1}, \tag{5.10}$$

and autocovariance function

$$\phi(\tau) = e^{-\mu|\tau|}, \tag{5.11}$$

and when the output filter has an "RC" form

$$K(\tau) = \beta\, e^{-\beta\tau}\, U(\tau), \tag{5.12}$$

the m.g.f. of the filtered output w of the quadratic rectifier, as shown by Kac and Siegert [21], is

$$h(z) = \frac{(\eta/2)^{\nu-1}}{\Gamma(\nu)\ I_{\nu-1}(\eta)}, \qquad \eta = 2(\nu z)^{1/2}, \qquad \nu = 2\mu/\beta, \tag{5.13}$$

where $I_{\nu-1}(\cdot)$ is the modified Bessel function. By using a continued fraction for the logarithmic derivative of the Bessel function, the saddlepoints of the integrands of (1.9) and (1.10) can be quickly determined, and the cumulative distribution $q^-(w)$ of w can be computed by integrating (1.21) by the trapezoidal rule. In this way we produced the curves for $q^-(w)$ shown in Fig. 5.1 [23].

Because good accuracy can be attained in these numerical saddlepoint integrations with only about a dozen steps, it becomes feasible to treat problems in which the m.g.f. is not -- as in (5.13) -- known in closed form, but must itself be computed numerically. To this end we have shown that the m.g.f. h(z) in (5.4) can be written as

$$h(z) = [D(z)]^{-1} \exp\left\{-\frac{z}{2}\int_0^T K(t)[\sigma^*(t;z^*)-S^*(t)][\sigma(t;z)-S(t)]dt\right\} \tag{5.14}$$

with $S(t) = S_0^*(T-t)$ and with the Fredholm determinant given by [24]

$$D(z) = \exp\left[-\int_0^T K(t)\ r(t,\ t;\ z)\ dt\right]. \tag{5.15}$$

Here [23, 25]

$$\sigma(t;\ z) = \int_0^t r(t,\ u;\ z)\ K(u)\ S'(u)\ du \tag{5.16}$$

might be called the "causal quasi-estimate" of the signal $S(t) = S_0^*(T-t)$. The function r(t, u; z), which is the solution of the integral equation

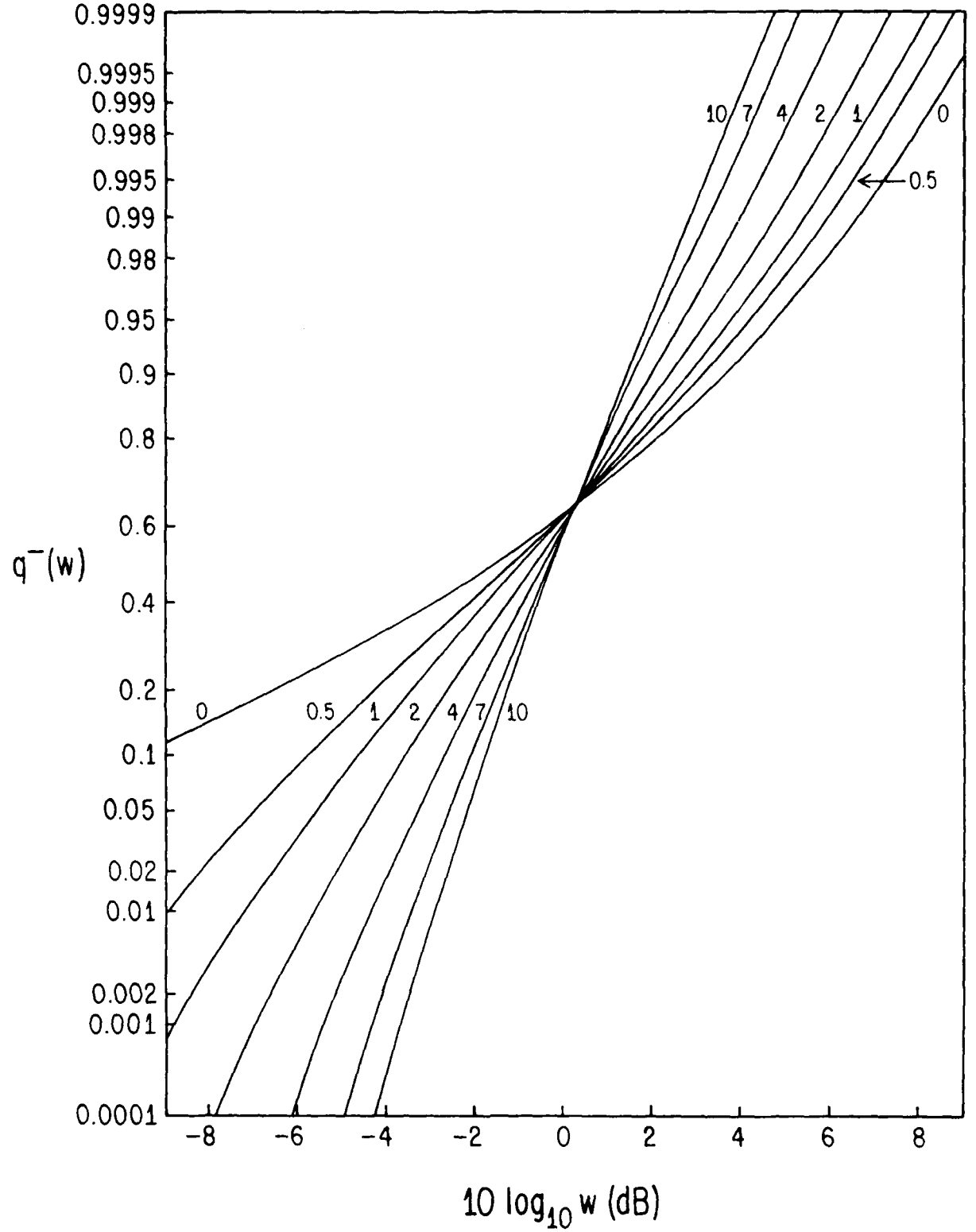


Fig. 5.1. Cumulative distribution $q^{-}(w)$ of RC-filtered output of a quadratic rectifier whose input is narrowband Gaussian noise with mean zero and a Lorentz spectral density. Curves are indexed with the value of $\nu = 2\mu/\beta$.

$$r(t, u; z) + z\int_0^t r(t, v; z)\, K(v)\, \phi(v-u)\, dv = z\phi(t-u),$$

$$0 < u < t < T, \tag{5.17}$$

is, for $K(\tau) = 1$ and z real and positive, the kernel of the minimum-mean-square-error estimator of the random process $z^{1/2}N(t)$ when it is observed in white Gaussian noise of unit spectral density.

It is this connection with estimation theory that shows a way of determining the m.g.f. h(z) numerically without having to find the eigenvalues $\lambda_k$ and the eigenfunctions $g_k(t)$ of the integral equation (5.5). When the spectral density $\Phi(\omega)$ of the noise is a rational function of the frequency, one can set up a state-space model of a linear, time-invariant system that is driven by circular-complex white noise W(t) and generates the process N(t). The state equations have the usual form

$$\frac{d\underset{\sim}{X}}{dt} = \underset{\sim}{F}\underset{\sim}{X} + \underset{\sim}{G}W(t), \tag{5.18}$$

where $\underset{\sim}{X}(t)$ is a column vector of n state variables, with 2n the degree of the denominator of the spectral density $\Phi(\omega)$, $\underset{\sim}{G}$ is a constant n-element vector, and $\underset{\sim}{F}$ is the n×n dynamical matrix of the system. For an appropriate n-element row vector $\underset{\sim}{C}$, the input noise can be represented as

$$N(t) = \underset{\sim}{C}\underset{\sim}{X}(t). \tag{5.19}$$

Then it can be shown that the kernel r(t, u; z) is given by

$$r(t, u; z) = \underset{\sim}{C}\underset{\sim}{k}_z(t, u), \tag{5.20}$$

where the n-element column vector $\underset{\sim}{k}_z(t, u)$ obeys the linear differential equation

$$\frac{\partial \underset{\sim}{k}_z(t, u)}{\partial t} = [\underset{\sim}{F} - \underset{\sim}{l}_z(t, t)K(t)\underset{\sim}{C}]\underset{\sim}{k}_z(t, u), \quad 0 < u < t < T, \tag{5.21}$$

and

$$\lim_{t \downarrow u} \underset{\sim}{k}_z(t, u) = \underset{\sim}{k}_z(u, u) = \underset{\sim}{\xi}(u; z)\underset{\sim}{C}^+ \tag{5.22}$$

with the n×n matrix $\underset{\sim}{\xi}(t; z)$ the solution of the matrix Ricatti equation

$$\frac{\partial \underset{\sim}{\xi}(t; z)}{\partial t} = \underset{\sim}{F}\underset{\sim}{\xi} + \underset{\sim}{\xi}\underset{\sim}{F}^+ - \underset{\sim}{C}^+K(t)\underset{\sim}{C}\underset{\sim}{\xi} + zQ\underset{\sim}{G}\underset{\sim}{G}^+$$

$$\underset{\sim}{\xi}(0; z) = z\underset{\sim}{\Lambda}_0, \tag{5.23}$$

where Q is the spectral density of the driving white noise W(t) in (5.18) and $\underset{\sim}{\Lambda}_0$ is the steady-state covariance matrix

$$\underset{\sim}{\Lambda}_0 = E[\underset{\sim}{X}(t)\ \underset{\sim}{X}^+(t)]$$

and obeys the equation

$$\underset{\sim}{F}\underset{\sim}{\Lambda}_0 + \underset{\sim}{\Lambda}_0\underset{\sim}{F} + Q\underset{\sim}{G}\underset{\sim}{G}^+ = 0. \tag{5.24}$$

The causal quasi-estimate σ(t; z) in (5.16) is

$$\sigma(t; z) = \underset{\sim}{C}\underset{\sim}{\varsigma}(t; z), \tag{5.25}$$

where the n-element column vector $\underset{\sim}{\varsigma}(t; z)$ is the solution of the vector differential equation

$$\frac{\partial \underset{\sim}{\varsigma}(t; z)}{\partial t} = \underset{\sim}{F}\underset{\sim}{\varsigma}(t; z) + \underset{\sim}{\xi}(t; z)\underset{\sim}{C}^+K(t)[S(t) - \underset{\sim}{C}\underset{\sim}{\varsigma}(t; z)],$$

$$\underset{\sim}{\varsigma}(0; z) = 0. \tag{5.26}$$

With J(T; z) denoting the integral in the exponent of the m.g.f. h(z) in (5.14), and with E(T; z) = ln D(z), one solves the differential equations (5.23) and (5.26) along with

$$\frac{\partial E(t; z)}{\partial t} = K(t)\underset{\sim}{C}\underset{\sim}{\xi}(t; z)\underset{\sim}{C}^+, \qquad E(0; z) = 0, \tag{5.27}$$

and

$$\frac{\partial J(t;\, z)}{\partial t} = K(t)[\sigma^*(t;\, z^*) - S^*(t)][\sigma(t;\, z) - S(t)],$$

$$J(0;\, z) = 0, \tag{5.28}$$

over the range $0 < t < T$. This can be accomplished by standard routines for solving sets of first-order differential equations. At $t = T$ one has the functions $E(T;\, z)$ and $J(T;\, z)$ for use in the phase

$$\Psi(z) = -E(T;\, z) - \frac{z}{2} J(T;\, z) + wz - \ln(\pm z) \tag{5.29}$$

in evaluating the saddlepoint integral (1.21). One carries out this procedure at each point z on the contour of integration after (1.21) has been replaced by a suitable quadrature formula such as the trapezoidal rule.

The derivatives of the phase $\Psi(z)$ for real values of z needed for finding the saddlepoint points $x_0^+$ and $x_0^-$ by Newton's method as in (1.16) and for determining the curvature $\kappa$ of the path of integration by (1.22) can be computed by solving along with (5.23), (5.26), (5.27), and (5.28) additional first-order differential equations obtained by differentiating these equations and their initial conditions with respect to z. This program has been carried through for RC-filtering of the output of a quadratic rectifier whose input is narrowband Gaussian noise with a Lorentz spectral density plus a signal with constant complex envelope. Good agreement was observed with the cumulative distribution computed by using (5.4) for the m.g.f. with the factor $[D(z)]^{-1}$ given by (5.13) and with the constants $s_k$ calculated by (5.8) [23].

## 6. Distribution of the Average Power of a Gaussian Process

A special case of the problem treated in Section 5 is that of finding the distribution of the average power

$$w = \frac{1}{2T}\int_0^T |N(t)|^2 \, dt \tag{6.1}$$

of a narrowband Gaussian random process Re $N(t)e^{i\Omega t}$ with carrier frequency $\Omega$ and mean zero, or of a lowpass Gaussian process $n(t)$,

$$w' = T^{-1}\int_0^T [n(t)]^2 \, dt \tag{6.2}$$

again with mean zero. The m.g.f. of w in (6.1) is

$$h(z) = E(e^{-zw}) = [D(z)]^{-1}$$

with $D(z)$ the Fredholm determinant given in (5.7) and (5.15), where the function $r(t, u; z)$ is by (5.17) now the solution of the integral equation

$$r(t, u; z) + \frac{z}{T}\int_0^t r(t, v; z)\, \phi(v-u)\, dv = z\phi(t-u),$$

$$0 < u < t < T. \tag{6.3}$$

For the random variable w' in (6.2), the m.g.f. is

$$h_1(z) = E(e^{-zw'}) = [D(2z)]^{-\frac{1}{2}}. \tag{6.4}$$

Slepian [22] calculated the p.d.f. and the cumulative distribution of w' for inputs $n(t)$ having Lorentz ("RC") and "RLC" spectral densities by determining $h_1(z)$ analytically and integrating the Laplace inversion formula numerically around cuts on the negative Re z-axis between pairs of branch points

$z_k = -1/\lambda_k$. His method requires finding a large number of eigenvalues $\lambda_k$ of the integral equation (5.5) with $K(v) = 2/T$; the larger the time-bandwidth product WT, with W the bandwidth of the input noise, the more of those cuts along which one needs to integrate. Saddlepoint integration provides a simple and efficient way of inverting the m.g.f. to determine the distribution of the average power.

When the circular complex Gaussian process N(t) has a rational spectral density $\Phi(\omega)$ that can be put into the form

$$\Phi(\omega) = 2\sum_{m=1}^{n} \frac{f_m\mu_m' + g_m(\omega-\mu_m'')}{(\omega-i\mu_m^*)(\omega+i\mu_m)}$$

$$= 2\sum_{m=1}^{n} \frac{f_m\mu_m' + g_m(\omega-\mu_m'')}{(\omega-\mu_m'')^2 + \mu_m'^2} \qquad (6.5)$$

where

$$-i\mu_k = -i\mu_k' + \mu_k'', \qquad i\mu_k^* = i\mu_k' + \mu_k'', \qquad 1 \le k \le n,$$

are the 2n poles of $\Phi(\omega)$, all of which we assume to be distinct, then the complex autocovariance function of N(t) is

$$\phi(\tau) = \sum_{m=1}^{n} (f_m + ig_m) \exp(-\mu_m^*\tau), \qquad \tau > 0$$

$$= \phi^*(-\tau) \qquad \tau < 0 \qquad (6.6)$$

When this is substituted into the integral equation (6.3), the kernel r(t, u; z) has the form

$$r(t, u; z) = \sum_{m=1}^{2n} c_m(t) \exp[\beta_m(t-u)], \qquad (6.7)$$

in which the coefficients $\beta_m$ are the 2n roots of the equations

$$1 + zT^{-1}\,\Phi(-ip) = 0, \qquad p = \beta_1, \beta_2, \ldots, \beta_m, \tag{6.8}$$

and the $c_m(t)$ satisfy a certain set of linear simultaneous equations. It is then possible to show from (5.15) that the Fredholm determinant D(z) is given by [23]

$$D(z) = \frac{\det(\underset{\sim}{D}_2^{-1}\underset{\sim}{M}^{*-1})\,\det\,(\underset{\sim}{C}_1 - \underset{\sim}{B}_2\underset{\sim}{D}_2\underset{\sim}{C}_2^{-1}\underset{\sim}{B}_1\underset{\sim}{D}_1^{-1})}{\det\,(\underset{\sim}{C}_1 - \underset{\sim}{B}_2\underset{\sim}{C}_2^{-1}\underset{\sim}{B}_1)}, \tag{6.9}$$

where the $n \times n$ matrices involved are defined by

$$\begin{aligned}
(\underset{\sim}{C}_1)_{mk} &= [(\beta_k - \mu_m)T]^{-1}, & (\underset{\sim}{C}_2)_{mk} &= [(\beta_{k+n} + \mu_m^*)T]^{-1},\\
(\underset{\sim}{B}_1)_{mk} &= [(\beta_k + \mu_m^*)T]^{-1}, & (\underset{\sim}{B}_2)_{mk} &= [(\beta_{k+n} - \mu_m)T]^{-1},\\
(\underset{\sim}{D}_1)_{mk} &= \exp\,(\beta_m T)\delta_{mk}, & (\underset{\sim}{D}_2)_{mk} &= \exp\,(\beta_{m+n}T)\,\delta_{mk},\\
(\underset{\sim}{M}^{*-1})_{mk} &= \exp\,(-\mu_m^* T)\,\delta_{mk}.
\end{aligned} \tag{6.10}$$

The roots $\beta_m$ of (6.8) are taken to have been arranged so that when the point z moves off to infinity in $0 \leq \arg z < \pi$, the first n roots trace paths finishing in the right half-plane and the rest ($k = n+1, \ldots, 2n$) trace paths finishing in the left half-plane. When z is real, $\beta_{m+n} = -\beta_m^*$, $1 \leq m \leq n$. The phase $\Psi(z)$ of the integrand of (1.21) is now

$$\Psi(z) = -\ln D(z) + wz - \ln(\pm z). \tag{6.11}$$

The form (6.9) is designed to avoid overflow in the computer. Because most computer libraries contain routines for multiplying complex matrices and forming their determinants and inverses, it is unnecessary to work out the Fredholm determinant in analytic form; instead one simply evaluates (6.9) at each point on the contour of integration. As good accuracy can be attained in integrating

(1.21) with only a few steps of the trapezoidal rule, this evaluation does not need to be carried out very often.

The spectral density of a lowpass process n(t) has the simpler form

$$\Phi(\omega) = \sum_{m=1}^{n} \frac{2\mu_m f_m}{\omega^2 + \mu_m^2}, \tag{6.12}$$

in which the $\mu_m$ are real or occur in complex-conjugate pairs. In calculating the distribution of the average power w' of such a process, as defined in (6.2), the form in (6.9) simplifies to

$$D(z) = \frac{\det\ (\underset{\sim}{D}\underset{\sim}{M}^{-1})\ \det\ (\underset{\sim}{C} - \underset{\sim}{B}\underset{\sim}{D}^{-1}\underset{\sim}{C}^{-1}\underset{\sim}{B}\underset{\sim}{D}^{-1})}{\det\ (\underset{\sim}{C} - \underset{\sim}{B}\underset{\sim}{C}^{-1}\underset{\sim}{B})}, \tag{6.13}$$

where

$$C_{mk} = [(\beta_k - \mu_m)T]^{-1}, \qquad B_{mk} = [(\beta_k + \mu_m)T]^{-1},$$

$$D_{mk} = \exp\ (\mu_k T)\ \delta_{mk}, \qquad M_{mk} = \exp\ (\mu_k T)\ \delta_{mk}, \tag{6.14}$$

and the $\beta_k$ are the n roots of

$$1 + 2zT^{-1}\ \Phi(-ip) = 0 \tag{6.15}$$

having non-negative real parts. The phase of the integrand in (1.21) is now

$$\Phi(z) = -\tfrac{1}{2} \ln D(z) - w'z - \ln\ (\pm z). \tag{6.16}$$

In [23] this method was applied to calculating the cumulative distribution of the average power of lowpass Gaussian processes having spectral densities characterizing RLC noise as well as those wih second- and fourth-order Chebyshev approximations to a bandlimited spectral density. The distribution of these last two were compared with that arising from a strictly bandlimited spectral density, as calculated by (1.21) with h(z) given by $[D(z)]^{-\frac{1}{2}}$ and D(z) by (5.7), in which

the eigenvalues $\lambda_k$ are proportional to those tabulated by Slepian and Sonnenblick for the prolate-spheroidal wave functions [26]. The distribution for the fourth-order Chebyshev approximation, calculated with the help of (6.13) and (1.21), agreed very closely with this one.

## 7. Intersymbol and Co-Channel Interference

In a typical binary channel suffering from intersymbol interference the output of the receiver has the form

$$y(t) = s(t) + n(t) \tag{7.1}$$

at time t, where the signal s(t) is

$$s(t) = \sum_{k=-\infty}^{\infty} b_k a(t-kT) \tag{7.2}$$

and n(t) is Gaussian noise with mean zero. The $b_k$'s are +1 or -1 with equal probability and express the transmitted binary message; we assume them uncorrelated. The output of the receiver from a single transmitted pulse is a(t), and T is the interval between pulses. The output is sampled at a time t to produce a variate

$$y = \sum_{k=-\infty}^{\infty} b_k a_k + n, \qquad a_k = a(t-kT), \tag{7.3}$$

on the basis of which the receiver decides whether a particular one of the $b_k$'s, say $b_0$, is + 1 or -1, choosing +1 if y > 0 and -1 if y < 0. The probability $P_e$ of error is then the probability that y < 0 when $b_0$ = +1,

$$P_e = Pr\ (y = \eta + a_0 + n < 0 \mid b_0 = +1), \tag{7.4}$$

where n is a Gaussian variate with mean zero and variance $\sigma^2$ resulting from the noise, and

$$\eta = \sum_{k=-\infty}^{\infty}{}' b_k a_k, \tag{7.5}$$

the prime indicating omission of the term $k = 0$.

Calculating the error probability $P_e$ exactly is most difficult, for all possible combinations of the "digits" $b_k = \pm 1$ must be taken into account, $1 \leq |k| < \infty$. Even if one assumes, as we for the most part have assumed, that only a finite number N of pulses before and after $a_0$ need to be included, exact computation of $P_e$ involves accounting for $2^{2N}$ combinations, and for accuracy N must ordinarily be very large. Some dozen papers have appeared in whch bounds on the error probability have been derived. The closer the bounds, the more complicated they are to evaluate.

The error probability can be calculated quite simply by saddlepoint integration of (1.9), in which now $V = 0$ and the m.g.f. $h(z)$ is given by

$$h(z) = \prod_{k=-N}^{N}{}' \cosh(a_k z) \exp(\tfrac{1}{2}\sigma^2 z^2 - a_0 z), \qquad (7.6)$$

the prime indicating omission of the term $k = 0$ [7]. Because of the Gaussian factor $\exp \tfrac{1}{2}\sigma^2 s^2$, the magnitude of the integrand of (1.9) drops off to zero rapidly along a vertical contour $\mathrm{Re}\ z = c > 0$ when that contour passes through the saddlepoint $c = x_0$ of the integrand.

In this problem the m.g.f. $h(z)$ and hence the integrand of (1.9) possesses an infinite number of zeros on the Im z-axis, lying at points $z = iy$ such that $a_k y = 2n\pi$ for some integers n and k. When the signal-to-noise ratio $a_0^2/\sigma^2$ is low, the path of steepest descent from the saddlepoint $x_0$ on the Re z-axis runs into one of those zeros and then passes from one zero to another on the way out to $+i\infty$. For large signal-to-noise ratio the path is slightly curved, but runs more or less parallel to the Im z-axis. Neither of these paths would be simple to approximate, and we have therefore adopted the original straight vertical path $z = x_0 + iy$ through the saddlepoint and found it adequate.

The saddlepoint $x_0$ is the solution of the equation

$$\Psi'(z) = \sum_{k=-\infty}^{\infty}{}' a_k \tanh(a_k z) + \sigma^2 z - a_0 - z^{-1} = 0, \qquad (7.7)$$

which is easily solved by Newton's method (1.16). As the saddlepoint $x_0$ is not needed to great accuracy, N in (7.7) can be replaced by a smaller value N" such that for $|k| > N"$ the values of the signal samples $a_k$ have fallen below a few percent of $a_0$. The integral in (1.9) is evaluated by the trapezoidal rule, and a simple bound on the error incurred has been determined [27]. The length of the computation of the error probability by this method is now roughly linear in N, in contrast to its exponential dependence on N when the combinatorial approach is taken.

If all possible interfering symbols were taken into account, the phase of the integrand in (1.9) would be

$$\Psi(z) = \sum_{k=-\infty}^{\infty}{}' \ln \cosh (a_k z) + \tfrac{1}{2}\sigma^2 z^2 - a_0 z - \ln z, \qquad (7.8)$$

and this can be approximated by

$$\Psi(z) \doteq \sum_{k=-N}^{N}{}' \ln \cosh (a_k z) + \tfrac{1}{2}\sigma_1^{\,2} z^2 - a_0 z - \ln z, \qquad (7.9)$$

where

$$\sigma_1^{\,2} = \sigma_0^{\,2} + \sum_{k=-\infty}^{-N-1} a_k^{\,2} + \sum_{k=N+1}^{\infty} a_k^{\,2}. \qquad (7.10)$$

When the sums in (7.10) can be evaluated, perhaps approximately, the pulses neglected in (7.6) can be roughly taken into account as contributing to the

Gaussian noise.

A similar problem is to calculate the effect on a binary communication system of signals leaking from adjacent channels, so-called "cochannel interference." Now (7.5) is replaced by

$$\eta = \sum_{k=1}^{L} r_k \cos \theta_k \tag{7.11}$$

where the $r_k$ are specified positive amplitudes and the angles $\theta_k$ are independently random and uniformly distributed over $(0, 2\pi)$; L is the number of interfering channels. The m.g.f. $h(z)$ in (1.9) is now

$$h(z) = \prod_{k=1}^{L} I_0(r_k z) \exp(\tfrac{1}{2}\sigma^2 z^2 - a_0 z),$$

where $I_0(\cdot)$ is the modified Bessel function. The resulting error probability $P_e$ can again be calculated by integrating (1.9) along a straight vertical contour passing through the saddlepoint $c = x_0 > 0$. A bound on the truncation error for this integration has also been determined [27].

## 8. The Distribution of Shot and Clutter Noise

Radar clutter noise can be considered a random process of the form

$$v(t) = \sum_{k=-\infty}^{\infty} a_k f(t-\tau_k) \tag{8.1}$$

in which the terms $a_k f(t-\tau_k)$ represent echoes of the transmitted radar pulses $f(t)$ from scatterers with various cross-sections located at randomly distributed ranges. The arrival times $\tau_k$ of the echoes can be taken as a Poisson point process, to which we assign a constant rate $\nu$. Only for a finite range of indices $k$ are the amplitudes $a_k$ significantly large, for the transmitting radar antenna illuminates only a limited area of the scattering surface. We can assume, however, that the interval of time during which the echoes arrive is so much longer than the duration of each pulse that the summation in (8.1) can be taken from $-\infty$ to $\infty$. The amplitudes $a_k$ in clutter noise can be assumed to be independent random variables with a common probability density function. We first consider the special case of shot noise.

(a) Shot Noise

When the amplitudes $a_k$ are all equal to 1, (8.1) represents shot noise. Rice [19, Sec. 1.4] showed that the m.g.f. of the random variable $v = v(t)$ at any time $t$ is then

$$h(z) = \exp\left\{\nu \int_{-\infty}^{\infty} \{\exp[zf(t)] - 1\}\, dt\right\}. \tag{8.2}$$

He also showed how to approximate the distribution of the amplitude $v$ by Edgeworth's series. Gilbert and Pollak [28] derived from (8.2) an integral equation for the cumulative distribution of $v$ and solved it for some simple pulse shapes. Lugannani and Rice [29] described how to evaluate the cumulative distri-

bution by numerically integrating (1.9) or (1.10) along the Im z-axis itself, and they also gave saddlepoint approximations and Chernoff bounds on this distribution. Yue et al. [30] developed series approximations for the distribution valid especially for low values of $\nu T$, where T is the pulse length.

In a preliminary investigation of the applicability of numerical saddlepoint integration to computing the cumulative distribution of the amplitude v of shot noise, we considered a pulse containing an arbitrary number M of cycles of a sinewave,

$$\begin{aligned} f(t) &= \cos \Omega t, \qquad 0 < t < T = 2\pi M/\Omega, \\ &= 0, \qquad\quad t < 0,\ t > T, \end{aligned} \tag{8.3}$$

for which the m.g.f. from (8.2) is

$$h(z) = \exp\{\nu T[I_0(z) - 1]\}, \tag{8.4}$$

where $I_0(\cdot)$ is the modified Bessel function. As the p.d.f. of v is an even function, we need to consider only negative values of the level V, for which we take the saddlepoint $x_0$ on the positive real axis.

The m.g.f.'s of shot noise, by (8.2), are entire functions and have no singularities anywhere in the finite portion of the z-plane. At infinity, however, they possess numerous singularities, as one can see by considering the asymptotic form of (8.4) for $|z|$ large, but with z going off to infinity in a direction other than that of the Im z-axis. The phase $\Psi(z)$ of the integrand in (1.10) is now, for $|z| \gg 1$, Re $z > 0$, $V < 0$,

$$\Psi(z) \sim (2\pi z)^{-\frac{1}{2}} \nu T\, e^z - |V|z - \ln z, \tag{8.5}$$

and if we put $z = re^{i\theta}$, the imaginary part becomes

$$\text{Im } \Psi(z) \sim \nu T(2\pi r)^{-\frac{1}{2}} e^x \sin(y - \tfrac{\theta}{2}) - |V|y - \theta. \tag{8.6}$$

This must remain constant on the path of steepest descent as z runs out to infinity in the right halfplane. The term with the factor $e^x$ will grow exponentially unless $\sin(y - \theta/2)$ goes to zero. This means that z must go off to infinity along a line on which y equals a multiple of $\pi$; along such a line the angle $\theta$ goes to zero as Re $z \to \infty$. The corresponding term in Re $\Psi(z)$ is proportional to

$$e^x \cos (y - \theta/2),$$

and if the integrand is to go to zero, y must approach an odd multiple of $\pi$. The path of steepest descent thus consists of hairpin curves opening toward $+\infty$ and approaching the lines Im $z = (2k+1)\pi$ asymptotically for all integers k. On the main branch lying symmetrically about the Re z-axis, $k = 0$ and Im $\Psi(z) = 0$. Each of these branches possesses one saddlepoint; for $k = 0$ it is the point we have denoted by $x_0$.

We have integrated (1.9) with the m.g.f. in (8.4) along the main branch of the path of steepest descent and along a number $n_{off}$ of the branches above the Re z-axis, and the results are exhibited in Table 8.1. The branches lying below the Re z-axis are mirror images of those above it and contribute equally to the cumulative probability $q^-(V)$. The branches were traced by the method described in Sec. I, part (b), and the integration along each was carried out by means of the five-point quadrature formula (1.27) of Birkhoff and Young [7]. The contribution of each branch was also estimated by the saddlepoint approximation (1.29), which agreed within a few percent with the result of the numerical integration.

The column marked "Ratio" in Table 8.1 lists the ratio of the contribution of the off-axis branches to the total probability $q^-(V)$. For $\nu T = 10$ the off-axis branches contributed only a small fraction of the probability, and five of

Table 8.1

$q^-(V)$: *Shot noise, sinusoidal pulses*

| V | Main branch | Off-axis branches | Ratio | Total probability $q^-(V)$ | LRY |
|---|---|---|---|---|---|
| | | $\nu T = 10$, $n_{off} = 5$ | | | |
| -1 | 0.32431 | -5.0163(-5) | -1.547(-4) | 0.32426 | 0.3242 |
| -3.5 | 0.58263(-1) | 4.7156(-6) | 8.093(-5) | 0.58268(-1) | 0.5827(-1) |
| -8 | 0.31845(-3) | 9.4186(-9) | 2.958(-5) | 0.31846(-3) | 0.3185(-3) |
| | | $\nu T = 1$, $n_{off} = 12$ | | | |
| -0.1 | 0.40362 | -0.11080 | -0.3784 | 0.29283 | 0.2920 |
| -1.1 | 0.60583(-1) | -0.14782(-1) | -0.3227 | 0.45801(-1) | 0.4607(-1) |
| -2.25 | 0.35009(-2) | -0.17276(-3) | -0.05191 | 0.33281(-2) | 0.3320(-2) |

them sufficed. For $\nu T = 1$, on the other hand, the off-axis branches contributed a substantial fraction of the total probability, and these amounts decreased very slowly and in an oscillatory fashion as one moved to branches farther and farther from the Re z-axis. Twelve branches above the axis were taken into account for $\nu T = 1$. The column marked "LRY" lists the values of $q^-(V)$ tabulated by Lugannani, Rice, and Yue [31]. The agreement is excellent at $\nu T = 10$, but not so good at $\nu T = 1$. The smaller the value of $\nu T$, the more slowly the m.g.f. $h(z)$ decreases as the value of z moves toward $\pm i\infty$.

(b) Clutter Noise

When as for clutter noise the amplitudes $a_k$ in (8.1) are independent and possess a common probability density function p(a), the m.g.f. of the random variable $v = v(t)$ is [32]

$$h(z) = \exp\left\{\nu \int_{-\infty}^{\infty} [H(zf(t)) - 1]\, dt\right\}, \tag{8.7}$$

where

$$H(z) = E(e^{-za}) = \int_{-\infty}^{\infty} p(a)e^{-za}\, da \tag{8.8}$$

is the m.g.f. of the amplitudes $a_k$. If, as we shall assume, these have identical Gaussian distributions with mean zero and variance $\sigma^2$,

$$H(z) = \exp\left(\tfrac{1}{2}\sigma^2 z^2\right), \tag{8.9}$$

then

$$h(z) = \exp\left\{\nu \int_{-\infty}^{\infty} [\exp(\tfrac{1}{2}\sigma^2 z^2 [f(t)]^2) - 1]dt\right\}. \tag{8.10}$$

We considered two types of signal: (i) a rectangular pulse,

$$f(t) = 1, \quad 0 < t < T; \quad f(t) = 0, \quad t < 0, \quad t > T, \tag{8.11}$$

for which

$$h_1(z) = \exp\{\nu T[\exp(\tfrac{1}{2}\sigma^2 z^2) - 1]\} \tag{8.12}$$

and (ii) the sinusoidal signal in (8.3), for which

$$h_2(z) = \exp\{\nu T[\exp(\tfrac{1}{4}\sigma^2 z^2) I_0(\tfrac{1}{4}\sigma^2 z^2) - 1]\}. \tag{8.13}$$

We wish to compare the cumulative distributions of v for these two signals, and we choose $\sigma^2$ so that both processes v(t) have the same variance $\nu T$, taking $\sigma^2 = 1$ for the first and $\sigma^2 = 2$ for the second. Thus

$$h_1(z) = \exp \nu T(e^{z^2/2} - 1), \tag{8.14}$$

$$h_2(z) = \exp \nu T[e^{z^2/2} I_0(z^2/2) - 1]. \tag{8.15}$$

Again taking $V < 0$, so that the principal saddlepoint $x_0$ lies on the positive real axis, we find that for signal (i) the path of steepest descent passing vertically through $x_0$ bends around and approaches zero along the hyperbola $xy = \pi$. Indeed, the phase of the integrand in (1.9) is now

$$\Psi_1(z) = \nu T(e^{z^2/2} - 1) - |V|z - \ln z, \tag{8.16}$$

and along the path of steepest descent

$$\begin{aligned} \operatorname{Im} \Psi_1(z) &= \nu T \exp \tfrac{1}{2}(x^2 - y^2) \sin xy - |V|y - \theta = 0, \\ z &= x + iy = re^{i\theta}. \end{aligned} \tag{8.17}$$

As the point z moves to the right, the exponential function increases rapidly, and sin xy must go to zero in order to keep $\operatorname{Im} \Psi_1(z)$ equal to zero; that is,

$xy \to \pi$. All the higher branches of the path of steepest descent in the upper halfplane are thus bent hairpins asymptotic, as $x \to \infty$, to the hyperbolas

$$xy = (2n+1)\pi, \qquad n = 0, 1, 2, \ldots . \tag{8.18}$$

Each such branch possesses a saddlepoint of the integrand. For signal (ii) the paths of steepest descent exhibit a similar configuration. Numerical integration along such a complicated set of curves would be quite lengthy and involved.

The real part of the phase $\Psi_1(z)$ is

$$\text{Re } \Psi_1(z) = \nu T \exp \tfrac{1}{2}(x^2-y^2) \cos xy - \nu T - |V|x - \ln r, \tag{8.19}$$

and the absolute value $\exp [\text{Re } \Psi_1(z)]$ of the integrand in (1.9) vanishes as z goes off toward infinity anywhere in the sector

$$\pi/4 < \arg z < \pi/2.$$

The originally vertical contour of integration in (1.9), with $c = x_0 > 0$, can therefore be deformed into a contour passing through the saddlepoint $x_0$ and approaching the line $x = y$ asymptotically. For this reason we have chosen to integrate (1.9) along a hyperbolic contour on which

$$z = (x_0^{\,2} + y^2)^{\frac{1}{2}} + iy, \tag{8.20}$$

whereupon (1.9) becomes

$$q^-(V) = \pi^{-1} \text{ Re} \int_0^\infty e^{\Psi(z)} \, z^* dy/x. \tag{8.21}$$

The trapezoidal rule was applied to integrating this numerically, and for the values of $\nu T$ considered, the trapezoidal sum converged rapidly enough for the numerical integration to be feasible.

In Figs. 8.1 and 8.2 we plot the complementary cumulative distributions

$q^+(V)$ for these two signals for $V > 0$ and values of $\nu T$ ranging from 1 to 50. The abscissa represents the variable $(\nu T)^{-\frac{1}{2}}V$. The ordinates were converted by the transformation $-\text{erfc}^{-1}(q^+)$, under which a normal distribution plots as a straight line. The dashed line marked '$\infty$' indicates the asymptote that the curves approach as with increasing $\nu T$ the distribution of the clutter amplitude becomes more nearly Gaussian. For the lowpass signal (i) the approach to normality is more rapid than for the sinusoidal rectangular pulse (ii).

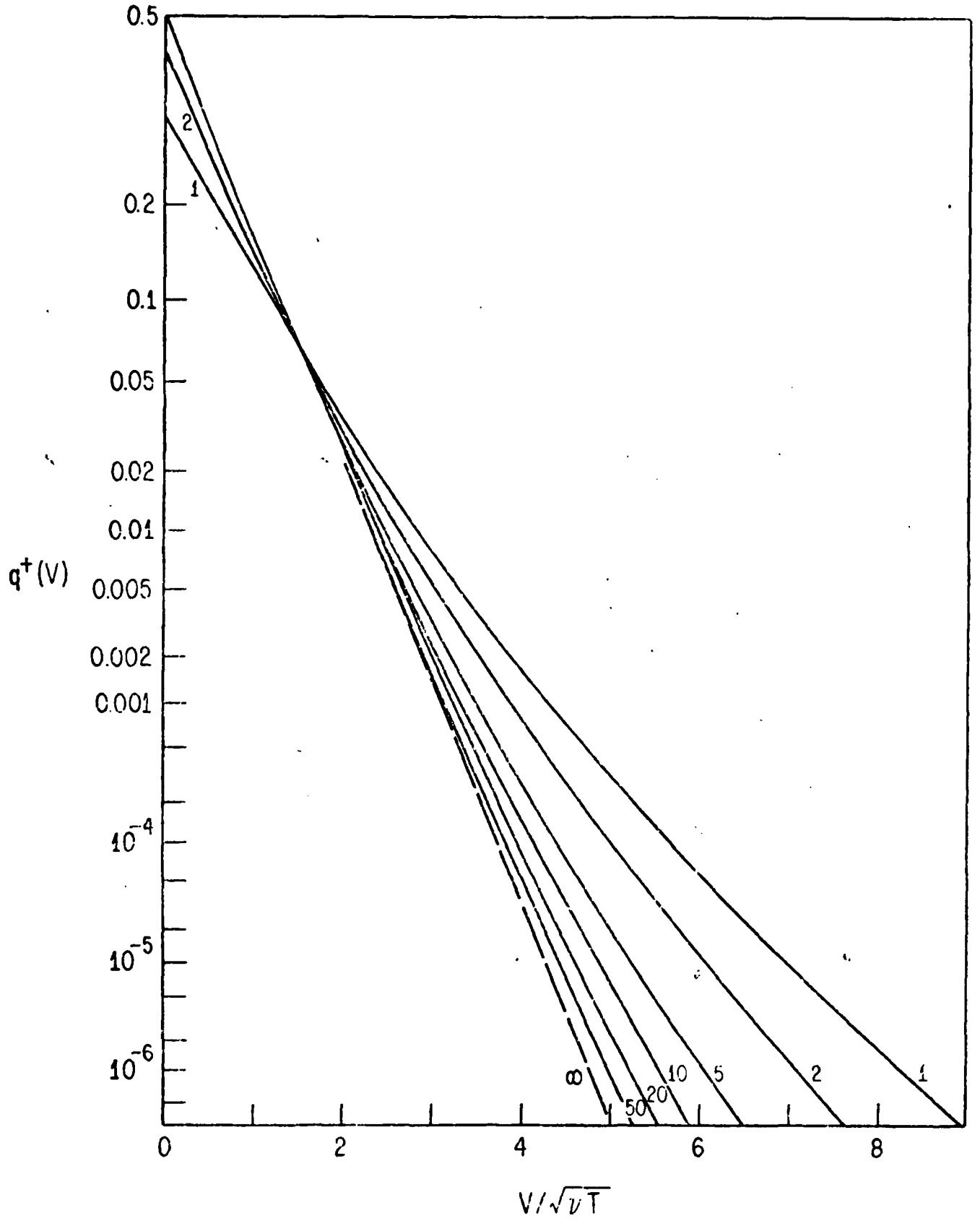


Fig. 8.1. Complementary cumulative distribution of clutter noise consisting of lowpass rectangular pulses with Gaussian-distributed amplitudes. Curves are indexed with the value of $\nu T$.

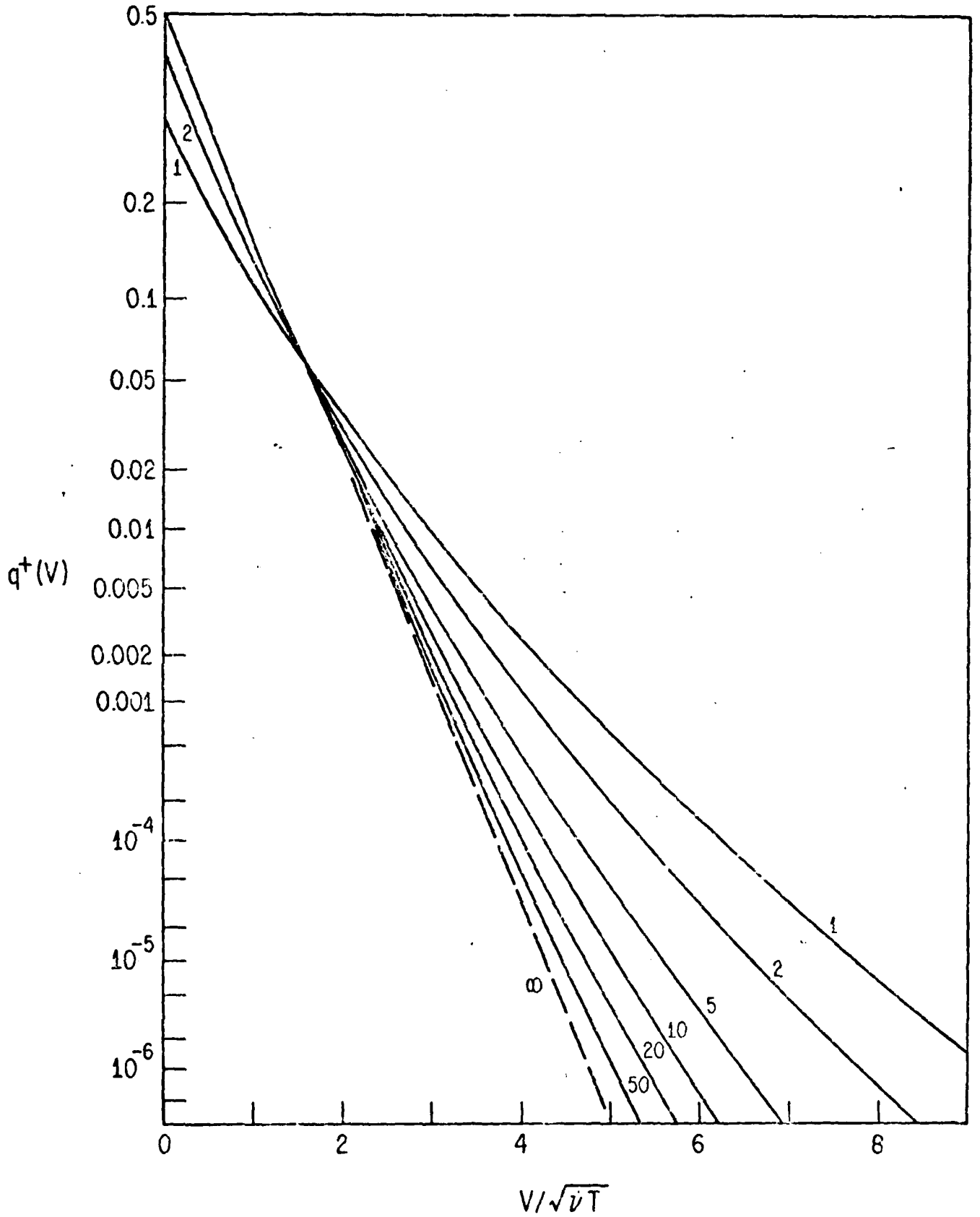


Fig. 8.2. Complementary cumulative distribution of clutter noise consisting of narrowband rectangular amplitude modulations of a carrier having Gaussian-distributed amplitudes. Curves are indexed with the value of $\nu T$.

## II. Integer-Valued Random Variables

### 9. Calculating Distributions from Probability Generating Functions

Let w be a positive integer-valued random variable with a probability distribution

$$\Pr(w = k) = p_k, \qquad k = 0, 1, 2, \ldots,$$

$$\sum_{k=0}^{\infty} p_k = 1,$$

with cumulative distribution function (c.d.f.)

$$Q_n^- = \Pr(w < n) = \sum_{k=0}^{n-1} p_k, \tag{9.1}$$

and with complementary cumulative distribution function (c.c.d.f.)

$$Q_n^+ = 1 - Q_n^- = \Pr(w \geq n) = \sum_{k=n}^{\infty} p_k. \tag{9.2}$$

In typical applications w is the number of electrons counted during a specific interval (0, T) at the output of some photoelectric device. The c.d.f. and the c.c.d.f. can be computed from the probability generating function (p.g.f.)

$$h(z) = E(z^w) = \sum_{k=0}^{\infty} p_k z^k \tag{9.3}$$

by the contour integrals

$$Q_n^- = \int_{C_-} \frac{z^{-n}\, h(z)}{1 - z} \frac{dz}{2\pi i}, \tag{9.4}$$

$$Q_n^+ = \int_{C_+} \frac{z^{-n}\, h(z)}{z - 1} \frac{dz}{2\pi i}, \tag{9.5}$$

in which $C_-$ and $C_+$ are circles centered at the origin $z = 0$; $C_+$ also encloses the point $z = 1$, $C_-$ does not; and the contours enclose no singularities of the p.g.f. $h(z)$, all of which lie outside the unit circle.

As shown in [33], the numerical evaluation of these integrals is most efficient when the contours pass through saddlepoints of the integrand, that is, through points $x_0$ that are solutions of

$$\Psi'(z) = \frac{h'(z)}{h(z)} - \frac{n}{z} - \frac{1}{z - 1} = 0, \tag{9.6}$$

where

$$\Psi(z) = \ln h(z) - n \ln z - \ln[\pm(z - 1)] \tag{9.7}$$

is the "phase" of the integrand, $\pm(z - 1)$ standing for $1 - z$ when (9.4) is integrated and for $z - 1$ when (9.5) is integrated. One such saddlepoint, $x_0 = \bar{x_0}$, lies in $0 < x_0 < 1$, the other lies on the real z-axis between $x = 1$ and the leftmost singularity of $h(z)$. The saddlepoint can usually be most expeditiously located by solving (9.6) by Newton's method or the secant method. Alternatively, the equivalent of (1.17) can be used, or $\Psi(x)$ can be minimized in the appropriate range of $x = \mathrm{Re}\ z$.

The circular contours in (9.4) and (9.5) often suffer the disadvantage that the integrand is oscillatory along them, so that too many steps may be needed in order to obtain an accurate value of $Q_n^+$ or $Q_n^-$ by numerical integration. The value of the integrand decreases most rapidly from its value at the saddlepoint when the contour is taken as the path of steepest descent through the saddlepoint. Along that path $\mathrm{Im}\ \Psi(z) = 0$. Determining the path of steepest descent, however, would much protract the evaluation of the contour integral. In many cases it has been found that the path of steepest descent, which lies symmetrically about the real axis, has nearly a parabolic form, and it is then expeditious to use instead its osculatory parabola, that is, a parabola passing through

the saddlepoint $z_0$ and having the same curvature

$$\kappa = \frac{1}{3} \Psi'''(z_0)/\Psi''(z_0) \tag{9.8}$$

at the point $z = z_0$. (Primes indicate differentiation.) Along this parabola

$$z = z_0 + 1/2\ \kappa y^2 + iy, \tag{9.9}$$

and the integral to be evaluated numerically is

$$Q_n^{\pm} = \pi^{-1} \int_0^{\infty} \mathrm{Re}\ \frac{h(z)z^{-n}}{\pm(z - 1)}\ (1 - i\kappa y)\ dy. \tag{9.10}$$

The initial step size is taken as

$$\Delta y = [\Psi''(z_0)]^{-1/2} \tag{9.11}$$

and successively halved until the values of the probability stabilize to the number of significant figures desired. The trapezoidal rule is used for reasons described by Schwartz [6] and Rice [3].

In other problems, such as the one to be treated in Sec. 10, the path of steepest descent may be more complicated. It is advisable first of all to trace a few such paths for typical parameter values by the method of Sec. 1(b). If one knows no simple alternative path along which the integral converges sufficiently rapidly, one can integrate along a close approximation of the path of steepest descent by, for instance, utilizing the five-point quadrature formula (1.27) as described in Sec. 1(d).

## 10. Single-Stage Photomultiplication

The contour-integration method has been applied to finding the distribution of the number of electrons at the output of a photomultiplier with a single stage of multiplication [34]. Light striking a photoelectrically emissive surface ejects a number k of photoelectrons during an interval (0, T) with probability $\Pi_k$. The p.g.f. of this distribution is

$$f(z) = \sum_{k=0}^{\infty} \Pi_k z^k. \tag{10.1}$$

Each such "primary" electron is accelerated by an applied voltage, impinges on a second metallic surface, and ejects from it a random number of secondary electrons. Let $p_m^{(s)}$ be the probability that a given primary electron ejects m secondary electrons; the p.g.f. of this distribution is

$$g(z) = \sum_{m=0}^{\infty} p_m^{(s)} z^m. \tag{10.2}$$

Then the p.g.f. of the total number of secondaries during (0, T) is

$$h(z) = \sum_{n=0}^{\infty} p_n z^n = f\big(g(z)\big), \tag{10.3}$$

where $p_n$ is the probability that n secondary electrons appear at the output of this device.

In this work it was assumed that the distribution of the number of secondary electrons per primary has the Poisson form, so that

$$g(z) = e^{G(z-1)}, \tag{10.4}$$

where G is the gain. The output distribution can then be computed from

$$p_n = \sum_{k=1}^{\infty} \Pi_k (kG)^n \, e^{-kG}/n! \tag{10.5}$$

with the cumulative distribution determined as in (9.1) by addition. Alternatively, one can use the finite relations

$$\begin{aligned} p_0 &= f(e^{-G}), \\ p_n &= G^n \sum_{k=1}^{n} f_k \, \bar{S}(n, k) \, e^{-kG}, \qquad n > 0, \end{aligned} \tag{10.6}$$

where

$$f_k = \frac{d^k}{dz^k} f(z) \bigg|_{z=e^{-G}}, \tag{10.7}$$

and where $\bar{S}(n, k)$ are modified Stirling numbers of the second kind and obey the recurrent relations

$$\begin{aligned} &\bar{S}(1, 1) = 1, \qquad \bar{S}(k, n) = 0, \qquad k > n, \\ &\bar{S}(n + 1, k) = [\bar{S}(n, k - 1) + k\bar{S}(n, k)]/(n + 1). \end{aligned} \tag{10.8}$$

These formulas were used to compute exact values of the probabilities $Q_n^-$ and $Q_n^+$ for comparison with those computed by our approximation methods. They involve lengthy computations when the number n is large, and round-off error introduces large relative error into the c.c.d.f. $Q_n^+ = 1 - Q_n^-$ when $Q_n^-$ is computed as in (9.1).

Three types of primary distribution $\{\Pi_k\}$ were treated: (i) that arising when the incident light has a Lorentz spectral density, and for which the probabilities $\Pi_k$ can be calculated by a method given by Bédard [35]; (ii) the negative binomial distribution

$$\Pi_k = \frac{\Gamma(M + k)}{k!\Gamma(M)} (1 - v)^M v^k, \qquad v = N_p/(N_p + M), \tag{10.9}$$

with $N_p$ the mean number of primary electrons and M the number of temporal modes or "degrees of freedom", given roughly by the product of the bandwidth W of the incident light and the duration T of the counting interval; and (iii) the Poisson distribution

$$\Pi_k = N_p{}^k \exp(-N_p)/k!, \tag{10.10}$$

for which the output distribution possesses the Neyman Type-A form.

For primary distributions of type (i) and, for M an integer, of type (ii), the p.g.f. f(z) possesses poles $z_k$ lying on the positive real z-axis to the right of z = 1, whereupon the output p.g.f. h(z) possesses poles at the points

$$\zeta_k^{(r)} = 1 + G^{-1}(\ln z_k + 2r\pi i), \tag{10.11}$$

for all positive and negative integral values of r, including r = 0. The contour integral (9.5) can then be evaluated as a residue series with terms corresponding to each point of this doubly infinite lattice of poles. For the negative-binomial primary distribution, the array shrinks to a vertical column of multiple poles of order M at the points

$$\zeta_r = 1 + G^{-1}(-\ln v + 2r\pi i). \tag{10.12}$$

When the number n of output electrons is of the order of or greater than the expected value

$$E(n) = N_p G, \tag{10.13}$$

only a very few of the poles above and below the real axis contribute significantly to the residue series. The number of columns of the lattice that need to

be included under case (i) (incident light with a Lorentz spectral density) is of the order of the time-bandwidth product WT. Formulas for computing the residues and numerical examples are given in [34]. Unless WT is very large, this residue method is most efficient for computing the c.c.d. $Q_n^+$ with $n > E(n)$.

Consideration was given to using the contour integrals in (9.4) and (9.5) for computing the c.d. and the c.c.d. of the number of output electrons. The path of steepest descent is now too complicated to be utilized or even approximated, for it consists of a number of hairpin-like branches opening to the right and passing around each of the poles of h(z). We therefore used instead a straight vertical path of integration passing through the saddlepoint of the integrand lying on the real z-axis; the one lying in $0 < z < 1$ was used for $Q_n^-$, and the one lying in $1 < z < \zeta_1^{(0)}$ was used for $Q_n^+$, these having been determined by solving (9.6) by Newton's method. A bound on the error incurred by truncating the numerical integration was worked out. Values of $Q_n^-$ and $Q_n^+$ over a broad range of values of n could be accurately computed in this way without requiring more than one hundred or so steps of numerical integration. Details are given in Sec. 4 of [34]. This method does not require that the number M in (10.9) be an integer. The contour-integration method can be used for all three types of primary distribution.

On each branch of the path of steepest descent of the integrand in (9.4) and (9.5) there is a point $z_k$ at which the magnitude of the integrand is maximum; this is a saddlepoint of the integrand. The contribution of each branch to an integration of (9.4) or (9.5) along its path of steepest descent can be crudely approximated by assuming that in the neighborhood of each saddlepoint $z_k$ the integrand has a Gaussian form, and this leads to the formula

$$Q_n^{\pm} = \sum_{k=-\infty}^{\infty} [2\pi\Psi''(z_k)]^{-1/2} \exp [\Psi(z_k)], \qquad (10.14)$$

where $\Psi(z_k)$ is the phase of the integrand as in (9.7) and $\Psi''(z_k)$ is its second derivative evaluated at the k-th saddlepoint [3]. For the most part two or three saddlepoints on each side of the principal one $x_0$ on the real z-axis are all that it is worth taking into account; often the one at $x_0$ alone suffices. Improved accuracy was obtained by evaluating the contribution of the principal branch of the path of steepest descent, which crosses the real axis at $z_0$, by means of the uniform asymptotic expansion described in [36] and [37]. The details of this method are to be found in Sec. 5 of [34].

## 11. Multistage Photomultiplier

A photomultiplier usually has not one, but several stages of electron multiplication. We number the stages, each associated with an electrode called a "dynode," from the final one. A single electron striking the k-th dynode ejects n secondary electrons from it with probability $p_n^{(k)}$; the collection of these probabilities constitutes the k-th "single-stage" distribution and has a p.g.f.

$$g_k(z) = \sum_{n=0}^{\infty} p_n^{(k)} z^n. \tag{11.1}$$

Then if there are N stages in all, the probabilities $p_n$ that n electrons emerge at the output when a single primary electron strikes the N-th dynode have the p.g.f.

$$H_N(z) = \sum_{m=0}^{\infty} p_m z^m, \tag{11.2}$$

where

$$\begin{aligned} H_1(z) &= g_1(z), \\ H_k(z) &= g_k\big(H_{k-1}(z)\big), \qquad k = 2, 3, \ldots, N. \end{aligned} \tag{11.3}$$

If the distribution of primary electrons again has the p.g.f. f(z) defined in (10.1), the total number of output electrons has the p.g.f. $f\big(H_N(z)\big)$.

In this study we have concentrated on calculating the cumulative output distributions, defined as in (9.1) and (9.2), for a single primary electron, so that in (9.3)-(9.5) the p.g.f. of the output is

$$h(z) = H_N(z).$$

We assumed that all the single-stage distributions have the same negative-binomi-

al or Polyà form, with common p.g.f.

$$g_k(z) = g(z) = [1 - bG(z - 1)]^{-1/b}, \qquad b > 0, \tag{11.4}$$

which corresponds to the distribution in (10.9) with

$$M = 1/b, \qquad v = bG/(1 + bG).$$

Again G is the gain per stage; the overall gain of the photomultiplier is

$$G_0 = G^N, \tag{11.5}$$

where N is the number of stages. The Poisson single-stage distribution represented by (10.4) arises in the limit $b \to 0$.

The singularities of the overall p.g.f. $H_N(z)$ now lie on or close to the portion of the real z-axis lying to the right of the point $z = 1$, and the path of steepest descent has roughly the form of a parabola lying symmetrically about the real z-axis and opening to the right. This path can be replaced by its osculatory parabola, whose curvature $\kappa$ at the saddlepoint is determined by (9.8). The first three derivatives of the phase $\Psi(z)$ of the integrand, defined as in (9.7), are computed by an N-fold set of three recurrent relations. The cumulative probabilities $Q_n^+$ are then computed by numerical integration of (9.10). The results were compared with values computed by the recurrent relations given by Prescott [38] for $N = 3$ and values of n up to 100, and the agreement was excellent [39]. The recurrent relations require of the order of $n^2$ operations to compute $p_n$ or $Q_n^+$, and this number is independent of the number of significant figures sought. Thus for $n = 3000$ of the order of nine million operations would be required, in contrast to the ten or twenty steps of numerical integration of (9.10) needed for adequate precision.

When the cumulative distributions $Q_n^+$ so calculated are plotted on a semi-

logarithmic grid for various numbers N of stages of multiplication, the overall gain $G_0 = G^N$ being kept fixed, one finds the points lying closer and closer to straight lines as N increases. The results are fitted quite closely by a geometric or "exponential" distribution,

$$\begin{aligned} p_0 &= 1 - (1 - v)G_0, \\ p_n &= G_0(1 - v)^2 v^{n-1}, \qquad n > 0, \\ Q_n^+ &= G_0(1 - v)v^{n-1}, \qquad n > 0, \end{aligned} \tag{11.6}$$

in which the parameter v is given by

$$v = a/(a + 1), \qquad a = \frac{\kappa_2(G_0 - 1)}{2G(G - 1)}, \tag{11.7}$$

where $\kappa_2$ is the second factorial moment of the single-stage distribution and G is the gain per stage,

$$G = g'(1), \qquad \kappa_2 = g''(1), \tag{11.8}$$

primes denoting differentiation. This value of v is chosen so that the distribution in (11.6) has the same variance as the exact distribution,

$$\text{Var } n = \frac{\sigma^2 G_0(G_0 - 1)}{G(G - 1)}, \qquad \sigma^2 = \kappa_2 + G - G^2. \tag{11.9}$$

A number of observers have reported approximately exponential distributions for the number of output electrons in photomultipliers, but an adequate explanation of this phenomenon seems to have been lacking [38]. In [39] the distribution in (11.6) was shown to approach the true output distribution under the conditions stated: the overall gain $G_0 = G^N$ is fixed, the single-stage distributions are identical, and the number N of stages increases, the gain G per stage decreasing simultaneously toward 1. A related limit theorem in the theory of branching processes has been derived by Fahady, Quine, and Vere-Jones [40].

## 12. Performance of Receivers with Avalanche Photodiodes

### (a) Distribution of the Output of an Avalanche Photodiode

In an avalanche photodiode primary electrons generated at one face by incident light are accelerated under an applied voltage and create hole-electron pairs in the body of the diode by collision. The holes and the secondary electrons are themselves accelerated and create more such pairs. The probability $Pr\ (n|\ N)$ that a fixed number N of primary electrons generate a total of n electrons at the output was calculated by McIntyre under the assumption that the collision-ionization probability for holes is a fixed fraction g of that for electrons, independently of their energy, $0 < g < 1$ [41]. Personick [42] showed under the same assumption that the probability generating function (p.g.f)

$$M(z) = \sum_{n=0}^{\infty} Pr\ (n|\ 1)\ z^n \tag{12.1}$$

of the distribution of the number of output electrons arising from a single primary electron is the solution of the equation

$$z = M[1 + a(M-1)]^{-b}, \qquad b = (1-g)^{-1} > 1, \tag{12.2}$$

where a is related to the gain G of the diode by

$$G = (1-ab)^{-1}, \qquad 0 < a < 1. \tag{12.3}$$

Ordinarily the number of primary electrons has a Poisson distribution with mean $\lambda$ proportional to the intensity of the incident light, and the number n of electrons at the output has a compound Poisson distribution,

$$p_n = \sum_{N=0}^{\infty} \frac{\lambda^N e^{-\lambda}}{N!}\ Pr\ (n|\ N). \tag{12.4}$$

The cumulative distribution, that is, the probability $q_k^-$ that fewer than k electrons are counted, must then be computed by summing the probabilities $p_n$,

$$q_k^- = \sum_{n=0}^{k-1} p_n, \tag{12.5}$$

and the complementary cumulative distribution is $q_k^+ = 1 - q_k^-$. Computing these probabilities in this manner is tedious because of the complexity of McIntyre's formula [41] for Pr (n| N), and when, as usually in a multiplicative device such as this, the numbers k are large, many summations are required and round-off error is serious.

The method of saddlepoint integration has been found most efficient for determining the cumulative distribution $q_k^-$ of the number of output electrons [43]. One computes $q_k^-$ or $q_k^+$ by numerical integration of (9.4) or (9.5), in which now the probability generating function is

$$h(z) = \exp[\lambda(M-1)], \tag{12.6}$$

M and z being related by (12.2). Rather than solving (12.2) for M at each point z on the contour of integration, we change variables in (9.4) and (9.5) and use M as the variable of integration, obtaining the formula

$$q_k^{\pm} = \pm \int_{C_\pm} e^{\lambda(M-1)} M^{-n}[1 + a(M-1)]^{bn-1} \times \left[\frac{1 - a + a(1-b)M}{M - [1 + a(M-1)]^b}\right] \frac{dM}{2\pi i}, \tag{12.7}$$

where $C_-$ and $C_+$ are curves in the M-plane passing through the image $M_0^-$ or $M_0^+$ of the saddlepoint $x_0^-$ or $x_0^+$ of the integrand in (9.4) or (9.5). The z-plane is cut along the real z-axis from a point

$$x_* = M_* [1 + a(M_*-1)]^{-b}, \quad M_* = (1-a)/[a(b-1)] > 1,$$

to $z = \infty$, in order to render the solution of (12.2) for M single-valued. A parabolic contour in the cut M-plane was found to yield the probabilities $q_k^+$ and $q_k^-$ to seven significant figures with fewer than twenty steps of numerical integration, even for values of k as high as 50000. Indeed, the larger the gain G and the mean number $\lambda$ of primary electrons, the more accurate this method of saddlepoint integration becomes.

(b) Distribution of the Sum of Diode Output and Gaussian Noise

In an optical receiver utilizing an avalanche photodiode, Gaussian noise corrupts the diode output in a subsequent amplifier. The performance of such a receiver was calculated by Personick, Balaban, Bobsin, and Kumar [44] by convolving the distribution of the number of output electrons, as computed by (12.4), with a Gaussian distribution representing the noise. This computation was so lengthy that they resorted instead to Monte Carlo simulation, crude Gaussian approximations, and Chernoff bounds. The distribution of the output can be computed easily by the method of saddlepoint integration.

The moment-generating function (m.g.f) of the sum v of the number of output electrons and a Gaussian noise variate with mean zero and variance $\sigma^2$ is

$$h(s) = E(e^{sv}) = \exp[\lambda(M-1) + \tfrac{1}{2}\sigma^2 s^2], \tag{12.8}$$

with $s = \ln z$ and z related to M again through (12.2),

$$s = f_s(M) = \ln M - b \ln [1 + a(M-1)]. \tag{12.9}$$

(We change from s to -s in our m.g.f. in order to avoid troublesome minus signs later.) The cumulative distribution of the noisy output v and its complement can be calculated by numerical integration of (1.9) and (1.10), with V replaced by

-V. We used the method of Sec. 1(d).

One computes an approximate path of steepest descent passing through the saddlepoint of the integrand of (1.9) or (1.10) by the method described in Sec. 1(b). The integration is carried out along this segmented path,

$$q^{\pm}(V) = \sum_{k=0}^{\infty} \int_{M_k}^{M_{k+1}} g(M)\, dM/\pi i, \tag{12.10}$$

where we have replaced the integration variable z by M, and

$$g(M) = (\pm s)^{-1} \exp[\lambda(M-1) + \tfrac{1}{2}\sigma^2 s^2](\frac{dM}{ds})^{-1} \tag{12.11}$$

with

$$\frac{dM}{ds} = \frac{M[1 + a(M-1)]}{1 + a(M-1) - abM} \tag{12.12}$$

and with s given by (12.9) as a function of M. The saddlepoint $s_0 = f_s(M_0)$ is obtained by solving the equation

$$\psi'(M) = \lambda \frac{dM}{ds} + \sigma^2 s - V - \frac{1}{s} = 0, \qquad s = f_s(M), \tag{12.13}$$

for $M = M_0$ by Newton's method. The contribution of each term in (12.10) is evaluated by the five-point formula (1.27) of Birkhoff and Young [7]. The initial length $|\Delta M| = \delta$ of the segments can be taken as

$$\delta = \tfrac{1}{2} \left(\frac{dM}{ds}\right)\Big|_{M=M_0} [\psi''(s_0)]^{-\frac{1}{2}}, \tag{12.14}$$

where $s_0 = f_s(M_0)$ is the saddlepoint on the Re s-axis; the second derivative $\psi''(s_0)$ will have been calculated in determining the saddlepoint by Newton's method.

One can also apply the saddlepoint approximation described in [8] and [46] to this problem, evaluating the tail probabilities $q^-(V)$ and $q^+(V)$ as

$$q^{\pm}(V) \tilde{=} [2\pi\Psi''(s_0)]^{-\frac{1}{2}} \exp \Psi(s_0), \tag{12.15}$$

where the phase $\Psi(s)$ is, as in (1.15),

$$\Psi(s) = \lambda(M-1) + \tfrac{1}{2}\sigma^2 s^2 - Vs - \ln(\pm s), \tag{12.16}$$

and the saddlepoint $s_0$ is the root of (12.13) lying to the right of the origin for $q^+(V)$ and to the left for $q^-(V)$. By using M as the independent variable, (12.13) can be solved by Newton's method, in the course of which $\Psi''(s_0)$ is determined.

In the binary receiver analyzed by Personick et al. [44] the decision level V above which it decides that a signal is present is set to minimize the average probability of error. As 0's and 1's were taken as equally frequent, this is the point at which

$$p_0(V) = p_1(V), \tag{12.17}$$

where $p_0(v)$ and $p_1(v)$ are the probability density functions of the output v under the hypotheses $H_0$ (no signal) and $H_1$ (signal present), respectively. The mean numbers $\lambda_i$ of input electrons under these two hypotheses are

$$\begin{aligned} \lambda_1 &= N_s + N_d, \\ \lambda_0 &= \eta N_s + N_d, \end{aligned} \tag{12.18}$$

where $N_d$ measures the strength of the dark current, $N_s$ the strength of the signal under $H_1$, and $\eta \ll 1$ the leakage in the optical transmitter. The aim of the computations described by Personick et al. [44] was to determine the minimum input signal strength $N_s$ and the associated decision level V so that the average probability of error

$$P_e = \tfrac{1}{2}[q_0^+(V) + q_1^-(V)] \tag{12.19}$$

takes on a pre-assigned value. Here the subscripts on $\lambda$, p, and $q^{\pm}$ refer to the hypothesis.

The density functions $p_0(V)$ and $p_1(V)$ needed for setting the decision level V through (12.17) can also be calculated approximately by the saddlepoint method [8, 46],

$$p_i(V) = h_i(\tilde{s}_i) \exp(-\tilde{s}_i V) [2\pi\Phi_i''(\tilde{s}_i)]^{-1/2}, \quad i = 0, 1, \tag{12.20}$$

where $h_i(s)$ is the m.g.f. of the output v under hypothesis $H_i$ and

$$\Phi_i(s) = \ln h_i(s) - sV = \lambda_i(M-1) + \tfrac{1}{2}\sigma^2 s^2 - sV \tag{12.21}$$

is the associated modified phase. The saddlepoints $\tilde{s}_i$ are the roots of the equation

$$\Phi_i'(s) = \lambda_i \frac{dM}{ds} + \sigma^2 s - V = 0, \quad i = 0, 1, \tag{12.22}$$

which can be solved by a few iterations of Newton's method for the saddlepoints $\tilde{s}_0$ and $\tilde{s}_1$, again treating M as an independent variable and determining s from (12.9). The equation (12.17) for the decision level V is in this approximation equivalent to

$$\begin{aligned} &\lambda_1(\tilde{M}_1-1) + \tfrac{1}{2}\sigma^2\tilde{s}_1^2 - \tilde{s}_1 V - \tfrac{1}{2}\ln \Phi_1''(\tilde{s}_1) \\ &\quad = \lambda_0(\tilde{M}_0-1) + \tfrac{1}{2}\sigma^2\tilde{s}_0^2 - \tilde{s}_0 V - \tfrac{1}{2}\ln \Phi_0''(\tilde{s}_0), \\ &\qquad \tilde{s}_i = f_s(\tilde{M}_i), \quad i = 0, 1. \end{aligned} \tag{12.23}$$

This equation is solved for V by the secant method.

One then uses this value of the decision level V in (12.19), computing $q_0^+(V)$ and $q_1^-(V)$ by the saddlepoint approximation (12.15) in order to obtain the error probability as a function $P_e(N_s)$ of the input signal strength $N_s$. By using

the secant method one can then determine the signal strength $N_s$ to yield the pre-assigned value of the error probability $P_e$.

The optimization procedure described in [45] starts with Gaussian approximations to the densities $p_i(V)$ and the cumulative probabilities $q_0^+(V)$ and $q_1^-(V)$. The means and variances of v needed for these are easily calculated, and the equation (12.17) for the decision level V reduces in this approximation to a quadratic equation. One uses the secant method to solve (12.19) in this Gaussian approximation to obtain starting values of $N_s$ and V for the computation with the saddlepoint approximations just outlined. Two or three iterations of each suffice to produce accurate estimates of the minimum signal strength $N_s$ and the decision level V needed to attain the pre-assigned false-alarm probability $P_e$.

In a further stage of this optimization procedure the probabilities $q_0^+(V)$ and $q_1^-(V)$ were computed by the numerical saddlepoint integration technique described earlier in this section. The decision level was still calculated by the saddlepoint approximation (12.20) - (12.23). Although one could also calculate the density functions $p_0(v)$ and $p_1(v)$ more accurately by numerical integration of (1.7), this refinement produced so slight a change in the final results as not to be worth the trouble. In Table 12.1 we list the values of the signal strength $N_s$ and the decision level V determined by the three successive parts of this optimization technique. It is seen that the third part, requiring numerical quadrature, alters the values of $N_s$ and V very little from those yielded by the saddlepoint approximations in the second part. For most practical purposes carrying the procedure through only the first and second parts suffices and yields results far more accurate than those of the Gaussian approximation alone, but without much additional computation.

Table 12.1

Examples of Optimization

$\eta = 0.01$, $N_d = 5$, $P_e = 10^{-9}$

| Gain | Gauss approx. (i) | | S'd'p't approx. (ii) | | Num. quad. (iii) | |
|---|---|---|---|---|---|---|
| G | $N_s$ | V | $N_s$ | V | $N_s$ | V |
| | | | $k = 0.5$, $\sigma^2 = 3.6\times10^7$ | | | |
| 10 | 7491 | 36858 | 7481.4 | 36837 | 7481.53 | 36836 |
| 30 | 3019 | 37512 | 2887.8 | 37555 | 2889.87 | 37578 |
| 40 | 2602 | 38100 | 2412.4 | 39445 | 2427.86 | 39701 |
| 50 | 2429 | 38898 | 2340.4 | 48549 | 2344.48 | 48679 |
| 60 | 2380 | 39952 | 2439.4 | 62806 | 2441.83 | 62876 |
| 70 | 2402 | 41321 | 2623.1 | 81012 | 2624.90 | 81074 |
| | | | $k = 0.1$, $\sigma^2 = 3.6\times10^7$ | | | |
| 50 | 1707 | 37435 | 1666.2 | 37435 | 1666.29 | 37434 |
| 70 | 1368 | 37966 | 1290.4 | 38045 | 1294.97 | 38164 |
| 90 | 1214 | 38672 | 1131.2 | 41291 | 1135.63 | 41524 |
| 110 | 1145 | 39588 | 1108.6 | 50373 | 1110.26 | 50483 |
| | | | $k = 0.04$, $\sigma^2 = 10^6$ | | | |
| 50 | 393 | 6779 | 367.4 | 7348 | 368.15 | 7361 |
| 70 | 359 | 7284 | 354.8 | 10149 | 355.08 | 10158 |
| 90 | 356 | 7981 | 379.6 | 14442 | 379.76 | 14449 |
| 110 | 368 | 8894 | 418.1 | 19917 | 418.25 | 19923 |

## 13. Photoelectron Counting

### (a) Incident Light of Arbitrary Spectral Density

When light falls on a photoelectrically emissive surface, the probability generating function of the number of electrons ejected during an interval (0, T) is given by

$$h(z) = E[e^{I(z-1)}], \tag{13.1}$$

where I is a random variable proportional to the total energy falling on the surface during that interval. If we assume the light to be plane-polarized, quasimonochromatic, and spatially coherent over the entire emissive surface, its field can be written

$$v(t) = \mathrm{Re}\,[V(t)e^{i\Omega t}], \qquad 0 < t < T,$$

in which the complex envelope V(t) is a circular complex Gaussian random process, and $\Omega = 2\pi\nu$ is the central angular frequency of the light. Then

$$I = \frac{1}{2}\,\eta \int_0^T |V(t)|^2\, dt \tag{13.2}$$

with $\eta$ a constant directly proportional to the quantum efficiency of the emissive surface and inversely proportional to the photon energy $h\nu$.

The expected value $E[V(t)] = S(t)$ represents the complex envelope of a coherent light signal, such as the output of a pulsed laser. The difference $V_b(t) = V(t) - S(t)$ represents incoherent light such as is produced by an ordinary incandescent source. It is assumed to be a stationary Gaussian random process with a temporal coherence function defined by

$$G(t_1-t_2) = \frac{1}{2}\,E[V_b(t_1)V_b^*(t_2)]. \tag{13.3}$$

The spectral density of tne light is

$$\Gamma(\omega)= \int_{-\infty}^{\infty} G(t)e^{i\omega t}\, dt. \tag{13.4}$$

The mean number $n_0$ of photoelectrons ejected by this incoherent component is

$$n_0 = nG(0)T; \tag{13.5}$$

the mean number $n_s$ ejected by the coherent component is

$$n_s = \frac{1}{2}\, n \int_0^T |S(t)|^2\, dt. \tag{13.6}$$

The p.g.f. h(z) can be expressed as [25]

$$h(z) = [D(\xi)]^{-1} \exp\{n_s(z-1)\{1 - \int_0^T \int_0^T \sigma^*(t)\psi(t,u;\xi;T)\sigma(u)\, dtdu\}\},$$

$$\xi = n_0(1-z), \tag{13.7}$$

where

$$D(\xi) = \prod_{k=1}^{\infty} (1+\lambda_k \xi) \tag{13.8}$$

is the Fredholm determinant associated with the integral equation

$$\lambda_k f_k(t) = T^{-1} \int_0^T \gamma(t-s)\, f_k(s)\, ds, \quad \gamma(\tau) = G(\tau)/G(0), \tag{13.9}$$

whose eigenvalues are $\lambda_k$. Furthermore, $\sigma(t)$ is a normalized signal envelope,

$$\sigma(t) = S(t) \Big/ \int_0^T |S(u)|^2\, du, \tag{13.10}$$

and $\psi(t,u;\xi;T)$ is the resolvent kernel defined by the integral equation

$$\psi(t,u;\xi;\tau) + \frac{\xi}{T}\int_0^\tau \psi(t,v;\xi;\tau)\gamma(v-u)\,dv$$

$$= \xi T^{-1}\gamma(t-u), \qquad 0 \le (t,u) \le \tau \le T. \tag{13.11}$$

In the past the distribution of the number of photoelectrons has been evaluated by decomposing the field V(t) into temporal modes by a Karhunen-Loève expansion, whereupon the p.g.f. can be written as a product of factors involving the eigenvalues $\lambda_k$ of (13.9) and the coefficients

$$S_k = \int_0^T f_k^*(t)\, S(t)\, dt$$

of the coherent component. The distribution corresponding to each factor or mode has the Laguerre form, and the distribution of the total number V of photoelectron counts is the convolution of as many of these as necessary [47]. Other modal decompositions can also be used [48]. (Further references are to be found in ref. [25].) Such methods require much computation time and storage, particularly when the product WT of the counting time T and the bandwidth W of $\Gamma(\omega)$ is large. The method of saddlepoint integration provides much greater efficiency in calculating the counting distribution.

When the light has a Lorentz spectral density,

$$\Gamma(\omega) = \frac{2\mu G(0)}{\omega^2+\mu^2}, \qquad \gamma(\tau) = e^{-\mu|\tau|}, \tag{13.12}$$

the Fredholm determinant has the well-known form [24]

$$D(\xi) = e^{-m}[(g+1)^2 e^{mg} - (g-1)^2 e^{-mg}]/(4g),$$

$$g = (1+2\xi/m)^{1/2}, \quad \xi = n_0(1-z), \quad m = \mu T. \tag{13.13}$$

If the signal is a sinusoid of constant amplitude and with a frequency displaced from $\Omega$ by $\Delta$, as we have shown, the p.g.f. $h(z)$ is [25]

$$h(z) = [D(\xi)]^{-1} \exp\{n_s(z-1)[\frac{1+\delta^2}{g^2+\delta^2} + \frac{4\xi\{(g+1(g-\delta^2)e^{mg} - (g-1)(g+\delta^2)e^{-mg} - 2g[(1-\delta^2)\cos m\delta - 2\delta \sin m\delta]\}}{m^2(g^2+\delta^2)^2[(g+1)^2e^{mg} - (g-1)^2e^{-mg}]}]\} \tag{13.14}$$

with $\delta = \Delta/\mu$ and the rest of the notation as in (13.13). After putting this into the integrals (9.4) and (9.5) we have computed the complementary cumulative distribution $q_k^+$ by evaluating the integrals numerically along a parabolic contour passing through the appropriate saddlepoint. Even for values of k of the order of thousands, accuracy of seven significant figures was attained by fewer than twenty steps of numerical integration.

For more complicated spectra $\Gamma(\omega)$ the p.g.f. $h(z)$ cannot be written down in closed form. It can be obtained numerically at points on the contour of integration, however, from the alternative expression [25]

$$h(z) = [D[\xi)]^{-1} \times \exp\{n_s(z-1)\int_0^T [\tilde{\sigma}^*(\tau;\xi^*)-\sigma^*(\tau)][\tilde{\sigma}(\tau;\xi)-\sigma(\tau)]d\tau\} \tag{13.15}$$

where

$$\tilde{\sigma}(\tau;\xi) = \int_0^\tau \bar{\psi}(\tau,u;\xi)\sigma(u)du \tag{13.16}$$

and $\bar{\psi}(\tau;u;\xi) = \psi(\tau,u;\xi;\tau)$ is the solution of the integral equation

$$\bar{\psi}(\tau,u;\xi) + \xi T^{-1}\int_0^{\tau}\bar{\psi}(\tau,v;\xi)\gamma(v-u)dv = \xi T^{-1}\gamma(\tau-u),$$

$$0 \le u \le \tau \le T. \tag{13.17}$$

In terms of this function the Fredholm determinant is given by [24]

$$D(\xi) = \exp\Big[\int_0^{T}\bar{\psi}(\tau,\tau;\xi)d\tau\Big]. \tag{13.18}$$

The function $\bar{\psi}(\tau,u;\xi)$ is the kernel of the minimum-mean-square-error causal estimator of the process $(\xi/T)^{1/2}V_b(t)$ in the presence of circular-complex white Gaussian noise with unit spectral density provided $\xi$ is real and positive. As such it can be computed by solving Kalman-Bucy differential equations as in (5.18) - (5.23) whenever one can establish a state-space model for generating $V_b(t)$ from white noise. Indeed, the procedures for determining the distribution of the average power of a Gaussian random process, described in Sec. 6, can be applied to evaluating the terms in h(z) in (13.15). In particular, the Fredholm determinant $D(\xi)$ can be expressed by the quotient of determinants in (6.9) when the spectral density $\Gamma(\omega)$ in (13.4) is a rational function of the frequency, like $\Phi(\omega)$ in (6.5). Equation (6.8) for the $\beta_k$'s appearing in (6.9) is now

$$1 + \xi T^{-1}\tilde{\Gamma}(-ip) = 0, \qquad \xi = n_0(1-z), \tag{13.19}$$

with $\tilde{\Gamma}(\omega) = \Gamma(\omega)/G(0)$ the Fourier transform of $\gamma(\tau)$ defined in (13.9). The form in (6.9) enables the integrands of (9.4) and (9.5) for the cumulative distribution of the number of photoelectron counts and its complement to be computed easily at the points on the contour of integration in the complex plane. In part (b) of this section, this method is applied to light with a spectral density composed of two overlapping Lorentz spectra, as in (6.5) with n = 2.

When the product WT of the counting time T and the bandwidth W of the

incoherent light is large, one can utilize the so-called "Toeplitz approximation" to write the p.g.f. as [25]

$$h(z) \cong \exp\{n_s(z-1)\int_{-\infty}^{\infty} \frac{|\Sigma(\omega)|^2}{1+\xi T^{-1}\tilde{\Gamma}(\omega)} \frac{d\omega}{2\pi} - T\int_{-\infty}^{\infty} \ln[1+\xi T^{-1}\tilde{\Gamma}(\omega)]d\omega/2\pi\},$$

$$\tilde{\Gamma}(\omega) = \Gamma(\omega)/G(0), \quad \Sigma(\omega) = \int_{-\infty}^{\infty} \sigma(t)e^{-i\omega t}dt, \quad \xi = n_0(1-z). \quad (13.20)$$

This can be substituted into (9.4) or (9.5) for numerical integration to determine the cumulative distribution of the number of photoelectrons approximately. For incident light with a Lorentz spectral density the result has been found quite close to the true distribution yielded by (13.14) for a time-bandwidth product $m = \mu T$ as low as [25].

(b) Bimodal Spectral Density (V. Staggs)

(i) Introduction

In the detection of incoherent narrowband light by counting photoelectrons, the counting statistics are specified completely by the Fredholm determinant, if one has a way of inverting the probability generating function for the number of photoelectrons. From [25] and (13.7), in the absence of a coherent light signal, the probability generating function of the number of photoelectrons is

$$h(z) = [D(x)]^{-1}, \qquad x = \eta PT(1-z),$$

where $\eta$ is the quantum efficiency divided by $h\nu$, P is the power in the spectrum, and T is the counting interval. The probabilities

$$Q_k^{+} = \sum_{l=k}^{\infty} P_l \qquad \text{and} \qquad Q_k^{-} = 1 - Q_k^{+}$$

can be obtained by a numerical contour integration involving h(z). For a spectrum consisting of a linear combination of Lorentz spectra, the function h(z) can be computed by using the matrix methods described in Section 6. Here we shall describe a numerical procedure written in FORTRAN to find $Q_k^+$ and $Q_k^-$ by the matrix method for Lorentz spectra.

This numerical procedure, named FRED, was compared with known methods in the case of a single Lorentz spectrum in order to test its accuracy. Furthermore, spectra consisting of a sum of two Lorentz spectra were used to explore cases where previously known techniques do not apply or are inefficient. In particular, the FRED algorithm can compute accurate results when the spectrum is bimodal, the counting time is short, and one examines large values of k where $Q_k^+$ is small. This is a regime where earlier approximations are inaccurate.

(ii) Description of the algorithm

The fundamental purpose of the FORTRAN program FRED is to mechanize the matrix procedure given in Section 6. The Fredholm-determinant algorithm is then used to perform a numerical contour integration for the computation of $Q_k^+$ or $Q_k^-$. An important secondary aspect of generating the FRED program was to be alert to the numerical conditioning of the various steps involved, and to take appropriate action to keep the results robust against roundoff error. The following is an overview of the numerical approach.

A. Fredholm Determinant

The spectrum of the narrowband process n(t) is expressed as

$$\Phi(\omega) = 2 \sum_{m=1}^{n} \frac{f_m \mu_m'}{(\omega - i\mu_m^*)(\omega + i\mu_m)},$$

as in (6.5), except that we have taken $g_m \equiv 0$. Here $\mu_m = \mu_m' + i\mu_m''$, or equivalently,

$$\Phi(\omega) = 2\sum_{m=1}^{n} \frac{f_m \mu_m'}{[(\omega-\mu_m'')^2 + \mu_m'^2]},$$

where $\mu_m''$ is the frequency offset of a Lorentz spectrum with width parameter $\mu_m'$ and power $f_m$. The solution of the integral equation for the Fredholm determinant involves finding the 2n roots $\beta_k$ of the equation

$$1 + \frac{z}{T}\Phi(-ip) = 0, \qquad p = \beta_1, \beta_2 \cdots, \beta_{2n}.$$

This is accomplished by calling subroutine FILPAR to fill the array P of coefficients of the polynomial numerator of the above equation, and then using IMSL subroutine ZCPOLY to find the roots p. Since the roots must be ordered so that $\beta_1, \ldots, \beta_n$ lie on the branches of the root locus originating at the poles $\mu_m$ of $\Phi(-ip)$ having positive real parts, a sorting procedure is applied after the roots are found.

Using the quantities $\beta_1, \beta_2, \ldots, \beta_{2n}, \mu_1, \mu_2, \ldots, \mu_{2n}$, and T, the matrices $\underset{\sim}{B}_1$, $\underset{\sim}{B}_2$, $\underset{\sim}{C}_1$, $\underset{\sim}{C}_2$, $\underset{\sim}{D}_1$, $\underset{\sim}{D}_2$, and $\underset{\sim}{M}^{*-1}$ are generated, and the Fredholm determinant is evaluated using (6.9),

$$D(z) = \frac{\det(\underset{\sim}{D}_2^{-1}\underset{\sim}{M}^{*-1}) \det(\underset{\sim}{C}_1 - \underset{\sim}{B}_2\underset{\sim}{D}_2\underset{\sim}{C}_2^{-1}\underset{\sim}{B}_1\underset{\sim}{D}_1^{-1})}{\det(\underset{\sim}{C}_1 - \underset{\sim}{B}_2\underset{\sim}{C}_2^{-1}\underset{\sim}{B}_1)}.$$

Within subroutine GETFRD, which computes D(z), the two determinants in the numerator, TERM1 and TERM2, and the denominator, TERM3, are computed separately. The quotient TERM2/TERM3 is computed first since its terms are of the same order of magnitude, in order to avoid overflow or underflow.

B. Parameters of Integration

In order to perform the numerical contour integration, one must know the parameters of the osculatory parabola which approximates the path of steepest descent as described in Sec. 1(c) and in [5]. As in (9.4) and (9.5), the tail

probabilities are

$$Q_k^- = \int_{C^-} \frac{z^{-k}\, h(z)}{1 - z} \frac{dz}{2\pi i} \tag{13.21}$$

$$Q_k^+ = \int_{C^+} \frac{z^{-k}\, h(z)}{z - 1} \frac{dz}{2\pi i} \tag{13.22}$$

where $C^-$ is a parabola intersecting the real axis between the origin and the point (1.0, 0.0), and $C^+$ similarly intersects the real axis between (1.0, 0.0) and the nearest singularity of h(z) greater than (1.0, 0.0). One uses (13.21) when $k \leq \bar{n}_0 = nPT$ and (13.22) when $k > \bar{n}_0$.

The integration procedure starts by finding the first eigenvalue lying to the right of the point z = 1. Subroutine LAMBDA performs this search. It starts with a simple Newton iteration (the secant method) and then switches to a second-order extrapolation method using inverse interpolation with relaxation. There is a reason for this elaborateness. Determinants are found in subroutine GETFRD by calling the IMSL suroutinte LEQT1C, which is also used to solve systems of linear equations involving complex matrices. LEQT1C always performs an LU factorization of the coefficient matrix, and whenever the matrix is nearly singular, the factorization algorithm may attempt to divide by a very small pivot, sometimes resulting in a fatal error. Thus, it makes sense to find the first eigenvalue without actually evaluating the Fredholm determinant with that eigenvalue, which implies that one needs a powerful predictor such as the second-order technique. Furthermore, in order to keep the predictor from jumping immediately to the first eigenvalue $\lambda$, a relaxation is performed, whereby the next value of $\lambda$ generated is only part way between the predicted value and the previous value. In this way, a sequence of approximations $\bar{\lambda}_i$ is generated that stays to the left of $\lambda$, and reasonably far from it, but which converges to $\lambda$ in a way that permits one to generate a predicted $\bar{\lambda}$ that converges well. This avoids numerical problems in

LEQT1C, it guarantees that $\lambda$ is approached from the left and that one does not jump over it because of roundoff error and erroneously deliver the next eigenvalue, and it converges adequately fast.

Once $\lambda$ is found, one can compute the quantities $x_0$, $\kappa$, and $\Psi''(x_0)$, where as in (9.7)

$$\Psi(z) = \ln [\pm z^{-k} h(z)/(1-z)],$$

i.e., $\Psi$ is the complex natural logarithm of the integrand, $\kappa$ is the curvature of the osculatory parabola as in (9.8), and $x_0$ solves

$$\Psi'(x_0) = 0. \tag{13.23}$$

Subroutine GETPAR gets the parameters of integration listed above. It solves (13.23) by using several iterations of the golden-section algorithm [2], and then it switches to a second-order Newton's method. The behavior of the integration procedure was found to depend somewhat sensitively on the accuracy of $x_0$, thus necessitating the extra elaboration.

Once $x_0$ is found, the second derivative $\Psi''(x_0)$ and curvature $\kappa$ are determined by taking differences. The curvature $\kappa$ is found directly from a difference formula assuming local second-order behavior (see [5], eq. 57). The differences in the independent variable are taken along the imaginary direction in order to avoid complications arising from the proximity of the point (1.0, 0.0), the first eigenvalue, and any nearby eigenvalues. One has the capability in GETPAR of successively refining $\Delta y$ and making new predictions of $\kappa$ and $\Psi''(x_0)$ by extrapolation to $\Delta y = 0$. However, the zeroth iteration has proved adequate thus far.

(iii) *The integration procedure*

The parabola approximating the path of steepest descent is parameterized by

using y, the distance from the real axis, as the parameter. Thus, one has

$$z(y) = x_0 + \frac{1}{2}\kappa y^2 + iy,$$

since

$$x(y) = x_0 + \frac{1}{2}\kappa y^2$$

on the osculatory parabola. One capitalizes on the fact that because the values of the integrand above Im z = 0 are the complex conjugates of those below, one needs only to follow the contour for positive y as in (9.10). The integration is by the trapezoidal rule, which is rewritten as a quadrature formula in terms of $y_k = k\Delta y$, and as in (9.11),

$$\Delta y = [\Psi''(z_0)]^{-1/2}.$$

Finally, one has

$$Q_k^{\pm} = \frac{1}{\pi}\left\{\frac{1}{2} f(z_0)(1 - i\frac{\kappa}{2}\Delta y)\Delta y + \sum_{j=1}^{\infty} f(z_j)(1-i\kappa y_j)\Delta y\right\}$$

with $f(z) = \exp[\Psi(z)]$. The summation is stopped when the absolute value of the summand falls below epsilon times the accumulated sum, where epsilon is a user-input variable of the order of $10^{-8}$. The integral is refined by repeating it for successively halved values of $\Delta y$. Three values of $Q_k^+$ and $Q_k^-$ are printed to permit confidence in the convergence of the integral.

(iv) Validity check

The algorithm of Bédard [35] was used to compute the probabilities $p_k$ and thus $Q_k^-$ by summation as in (9.1), and $Q_k^+ = 1-Q_k^-$, for a single Lorentz spectrum. The FRED algorithm was reduced nearly to a single spectrum by choosing

a very small power for the second peak and by displacing it only slightly from the first. Table 13.1 presents the results, which agree within the ability of FRED to simulate a single spectrum. Figure 13.1 is a plot of Table 13.1, also showing the results of the saddlepoint approximation (see [5], eqs. (48) and (49)), which is not guaranteed to be accurate near the mean. The results of the Fredholm-determinant method fall so close to those of Bédard that it is not possible to separate them on a plot.

One can image a spectrum consisting of two displaced Lorentz spectra whose width parameters are permitted to approach zero. The spectra thus become delta functions, and this permits one to solve the integral equation for D(z) easily, and thus to obtain explicit expressions for $Q_k^+$ and $Q_k^-$. If one imposes the condition $f_1T \neq f_2T$, and insists that $\mu_1 T = 2\pi k_1$, $\mu_2 T = 2\pi k_2$, $k_1$ and $k_2$ being distinct integers, then the formulas are

$$\begin{aligned} Q_k^+ &= \sum_{l=k}^{\infty} p_l = \frac{1}{a-b}\left\{a\left(\frac{a}{1+a}\right)^k - b\left(\frac{b}{1+b}\right)^k\right\} \\ Q_k^- &= 1 - Q_k^+ \\ a &= \bar{n}_{01} = nf_1T \\ b &= \bar{n}_{02} = nf_2T. \end{aligned} \tag{13.24}$$

A comparison of results from this formula and from an appropriately chosen spectrum in program FRED is given in Table 13.2. Here the agreement is not so precise as in the previous example, since too small a value of $\mu_1 = \mu_2$ would cause problems in the algorithm. However, it is clear that there is no serious disagreement.

(v) New results

In this section, we let $\beta = \mu_1'$ be the frequency offset of the second Lorentz spectrum relative to the first, and $\mu_1$ and $\mu_2$ be the width parameters of

Table 13.1

Counting statistic $Q_k^+$ for a single Lorentz spectrum, $\mu = 10$, $\bar{n}_0 = 5$, $T = 1.0$, calculated by the Bédard algorithm, the Fredholm determinant algorithm, and the saddlepoint approximation.

| k | $Q_k^+$, Bédard | $Q_k^+$, Fred | $Q_k^+$, Saddlepoint approx'n |
|---|---|---|---|
| 2 | 0.92939535 | 0.92939536 | 0.93404541 |
| 4 | 0.68036006 | 0.68036009 | 0.71836016 |
| 6 | 0.37859723 | 0.37859724 | 0.33516088 |
| 8 | 0.16831838 | 0.16831839 | 0.15129038 |
| 10 | 6.3351307E-2 | 6.3351306E-2 | 5.7515912E-2 |
| 12 | 2.1133291E-2 | 2.1133289E-2 | 1.9315245E-2 |
| 14 | 6.4594820E-3 | 6.4594811E-3 | 5.9339735E-3 |
| 16 | 1.8521763E-3 | 1.8521759E-3 | 1.7090362E-3 |
| 18 | 5.0661615E-4 | 5.0661598E-4 | 4.6941913E-4 |
| 20 | 1.3377483E-4 | 1.3377477E-4 | 1.2446659E-4 |

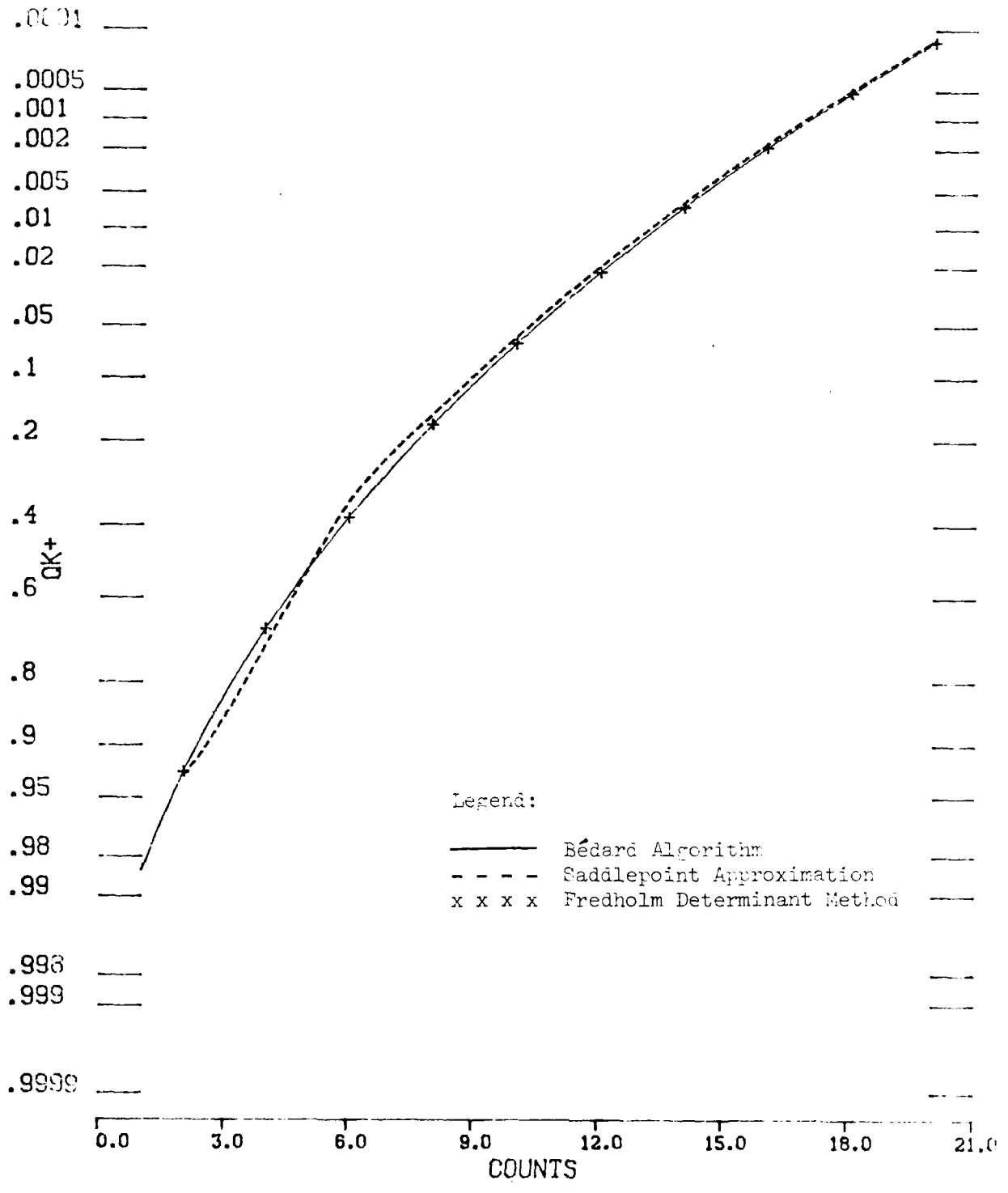


Figure 13.1 Plot of $Q_k^+$ vs counts, k, as computed by the Bédard algorithm, the Fredholm determinant method, and the saddlepoint approximation. Here, $\mu = 10$, $T = 1.0$, and $n_0 = 5$. For the Fredholm determinant method, $\mu_1 = \mu_2 = 10$, $f_1/f_2 = 999$.

Table 13.2

Counting statistic $Q_k^+$ for two discrete Lorentz spectra, approximated in FRED by $\mu_1' = \mu_2' = 0.01$, $\mu_2'' = 10$, $\bar{n}_0 = 5$, $T = 1.0$, $a = 3.75$, $b = 1.25$.

| k | $Q_k^+$, eq. (13.24) | $Q_k^+$, FRED |
|---|---|---|
| 2 | 0.7805820 | 0.77919718 |
| 4 | 0.5350658 | 0.53318556 |
| 6 | 0.3484754 | 0.34739919 |
| 8 | 0.2218190 | 0.22166426 |
| 10 | 0.1396803 | 0.14011555 |
| 12 | 8.749901E-2 | 8.8187526E-2 |
| 14 | 5.467138E-2 | 5.5393858E-2 |
| 16 | 3.411693E-2 | 3.4762644E-2 |
| 18 | 2.127697E-2 | 2.1805994E-2 |
| 20 | 1.326526E-2 | 1.3675749E-2 |

AD-A175 002 CALCULATION OF CUMULATIVE DISTRIBUTIONS AND DETECTION PROBABILITIES IN CO.. (U) CALIFORNIA UNIV SAN DIEGO LA JOLLA DEPT OF ELECTRICAL ENGINEE.. C W HELSTROM 2/2

UNCLASSIFIED 31 MAR 86 AFOSR-TR-86-2183 AFOSR-82-0343 F/G 9/4 NL

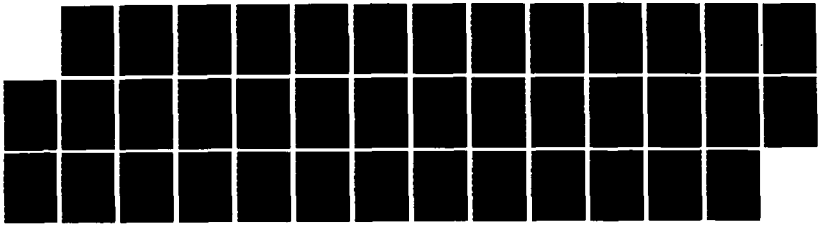

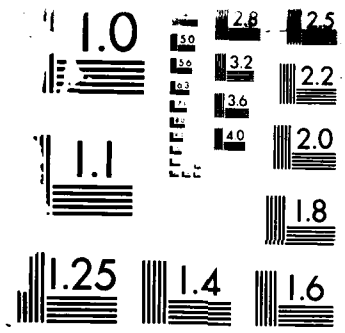


RESOLUTION TEST CHART

the spectra. Figure 13.2 shows the plot of $Q_k^+$ versus k for two spectra with $\mu_1 = \mu_2 = 10$, $\beta = 50$, and values of $f_2/f_1$ equal to 1, 5, and 10. When $f_1 = f_2$, the spectrum is maximally bimodal, and as $f_2/f_1$ increases it becomes unimodal, so that the curve approaches that of Figure 13.1. The curves diverge perceptibly for large values of k. Figure 13.3 is the same type of plot, but here we let $\mu_1 = \mu_2 = 1.0$, $\beta = 5.0$, $T = 1.0$, and $f_2/f_1 = 1$, 5, and 10. This is a case where $\mu_1 T = \mu_2 T$ is small. The curves have the same general behavior. Since the vertical axis is drawn on a probability scale, a Gaussian random variable would plot as a straight line, and obviously the variable $Q_k^+$ is not Gaussian. Actually, these plots should be staircase functions continuous from the right at the integers, but they are represented here as curved lines for simplicity.

Figures 13.4 and 13.5 are cases where everything about the two Lorentz spectra is fixed except their displacement $\beta$ in radian frequency. We let $\beta/\mu_1 =$ .001, 1.0, and 10.0 on each figure. For Figure 13.4, $\mu_1 = \mu_2 = 10$, $f_1 = f_2 = 0.5$, $T = 1.0$, and $\bar{n}_0 = 5$. For Figure 13.5, we have $\mu_1 = \mu_2 = 1.0$, and otherwise the variables are the same. In these cases, the increasingly bimodal character increases $Q_k^+$ for a given k when $k > \bar{n}_0$.

The coding in program FRED is general in the sense that it does not care how many Lorentz spectra are combined to make up the power spectral density. Only subroutine FILPAR and some dimension statements need to be changed to handle an arbitrary number of spectra. Thus the matrix approach to finding the Fredholm determinant and the counting statistics of incoherent narrowband light can be applied with program FRED to a nearly arbitrary power spectral density.

(c) Coherent plus Chaotic Light

When the incident light consists of a finite number of sinusoidal components in the presence of Gaussian background light with a rational spectral density, the moment-generating function h(z) in (13.7) can be expressed in terms of

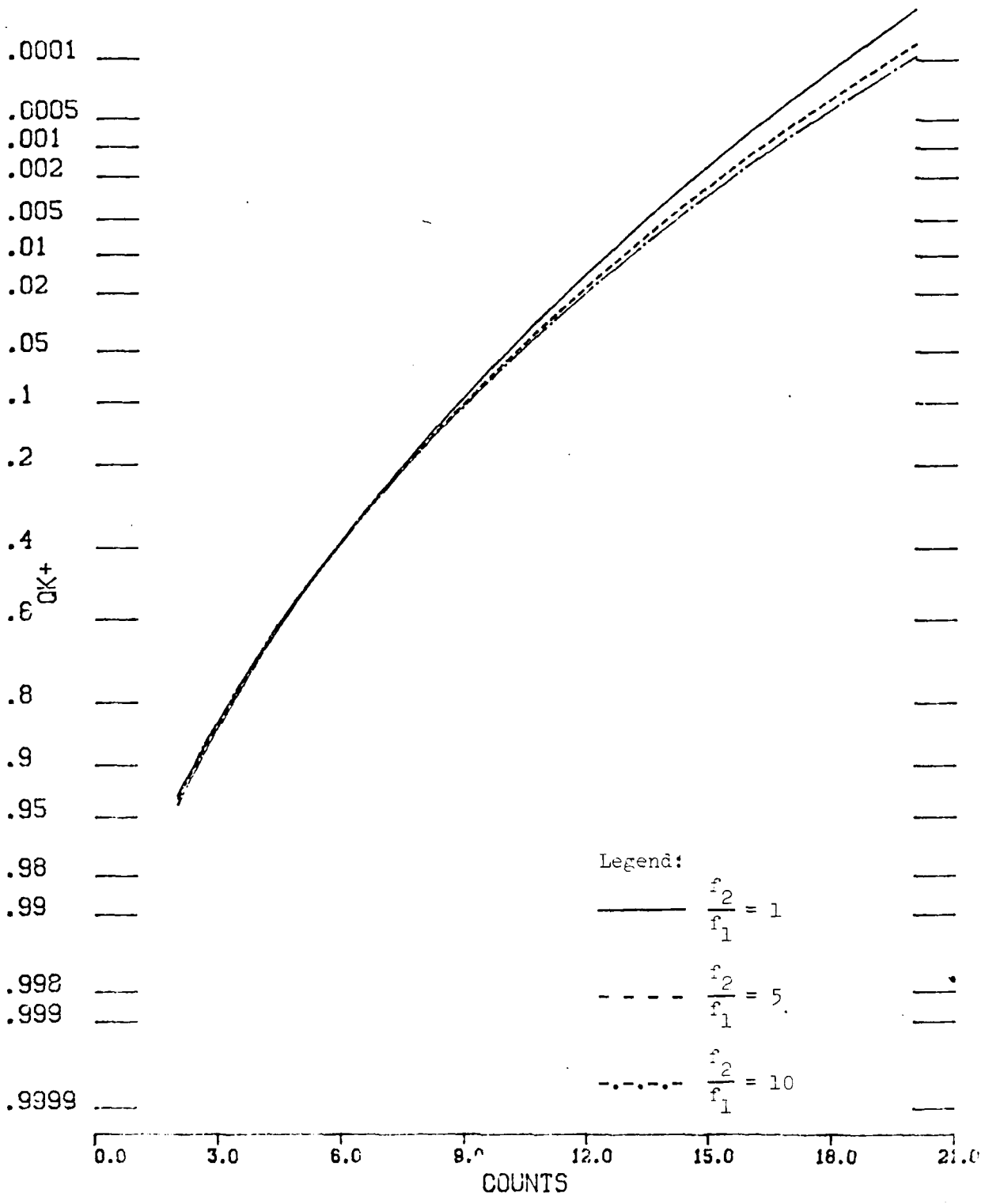


Figure 13.2 Plot of $Q_k^+$ vs. counts, k, for different relative powers of two component Lorentz spectra, computed by the Fredholm determinant method. Here, $\mu_1 = \mu_2 = 10$, $\beta = 50$, $T = 1.0$, $\bar{n}_0 = 5$, and $f_2/f_1 = 1$, 5, and 10.

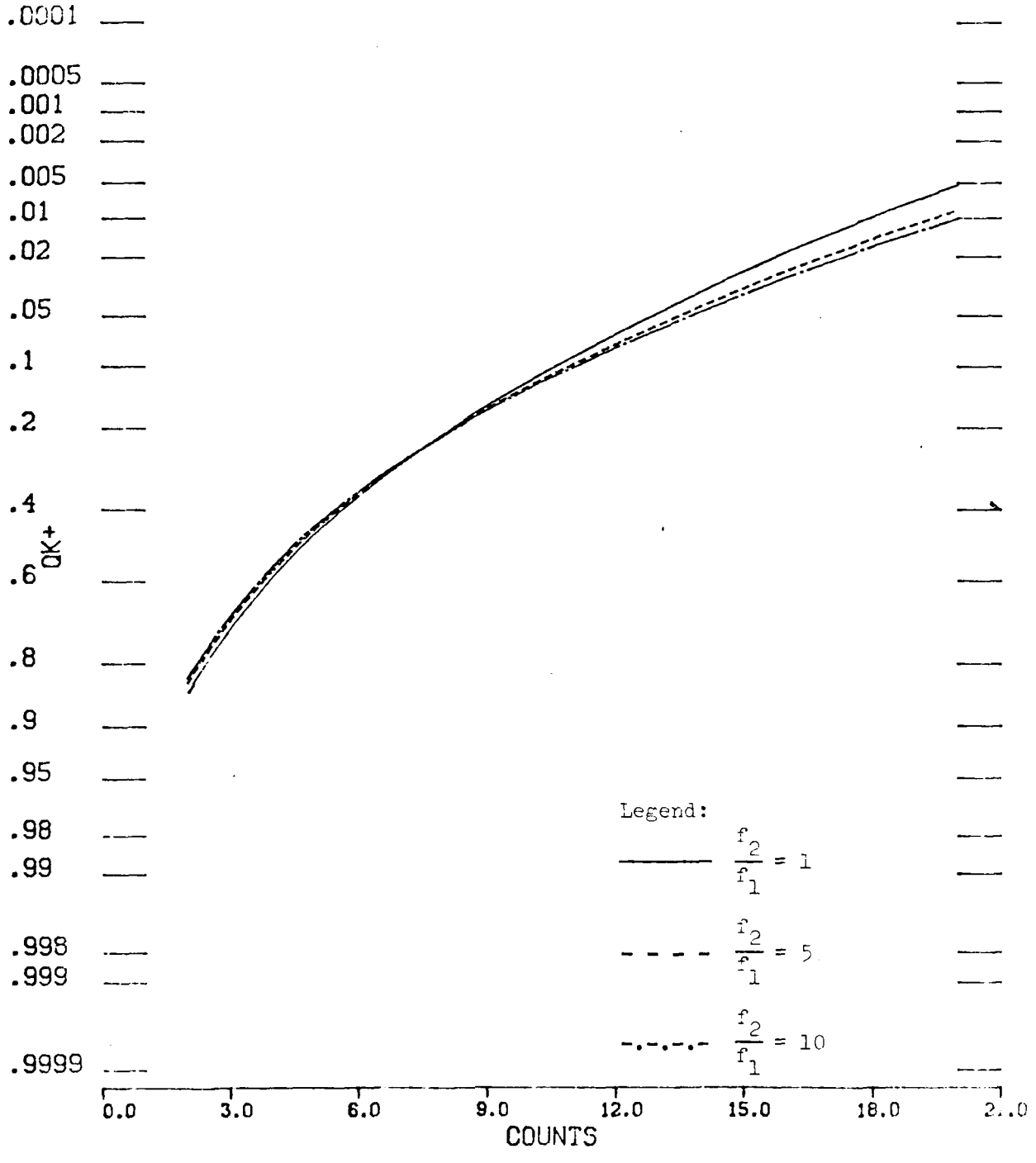


Figure 13.3 Plot of $Q_k^+$ vs. counts, k, for different relative powers of two component Lorentz spectra, computed by the Fredholm determinant method. Here, $\mu_1 = \mu_2 = 1$, $\beta = 5$, $T = 1.0$, $\bar{n}_0 = 5$, and $f_2/f_1 = 1$, 5, and 10.

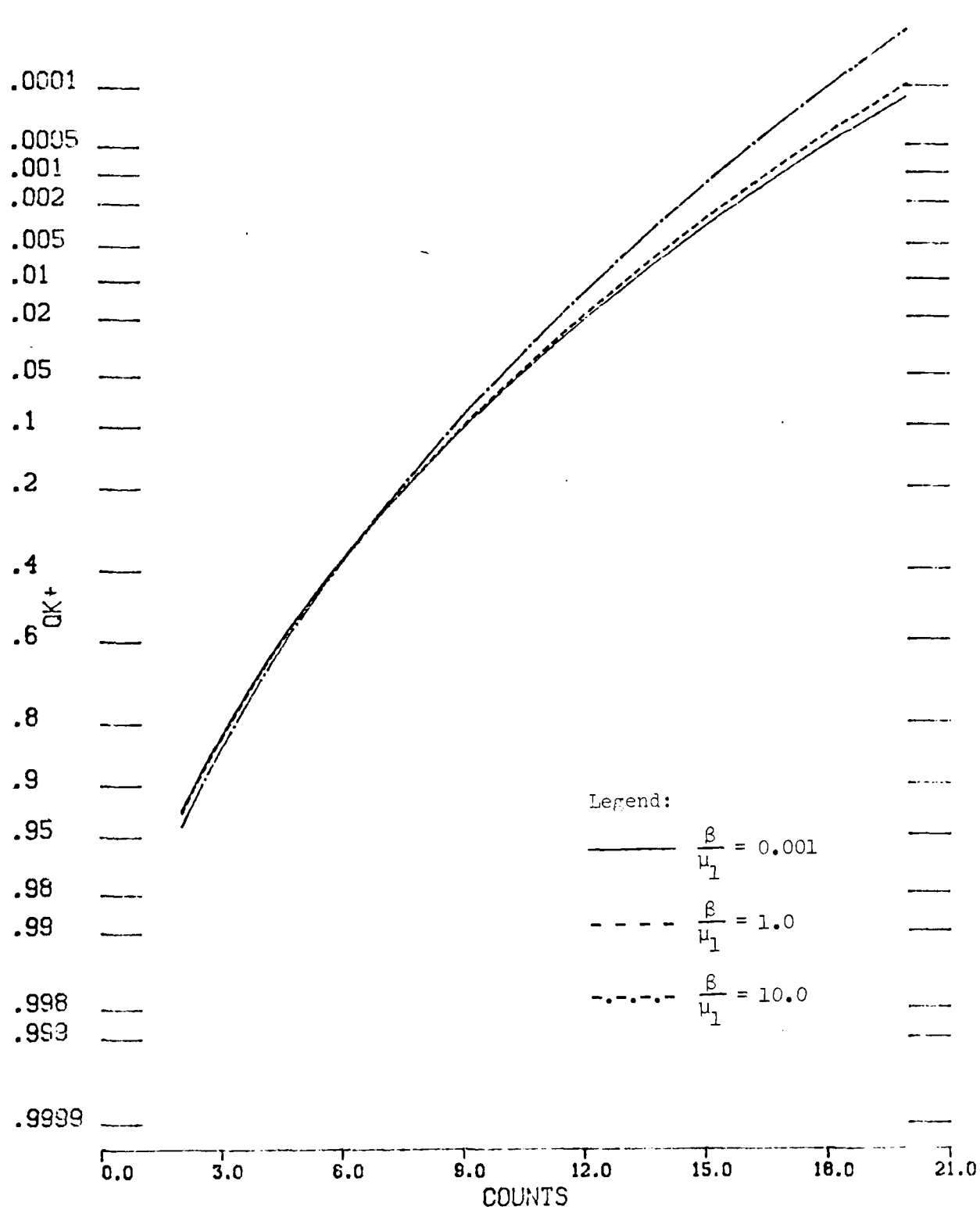


Figure 13.4 Plot of $Q_k^+$ vs. counts, k, for different values of frequency of separation of two component Lorentz spectra, computed by the Fredholm determinant method. Here, $\mu_1 = \mu_2 = 10$, $f_1 = f_2 = 0.5$, $T = 1.0$, $\bar{n}_0 = 5$, and $\beta/\mu_1 = 0.001$, 1.0, and 10.0.

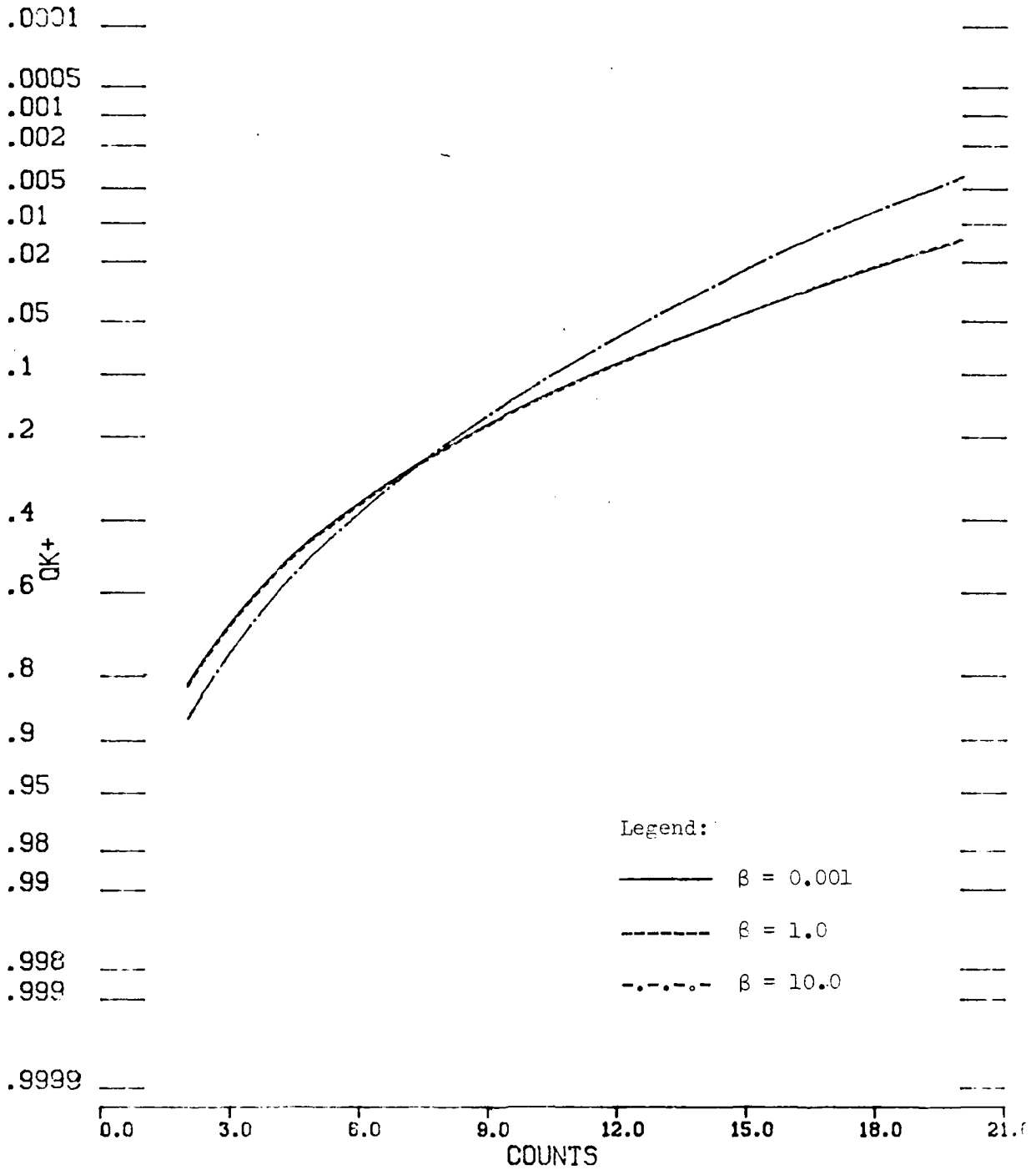


Figure 13.5 Plot of $Q_k^+$ vs. counts, k, for different values of frequency of separation of two component Lorentz spectra, computed by the Fredholm determinant method. Here, $\mu_1 = \mu_2 = 1.0$, $f_1 = f_2 = 0.5$, $T = 1.0$, $\bar{n}_0 = 5$, and $\beta/\mu_1 = 0.001$, 1.0, and 10.0.

determinants by an extension of the analysis in Section 6. The complex envelope of the normalized signal is taken to have the form

$$\sigma(t) = T^{-\frac{1}{2}} \sum_r \alpha_r \exp(i\nu_r t), \qquad 0 < t < T, \tag{13.25}$$

in which the $\nu_r$ are the angular frequencies of the coherent components of the light and the $\alpha_r$ are their complex amplitudes. The normalized spectral density $\tilde{\Gamma}(\omega)$ of the background light can be written in the form

$$\tilde{\Gamma}(\omega) = 2 \sum_{k=1}^{n} \frac{f_k \mu_k' + g_k(\omega - \mu_k'')}{(\omega - \mu_k'')^2 + \mu_k'^2}$$

as in (6.5). Its normalized autocovariance function is then

$$\begin{aligned} \gamma(t-u) &= \sum_{k=1}^{n} \phi_k \exp[-\mu_k^*(t-u)], \qquad t > u, \\ &= \sum_{k=1}^{n} \phi_k^* \exp[\mu_k(t-u)], \qquad t < u, \end{aligned} \tag{13.26}$$

with $\phi_k = f_k + ig_k$, $\mu_k = \mu_k' + i\mu_k''$. The spectral density $\tilde{\Gamma}(\omega)$ is assumed to have only simple poles.

We first obtain an expression for the square bracket multiplying $n_s(z-1)$ in (13.7); we denote it by J. In terms of the eigenfunctions and eigenvalues of the integral equation (13.9), it is [25]

$$\begin{aligned} J(\xi) &= \sum_k \frac{|\sigma_k|^2}{1 + \xi\lambda_k}, \quad \sigma_k = \int_0^T f_k^*(t)\, \sigma(t)\, dt, \\ &\sum_k |\sigma_k|^2 = 1, \qquad \xi = n_0(1-z). \end{aligned} \tag{13.27}$$

Now define the signal $q(t;\xi)$ as the solution of the integral equation

$$\sigma(t) = q(t;\xi) + \xi T^{-1} \int_0^T \gamma(t-u)\, q(u;\xi)\, du, \qquad 0 < t < T. \tag{13.28}$$

It is not difficult to show from the orthonormality of the eigenfunctions $f_k(t)$ of (13.9) that

$$J(\xi) = \int_0^T \sigma^*(t)\, q(t;\xi)\, dt. \tag{13.29}$$

The integral equation (13.28) has a solution of the form

$$q(t;\xi) = q_\infty(t;\xi) + \sum_{k=1}^{2n} d_k \exp(\beta_k t), \tag{13.30}$$

in which as in Sec. 6 the $\beta_k$'s are the roots of (13.19), and

$$q_\infty(t;\xi) = T^{-1/2} \sum_r \frac{\alpha_r \exp(iv_r t)}{\Phi(v_r)}, \qquad \Phi(v) = 1 + \xi T^{-1}\, \tilde{\Gamma}(v). \tag{13.31}$$

Substituting (13.30) into (13.28), one finds that the coefficients $d_k$ have the form

$$d_k = T^{-1/2} \sum_r \alpha_r d_{kr} \tag{13.32}$$

with the $d_{kr}$ the solutions of the 2n linear simultaneous equations

$$\sum_{k=1}^{2n} \frac{d_{kr} \exp(\beta_k T)}{\beta_k - \mu_m} = \frac{\exp(iv_r T)}{\Phi(v_r)(\mu_m - iv_r)}, \qquad 1 \le m \le n,$$

$$\sum_{k=1}^{2n} \frac{d_{kr}}{\beta_k - \mu_m} = \frac{1}{\Phi(v_r)(\mu_m - iv_r)}, \qquad n+1 \le m \le 2n, \tag{13.33}$$

in which $\mu_m = -\mu^*_{m-n}$, $n+1 \le m \le 2n$. Writing the right-hand terms of these equations as $[\phi(v_r)]^{-1} f_{mr}$, $1 \le m \le 2n$, denoting by $G_{mk}$ the elements of the $2n \times 2n$ matrix $\underline{G}$ of the coefficients of the unknowns $d_{kr}$ on the left, we express these equations as

$$\sum_{k=1}^{2n} G_{mk}\, d_{kr} = [\phi(v_r)]^{-1} f_{mr}, \qquad 1 \le m \le 2n, \tag{13.34}$$

and their solutions are

$$d_{kr} = [\phi(v_r)]^{-1} \sum_{m=1}^{2n} g_{km} f_{mr}, \qquad 1 \le k \le 2n, \tag{13.35}$$

where the $g_{km}$ are the elements of the inverse matrix $\underline{G}^{-1}$.

If we now substitute (13.25), (13.30), and (13.31) into (13.29), we find

$$J(\xi) = J_1 + J_2 \tag{13.36}$$

with

$$J_1 = \sum_r \sum_s \frac{\alpha_s^* \alpha_r}{\phi(v_r)} \int_0^T \exp[i(v_r - v_s)t]\, dt/T = \sum_r \sum_s \frac{\alpha_s^* \alpha_r}{\phi(v_r)} J_{sr},$$

$$J_{rr} = 1, \qquad J_{sr} = \frac{\exp[i(v_r - v_s)T] - 1}{i(v_r - v_s)T}, \qquad s \ne r, \tag{13.37}$$

and

$$J_2 = \sum_r \alpha_r \sum_s \alpha_s^* \sum_{k=1}^{2n} d_{kr} \int_0^T \exp[(\beta_k - iv_s)t]\, dt/T$$

$$= \sum_r \sum_s \alpha_s^* \alpha_r \sum_{k=1}^{2n} e_{sk} d_{kr},$$

$$e_{sk} = \frac{\exp[(\beta_k - iv_s)T] - 1}{(\beta_k - iv_s)T}. \tag{13.38}$$

With (13.35) this becomes

$$J_2 = \sum_r \sum_s \frac{\alpha_s^* \alpha_r}{\phi(v_r)} \sum_{k=1}^{2n} \sum_{m=1}^{2n} e_{sk} g_{km} f_{mr} = \sum_{k=1}^{2n} \sum_{m=1}^{2n} E_k g_{km} F_m,$$

$$E_k = \sum_s \alpha_s^* e_{sk}, \qquad F_m = \sum_r \alpha_r f_{mr}/\phi(v_r). \tag{13.39}$$

By defining the $(n+1) \times (n+1)$ augmented matrix $\underline{\bar{G}}$ as

$$\underline{\bar{G}} = \begin{bmatrix} 0 & \underline{E} \\ \underline{F} & \underline{G} \end{bmatrix}, \tag{13.40}$$

where $\underline{E}$ is the $2n$-element row vector of the $E_k$'s and $\underline{F}$ is the $2n$-element column vector of the $F_m$'s, we can write

$$J_2 = -\det \underline{\bar{G}}. \tag{13.41}$$

The Fredholm determinant $D(z)$ in (13.7) is

$$D(z) = \exp\left(-\sum_{k=1}^{2n} \beta_k T + \sum_{m=1}^{n} \mu_m^* T\right) \frac{\det \underline{G}(T)}{\det \underline{G}(0)}, \tag{13.42}$$

where $\underline{G}(0)$ is the $2n \times 2n$ matrix obtained by setting $T = 0$ in the elements of the matrix $\underline{G} = \underline{G}(T)$. The probability-generating function of the photoelectron counts is, as in (13.7),

$$h(z) = [D(z)]^{-1} \exp[n_s(z-1)](J_1 + J_2)], \qquad \xi = n_0(1-z); \tag{13.43}$$

$J_1$ and $J_2$ depend on $\xi$ through the $\beta_k$'s and $\phi(v)$ defined in (13.31) and (13.19); $\phi(-i\beta_k) = 0$, $1 \le k \le 2n$.

For a single sinusoidal component, $\alpha_1 = 1$, $v_1 = v$, $J_1 = T/\phi(v)$,

$$E_k = \frac{\exp[(\beta_k - iv)T] - 1}{(\beta_k - iv)T},$$

$$F_k = \frac{e^{ivT}}{\mu_k - iv}, \qquad 1 \le k \le n,$$

$$F_k = \frac{1}{\mu_k - iv}, \qquad n+1 \le k \le 2n, \qquad \mu_k = \mu^*_{k-n}. \tag{13.44}$$

The expression in (13.14) is a special case of (13.43) and (13.44) for n = 1.

This formulation enables the probability generating function h(z) to be evaluated entirely by finite operations for all values of z involved both in locating the saddlepoints of the integrands of (9.4) and (9.5) and in evaluating those integrals for the cumulative probabilities by numerical quadrature in the complex plane. The evaluation entails solving the algebraic equation of degree 2n with complex coefficients arising from (13.19) and calculating the determinants in (13.41) and (13.42); standard computer routines can be employed. Any finite number of sinusoidal components can be handled.

If the coherent signal S(t) is a pulse confined to the counting interval (0, T), the complex amplitudes $\alpha_r$ in (13.25) can be determined by numerical Fourier transformation of the normalized signal $\sigma(t)$; a large enough number of Fourier components must be utilized to provide adequate accuracy in the cumulative distribution. The term $J_1$ in (13.37) and (13.43) becomes

$$J_1 = \int_{-\infty}^{\infty} \frac{|\Sigma(\omega)|^2}{\Phi(\omega)} \frac{d\omega}{2\pi}, \tag{13.45}$$

with $\Phi(\cdot)$ as in (13.31) and with $\Sigma(\omega)$ the Fourier transform of the normalized signal $\sigma(t)$; this is just the first integral in the Toeplitz approximation in (13.20). The terms $E_k$ and $F_m$ in (13.39) become

$$E_k = \int_0^T \sigma^*(t)\, \exp(\beta_k t)\, dt/T = T^{-1}(\Sigma(-i\beta_k^*))^*,$$

$$F_m = \int_{-\infty}^{\infty} \Sigma(\omega)\, \frac{[e^{i\omega T}]_m}{\Phi(\omega)(\mu_m - i\omega)}\, \frac{d\omega}{2\pi}, \qquad (13.46)$$

in which

$$[e^{i\omega T}]_m = e^{i\omega T}, \qquad 1 \leq m \leq n,$$

$$= 1, \qquad n+1 \leq m \leq 2n.$$

The details of applying these new methods to computing the photoelectron counting distribution remain to be elaborated.

## 14. Significance Probabilities for Rank Tests

The method of saddlepoint integration described in Sec. 9 has been applied to computing the distributions of the Wilcoxon signed-rank and ranksum statistics [49] and the Jonckheere statistic [50]. Tables of the distributions of the Wilcoxon statistics and of their percentage points take up a great many pages because of the numbers of parameters involved [49], and the distribution of the Jonckheere statistic, which is a generalization of the ranksum statistic and depends on even more parameters, seems to have been tabulated only for a few very small sample sizes [50]. Although recurrent relations exist whereby these distributions can be computed, the algorithms are extremely time-consuming and require extensive computer memory when the sample sizes are large. By saddlepoint integration one can compute the significance probabilities directly and accurately for sample sizes beyond those at which the recurrent algorithms become infeasible. The saddlepoint-integration method, furthermore, requires storing only a dozen or so numbers utilized in the computation , in contrast to the hundreds or thousands that may need to be stored in the recurrent computations.

### Signed-Rank Statistic

The one-sample Wilcoxon test, or "signed-rank test," decides between a null hypothesis $H_0$ that M independent data $x_1, x_2, \ldots, x_M$ possess a common distribution symmetrical about 0 and an alternative hypothesis $H_1$ that the data are stochastically larger. The data are first ordered according to their absolute values. If $r_i$ denotes the rank of $x_i$ in that ordering, one forms the statistic

$$W = \sum_{i=1}^{M} r_i \, U(x_i), \tag{14.1}$$

where $U(\cdot)$ is the unit step-function. When a given set of data yields a value $W_0'$ for this statistic, one quotes the significance probability

$$P = Pr\ (W \geq W_0' |\ H_0)$$

that a value of W as large as $W_0'$ or larger could occur under the null hypothesis, and one states that the null hypothesis is rejected at probability level P. Detailed explanations of this test and its two-sided extension can be found in texts on statistics.

Because the distribution of W under hypothesis $H_0$ is symmetric about its mean

$$\bar{W} = E(W |\ H_0) = M(M+1)/4, \tag{14.2}$$

this probability is the same as the probability

$$P = Pr\ (W \leq W_0 |\ H_0), \quad W_0 = \frac{1}{2} M(M+1) - W_0'.$$

We need, therefore, the cumulative distribution of W, which by (9.4) is given by the contour integral

$$q_k = Pr\ (W \leq k) = \int_C \frac{z^{-(k+1)}\ h(z)}{1 - z}\ \frac{dz}{2\pi i} \tag{14.3}$$

in terms of the p.g.f. h(z) of the signed-rank statistic [49]

$$h(z) = \prod_{j=1}^{M} \left(\frac{1 + z^j}{2}\right). \tag{14.4}$$

Here C is initially a circle concentric with the origin and of radius less than 1.

It has been found simplest to deform the contour C into a vertical straight

line through the saddlepoint $x_0$ of the integrand of (14.3) lying on the Re z-axis, $0 < x_0 < 1$, completed by the portion of the unit circle lying to the left of that straight line, whereupon

$$q_k = \mathrm{Re} \int_0^Y \frac{z^{-(k+1)}\, h(z)}{1 - z} \frac{dy}{\pi} + I_c, \qquad z = x_0 + iy, \qquad Y = (1-x_0^2)^{1/2}. \tag{14.5}$$

The second term

$$I_c = \int_{\theta_0}^{\pi} \prod_{j=1}^{M} \cos\left(\tfrac{1}{2} j\theta\right) \mathrm{Re}\left[\frac{\exp[i(\bar{W}-k)\theta]}{1-\exp(i\theta)}\right] \frac{d\theta}{\pi}, \quad \theta_0 = \cos^{-1} x_0, \tag{14.6}$$

represents the integral along the unit circle, on which $z = \exp(i\theta)$.

For the large values of M for which this method is intended, the term $I_c$ is neglibible, and sufficient accuracy is achieved by integrating only the first term in (14.5). The product of cosines in (14.6) possesses $M(M+1)/4$ zeros, some multiple, in $0 \le \theta \le \pi$. Between any pair of these zeros, which lie close together when M is large, the oscillatory integrand perforce remains very small, and the value of $I_c$ itself must be very small in comparison with the first term in (14.5). Our computations have borne out the insignificance of the term $I_c$ when M is greater than about 20, as manifested by the relative errors to be exhibited in Table 14.1.

The saddlepoint $x_0$ is the root of the equation

$$\psi'(x) = \sum_{j=1}^{M} \frac{j x^{j-1}}{1+x^j} - \frac{k+1}{x} - \frac{1}{x-1} = 0, \tag{14.7}$$

where

$$\psi(z) = \sum_{j=1}^{M} \ln\left(\frac{1 + z^j}{2}\right) - (k+1) \ln z - \ln(1-z) \tag{14.8}$$

is the phase of the integrand of (14.3). Equation (14.7) is quickly and conveniently solved by Newton's method, as in (1.16). The second derivative $\Psi''(x)$ in that algorithm is not needed to great accuracy and can be approximated by

$$\Psi''(x) \doteq \rho + (k+1)x^{-2} + (x-1)^{-2} \tag{14.9}$$

with

$$\rho = \text{Var } W - \bar{W} = M(M+1)(2M-5)/24. \tag{14.10}$$

This approximation derives from the first two terms of the series expansion

$$\ln h(z) = \bar{W}(z-1) + \tfrac{1}{2}\rho(z-1)^2 + \ldots \tag{14.11}$$

of the logarithm of the p.g.f. about the point $z = 1$. From this we also obtain a convenient starting value

$$x_0^{(0)} = 1 + \frac{k+1-\bar{W} - [(k+1-\bar{W})^2 + 4\rho]^{1/2}}{2\rho} \tag{14.12}$$

for the search for the saddlepoint.

In the numerical integration a convenient step size is

$$\Delta y = [\Psi''(x_0)]^{-1/2} \tag{14.13}$$

with $\Psi''(x_0)$ calculated from (14.9). One halts the numerical integration when the absolute value of the integrand falls below $\varepsilon\Delta y$ times the accumulated trapezoidal sum. For $M > 20$ this usually occurs before the point $z = x_0 + iy$ on the contour of integration of the first term of (14.5) reaches the unit circle at $y = Y$. One can repeat the numerical integration, halving the step size until the result converges in the number of significant figures desired.

In Table 14.1 we exhibit typical results of these computations in order to

Table 14.1

Signed Rank Statistic

| M | k | $q_k$ | Number of steps | Relative error |
|---|---|---|---|---|
| 20 | 21 | 4.24988(-4) | 15 | -8.2(-4) |
| | | 4.24993(-4) | 30 | -8.1(-4) |
| | | 4.24994(-4) | 60 | -8.1(-4) |
| | 43 | 9.61708(-3) | 11 | 2.4(-5) |
| | | 9.61710(-3) | 22 | 2.6(-5) |
| | | 9.61714(-3) | 43 | 3.0(-5) |
| | 81 | 0.194199 | 5 | 5.7(-5) |
| | | 0.194188 | 10 | -2.2(-6) |
| | | 0.194187 | 20 | -4.3(-6) |
| 30 | 78 | 4.75886(-4) | 11 | -1.6(-6) |
| | | 4.75889(-4) | 22 | 3.3(-6) |
| | | 4.75890(-4) | 44 | 5.7(-5) |
| | 120 | 9.83041(-3) | 6 | 6.0(-7) |
| | | 9.83043(-3) | 12 | 2.5(-6) |
| | | 9.83043(-3) | 24 | 2.5(-6) |
| | 190 | 0.196536 | 6 | 5.5(-5) |
| | | 0.196525 | 11 | -6.4(-8) |
| | | 0.196525 | 21 | -5.3(-7) |
| 40 | 172 | 4.96817(-4) | 7 | -8.5(-7) |
| | | 4.96818(-3) | 14 | 8.8(-7) |
| | | 4.96818(-3) | 28 | 1.7(-6) |
| | 238 | 9.99397(-3) | 6 | 5.6(-7) |
| | | 9.99396(-3) | 11 | -6.7(-7) |
| | | 9.99395(-3) | 22 | -1.5(-6) |
| | 346 | 0.198723 | 6 | 5.5(-5) |
| | | 0.198712 | 11 | -7.6(-8) |
| | | 0.198712 | 21 | 2.5(-7) |

| M | k | $q_k$ | Number of steps | Relative error |
|---|---|---|---|---|
| 70 | 689 | 4.96333(-4) | 6 | 3.7(-8) |
| | | 4.96333(-4) | 12 | -9.4(-8) |
| | | 4.96333(-4) | 23 | -2.7(-7) |
| | 846 | 9.91121(-3) | 6 | 7.8(-7) |
| | | 9.91120(-3) | 11 | -2.6(-8) |
| | | 9.91120(-3) | 22 | 3.6(-8) |
| | 1097 | 0.199230 | 6 | 5.5(-5) |
| | | 0.199219 | 11 | 1.4(-7) |
| | | 0.199219 | 22 | 3.6(-7) |
| 100 | 1578 | 4.94497(-4) | 6 | 4.7(-8) |
| | | 4.94497(-4) | 11 | 8.9(-8) |
| | | 4.94497(-4) | 22 | 2.9(-7) |
| | 1850 | 9.96548(-3) | 6 | 9.1(-7) |
| | | 9.96547(-3) | 11 | 3.5(-8) |
| | | 9.96547(-3) | 22 | 1.0(-7) |
| | 2278 | 0.199166 | 6 | 5.6(-5) |
| | | 0.199155 | 12 | 1.4(-8) |
| | | 0.199155 | 23 | 1.4(-7) |

show how the integrals evaluated by the trapezoidal rule in double-precision arithmetic converge as the step size is halved. We took $\epsilon = 10^{-3}$ in truncating the numerical integration. The relative error tabulated there is the difference between the probability as calculated by saddlepoint integration and the exact probability, divided by the latter. The exact probability was computed by the recurrent method of Mann and Whitney [51] carried out in double-precision arithmetic. These computations were executed on a VAX 11/780.

In order to compare the time required by the saddlepoint integration method with that required by the recurrent algorithm [51] we programmed both in Basic on an HP-71B handheld computer. Results are exhibited in Table 14.2. The recurrent algorithm may need to compute and store as many as $\bar{W} = M(M+1)/4$ values of the probabilities $p_k = Pr\ (W = k)$, and the time $T_R$ listed in Table 14.2 is that needed to do so. The time to sum those probabilities to obtain the cumulative probability $q_k$ is not included. The times in the column labeled $T_I$ are those for the entire computation of $q_k$ by saddlepoint integration. Again we took $\epsilon = 10^{-3}$; $N_{st}$ is the number of steps in the numerical quadrature.

Once the number M of samples exceeds thirty or so, the saddlepoint integration method is decidedly faster than the recurrent algorithm. It should be kept in mind that the statistician usually needs only a single significance probability $Pr\ (W \leq W_0)$ in assessing a set of experimental data. The recurrent algorithm must compute and store the probabilities $p_k$ for all values of k up to and including $k = W_0$ and sum them, and if $W_0$ is near the mean $\bar{W}$, this may take a long time and require storing many numbers.

(b) The Ranksum Statistic

In the two-sample Wilcoxon test, or "rank-sum test," one arranges the N+M data $x_1, x_2, \ldots, x_M, y_1, y_2, \ldots, y_N$ in ascending order. Let $r_i$ denote the rank of the datum $x_i$ in that arrangement. One forms the rank-sum statistic

Table 14.2

Signed-rank Statistic

| k | $N_{st}$ | $T_I$(sec.) | $q_k$ | Relative error |
|---|---|---|---|---|
| | | M = 25, $T_R$ = 67.6 sec. | | |
| 45 | 14 | 78.0 | 4.55944(-4) | 3.11(-6) |
| 76 | 8 | 41.4 | 9.37229(-3) | 6.39(-6) |
| 130 | 6 | 29.8 | 1.97867(-1) | -5.68(-5) |
| | | M = 30, $T_R$ = 117.6 sec. | | |
| 78 | 12 | 77.0 | 4.75860(-4) | 5.81(-5) |
| 120 | 7 | 43.2 | 9.83011(-3) | 3.02(-5) |
| 190 | 7 | 39.4 | 1.96541(-1) | -8.21(-5) |
| | | M = 40, $T_R$ = 281.6 sec. | | |
| 172 | 8 | 70.9 | 4.96793(-4) | 4.93(-5) |
| 238 | 7 | 53.4 | 9.99337(-3) | 5.99(-5) |
| 346 | 7 | 50.8 | 1.98727(-1) | -7.57(-5) |
| | | M = 50, $T_R$ = 554.0 sec. | | |
| 304 | 8 | 83.9 | 4.93541(-4) | 4.06(-5) |
| 397 | 7 | 66.0 | 9.79352(-3) | 3.76(-5) |
| 549 | 7 | 63.3 | 1.99441(-1) | -6.82(-5) |

$$V = \sum_{i=1}^{M} r_i .$$

If for a particular set of data this yields the value $V_0$, one quotes the significance probability $P = Pr\ (V \geq V_0 | H_0)$ that as large a value of V as $V_0$, or a larger value, could arise under the null hypothesis $H_0$ that the x's have the same distribution as the y's; and one reports that the null hypothesis is rejected at probability level P.

The maximum possible value of V is $NM + \frac{1}{2} M(M+1)$. The significance probability P is given by

$$P = Pr\ (V \geq V_0 |\ H_0) = Pr\ (U \leq U_0 |\ H_0), \tag{14.14}$$

where

$$U = NM + \frac{1}{2} M(M+1) - V, \quad U_0 = NM + \frac{1}{2} M(M+1) - V_0. \tag{14.15}$$

The random variable U has the following significance. Consider all $_{N+M}C_M$ arrangements of M x's and N y's; under $H_0$ these are equally likely. Then in a randomly selected one of these arrangements U is the number of times that an x precedes a y. The value of U ranges from 0 to NM, and its distribution is symmetrical about its mean

$$\bar{U} = E(U |\ H_0) = MN/2. \tag{14.16}$$

We treat the computation of the cumulative probabilities

$$q_k = Pr\ (U \leq k | H_0) \tag{14.17}$$

for $0 < k \leq MN/2$, from which the significance probability $P = Pr\ (V \geq V_0 |\ H_0)$ can be calculated by (14.14) and (14.15). For the sake of efficiency one will always take M as the smaller of the two sample sizes, $M \leq N$, interchanging the labels x

and y on the data if necessary.

The probability generating function of the random variable U is [49]

$$h(z) = c \prod_{j=1}^{M} \left(\frac{z^{N+j}-1}{z^{j}-1}\right), \qquad c = \left({}_{N+M}C_{M}\right)^{-1}. \tag{14.18}$$

Again we can write the probability $q_k$ as the contour integral (14.3), and again we pick a closed contour C surrounding the origin, symmetrical about the Re z-axis, excluding the point z = 1, and passing vertically through the saddlepoint $z = x_0$ of the integrand lying in $0 < x = \text{Re } z < 1$. The phase of the integrand is now

$$\begin{aligned}\Psi(z) = &\sum_{j=1}^{M}[\ln (z^{N+j}-1) - \ln(z^{j}-1)] \\ &+ \ln c - (k+1) \ln z - \ln (1-z),\end{aligned} \tag{14.19}$$

and the saddlepoint $x_0$ is the root of the equation

$$\Psi'(z) = \sum_{j=1}^{M} \left[\frac{(N+j)z^{N+j-1}}{z^{N+j}-1} - \frac{jz^{j-1}}{z^{j}-1}\right] - \frac{k+1}{z} - \frac{1}{z-1} = 0 \tag{14.20}$$

lying in that interval. As before, we integrate instead along the straight vertical line segment passing through the saddlepoint $z = x_0$ and lying within the unit circle, and we integrate thence counterclockwise around the unit circle. The contour integral (14.3) takes on the same form as in (14.5), except that now the integral $I_c$ along the unit circle to the left of the line $\text{Re } z = x_0$ is written

$$I_c = \int_{\theta_0}^{\pi} \prod_{j=1}^{M} \frac{\sin \frac{1}{2}(N+j)\theta}{\sin \frac{1}{2} j\theta} \text{ Re } \left[\frac{\exp i(\bar{U}-k)\theta}{1-\exp(i\theta)}\right] \frac{d\theta}{\pi}, \quad \theta_0 = \cos^{-1} x_0. \tag{14.21}$$

The same argument as in part (a) leads us to expect that when M and N are

large, the term $I_c$ can be neglected. The product in the integrand of (14.21) has MN/2 zeros -- some of them multiple -- lying in $0 \le \theta \le \pi$, and the integrand, which is oscillatory, perforce remains small between them. The principal contribution to $q_k$ comes from the first term of (14.5), with h(z) as in (14.18), and in that term it arises from the neighborhood of the saddlepoint $z = x_0$. The larger M, N, and k, the more rapidly the integrand in that term drops off from its peak value at y = 0.

The first term of (14.5), with (14.18), is integrated by the trapezoidal rule, and the integration is stopped when the absolute value of the integrand falls below $\varepsilon$ times the accumulated sum times the step size $\Delta y$, provided $y < Y$; again we took $\varepsilon = 10^{-3}$. The step size $\Delta y$ is chosen as in (14.13), with the second derivative $\Psi''(x)$ of the phase again approximated as in (14.9), where now

$$\rho = \text{Var } U - \bar{U} = MN(M+N-5)/12. \qquad (14.22)$$

The saddlepoint is calculated as in part (a) by solving (14.20) by Newton's method (1.16), the initial trial value being determined by (14.12) with $\bar{w}$ replaced by $\bar{U} = MN/2$ and $\rho$ by (14.22).

In Table 14.3 we show how the values of the probability $q_k$ calculated by numerical integration converge as the step size is halved. Exact values of the probabilities were computed by Harding's algorithm [52] carried out in double-precision arithmetic, and the relative errors were determined as in part (a). The numerical quadrature was terminated as before, with $\varepsilon = 10^{-3}$. Good accuracy is attained with only a few steps of numerical integration.

Table 14.4 compares the times required by an HP-71B computer to carry out the numerical-quadrature algorithm and Harding's. The time $T_R$ is that occupied by the latter when computing and storing all the probabilities $p_k$, $0 \le k \le \bar{U}$, as it potentially must do; $T_R$ increases as $M^2N$ as M and N increase [52]. The times

Table 14.3

Ranksum Statistic

| M | N | k | $q_k$ | Number of steps | Relative error |
|---|---|---|---|---|---|
| 15 | 15 | 37 | 4.98338(-4) | 7 | -2.6(-5) |
| | | | 4.98342(-4) | 14 | -1.9(-5) |
| | | | 4.98343(-4) | 28 | -1.6(-5) |
| | | 57 | 9.27685(-3) | 6 | -1.8(-6) |
| | | | 9.27684(-3) | 11 | -2.1(-6) |
| | | | 9.27682(-3) | 21 | -5.1(-6) |
| | | 92 | 0.194630 | 5 | 6.6(-5) |
| | | | 0.194617 | 10 | 1.8(-7) |
| | | | 0.194617 | 19 | 2.4(-6) |
| 15 | 30 | 93 | 4.88862(-4) | 7 | -8.4(-7) |
| | | | 4.88863(-4) | 13 | 2.0(-6) |
| | | | 4.88862(-4) | 25 | -4.1(-7) |
| | | 129 | 9.45642(-3) | 6 | 6.8(-7) |
| | | | 9.45641(-3) | 11 | -2.3(-6) |
| | | | 9.45640(-3) | 21 | -1.7(-6) |
| | | 190 | 0.198499 | 5 | 6.1(-5) |
| | | | 0.198487 | 10 | 4.6(-7) |
| | | | 0.198487 | 20 | 1.4(-6) |
| 20 | 30 | 138 | 4.75283(-4) | 6 | 3.9(-7) |
| | | | 4.75283(-4) | 12 | -7.2(-8) |
| | | | 4.75282(-4) | 23 | -2.1(-6) |
| | | 183 | 9.48660(-3) | 5 | 6.3(-7) |
| | | | 9.48659(-3) | 10 | -2.3(-7) |
| | | | 9.48660(-3) | 20 | 6.0(-7) |
| | | 257 | 0.196244 | 6 | 6.0(-5) |
| | | | 0.196232 | 11 | 2.0(-8) |
| | | | 0.196232 | 21 | 4.9(-7) |

| M | N | k | $q_k$ | Number of steps | Relative error |
|---|---|---|---|---|---|
| 30 | 60 | 522 | 4.98938(-4) | 6 | 4.7(-8) |
| | | | 4.98938(-4) | 11 | -4.5(-8) |
| | | | 4.98938(-4) | 22 | 1.6(-7) |
| | | 630 | 9.99919(-3) | 6 | 9.5(-7) |
| | | | 9.99918(-3) | 11 | 6.3(-8) |
| | | | 9.99919(-3) | 21 | 3.2(-7) |
| | | 801 | 0.198277 | 6 | 5.7(-5) |
| | | | 0.198265 | 11 | 1.5(-7) |
| | | | 0.198266 | 22 | 3.3(-7) |

Table 14.4

Ranksum Statistic

| k | $N_{st}$ | $T_I$(sec.) | $q_k$ | Relative error |
|---|---|---|---|---|
| | | M = 10, N = 40, $T_R$ = 120.2 sec. | | |
| 69 | 10 | 52.8 | 4.59224(-4) | 2.44(-6) |
| 104 | 8 | 30.3 | 9.41982(-3) | -3.50(-6) |
| 164 | 6 | 25.4 | 1.97525(-1) | 5.63(-5) |
| | | M = 20, N = 20, $T_R$ = 247.5 sec. | | |
| 81 | 7 | 50.9 | 4.66710(-4) | 2.28(-6) |
| 114 | 6 | 51.1 | 9.76839(-3) | 5.52(-7) |
| 168 | 6 | 44.9 | 1.99164(-1) | 6.37(-5) |
| | | M = 15, N = 45, $T_R$ = 316.7 sec. | | |
| 149 | 8 | 55.1 | 4.67736(-4) | -2.94(-7) |
| 201 | 7 | 42.6 | 9.55136(-3) | 6.28(-7) |
| 287 | 7 | 40.0 | 1.98662(-1) | 5.75(-5) |
| | | M = 20, N = 40, $T_R$ = 510.4 sec. | | |
| 194 | 7 | 57.5 | 4.80410(-4) | 2.29(-7) |
| 252 | 7 | 54.3 | 9.90422(-3) | 8.53(-7) |
| 345 | 7 | 51.0 | 1.97986(-1) | 5.86(-5) |
| | | M = 30, N = 30 $T_R$ = 870.1 sec. | | |
| 231 | 7 | 72.7 | 4.87380(-4) | 6.32(-8) |
| 293 | 6 | 68.6 | 9.95029(-3) | 9.22(-7) |
| 392 | 7 | 72.8 | 1.99014(-1) | 5.99(-5) |

$T_I$ for computing the probabilities $q_k$ by saddlepoint integration are considerably shorter, and they are proportional roughly to the smaller of M and N. It requires storing only a dozen or so numbers; the recursive Harding algorithm requires storing as many as $\bar{U} = MN/2$, and this might well strain the capacity of a small computer.

(c) The Jonckheere Statistic

The Jonckheere test extends the rank-sum test to an arbitrary number $s \geq 2$ of the samples of sizes $M_1, M_2, \ldots, M_s$ [50]. One has s groups of independent data

$$(x_1^{(i)}, x_2^{(i)}, \ldots x_{M_i}^{(i)}), \qquad i = 1, 2, \ldots, s.$$

With $U_{ij}$ denoting the number of pairs (a, b) for which $x_a^{(i)} < x_b^{(j)}$, $i < j$, the test statistic is

$$U = \sum_{j=2}^{s} \sum_{i=1}^{j-1} U_{ij}. \tag{14.23}$$

For $s = 2$, $M_1 = M$, $M_2 = N$, U is the ranksum statistic treated in part (b). We are concerned with the distribution of U under the null hypothesis that all the data $x_j^{(i)}$ have a common probability distribution.

The probability generating function of U under the null hypothesis H is

$$h(z) = c \prod_{r=1}^{N_t} (1-z^r) \cdot \prod_{m=1}^{s} \prod_{j_m=1}^{M_m} (1-z^{j_m})^{-1},$$

$$c = \prod_{m=1}^{s} M_m!/N_t!, \tag{14.24}$$

with

$$N_t = M_1 + M_2 + \ldots + M_s \tag{14.25}$$

the total number of data. Harding [52] has shown how the probabilities

$$p_n = Pr\ (U = n \mid H)$$

can be computed by s - 1 repetitions of his minimal-storage algorithm for the ranksum statistic.

Saddlepoint integration can conveniently be applied to computing the significance probabilities

$$q_k = \sum_{n=0}^{k} p_n = Pr\ (U \leq k \mid H). \tag{14.26}$$

It suffices to consider the range $0 \leq k \leq \bar{U}$, where

$$\bar{U} = \frac{1}{4}\left(N_t^2 - \sum_{j=1}^{s} M_j^2\right) \tag{14.27}$$

is the mean of the distribution, about which it is symmetrical,

$$q_k = 1 - q_{2\bar{U}-k}.$$

The probability $q_k$ is again written as the contour integral (14.3).

For the sake of fast computation we rewrite h(z) in terms of the numbers $\mu_1, \mu_2, \ldots, \mu_p$ of different sample sizes, of which there are p. Let $r_j$ be the multiplicity of size $\mu_j$. If, for example, s = 5 and

$$M_1 = M_2 = 5,\ M_3 = M_4 = M_5 = 10,$$

then $p = 2$, $\mu_1 = 5$, $r_1 = 2$, $\mu_2 = 10$, $r_2 = 3$. If all s samples have the same size M, then $p = 1$, $\mu_1 = M$, $r_1 = s$. Now

$$N_t = \sum_{j=1}^{p} r_j \mu_j, \tag{14.28}$$

the mean is

$$\bar{U} = \frac{1}{4} \left( N_t^2 - \sum_{j=1}^{p} r_j \mu_j^2 \right), \tag{14.29}$$

and the p.g.f. is

$$H(z) = c \frac{\prod_{m=1}^{N_t} (1-z^m)}{\prod_{j=1}^{p} \left[ \prod_{m=1}^{\mu_j} (1-z^m) \right]^{r_j}}. \tag{14.30}$$

For later convenience the sample sizes $\mu_j$ are arranged in ascending order,

$$\mu_1 < \mu_2 < \ldots < \mu_p.$$

The phase of the integrand in (14.3) is

$$\Psi(z) = \ln c + \sum_{m=1}^{N_t} \ln(1-z^m) - \sum_{j=1}^{p} r_j \sum_{m=1}^{\mu_j} \ln(1-z^m) - (k+1)\ln z - \ln(1-z). \tag{14.31}$$

Its derivative

$$\Psi'(z) = z^{-1} \left\{ \sum_{m=1}^{N_t} \frac{m}{1-z^{-m}} - \sum_{j=1}^{p} r_j \sum_{m=1}^{\mu_j} \frac{m}{1-z^{-m}} - (k+1) \right\} - \frac{1}{z-1} \tag{14.32}$$

is again set to zero, and the resulting equation is solved for the saddlepoint $x_0$

lying in (0, 1). Newton's method (1.16) is used, in which the second derivative $\Psi''(x)$ is approximated as in (14.9), where now

$$\rho = \frac{1}{36} \left\{ N_t^3 - \sum_{j=1}^{p} r_j \mu_j^3 - 30\bar{U} \right\} \tag{14.33}$$

The integration is again taken over a straight vertical contour, completed around the part of the unit circle lying to the left of it, as in (14.5). Because the p.g.f. h(z) is a product of p.g.f.'s of the type in (14.18), h(z) will have a large number of zeros on the unit circle $|z| = 1$ when $N_t >> 1$, and the contribution of the term $I_c$ will be small. The integral along the vertical path is approximated by the trapezoidal rule with a step-size $\Delta y$ given by (14.13), with (14.9) and (14.33). The integration is stopped when the absolute value of the integrand falls below $\varepsilon \Delta y$ times the accumulated trapezoidal sum. Provided this occurs before the point $z = x_0 + iy$ reaches the unit circle, the term $I_c$ can be neglected. We found $\varepsilon = 10^{-3}$ sufficiently small for accurate evaluation of $q_k$.

The bracketed portion of (14.32) is easily programmed. One accumulates the sum

$$\sum_{m=1}^{N_t} m(1-z^{-m})^{-1}$$

in the first term, picking off the values of the sums

$$\sum_{m=1}^{\mu_j} m(1-z^{-m})^{-1} \tag{14.34}$$

for the second term when m passes through successive values of $\mu_j$. The p.g.f. h(z) in (14.30) is computed in a similar manner. As the product

$$\prod_{m=1}^{N_t} (1-z^m)$$

in its numerator is being accumulated, the products

$$\prod_{m=1}^{\mu_j} (1-z^m)$$

in its denominator are picked off when m passes through the successive sample sizes $\mu_j$, $1 \le j \le p$. The time needed by the saddlepoint integration method is roughly proportional to $N_t$. Written to accommodate a variety of sample sizes and numbers s of samples, our program is not so efficient for $s = 2$ as the one based on the equations given in part (b).

Table 14.5 compares the performance of this method with that of Harding's algorithm [52]. The basis of comparison is the same as in Table 14.4. Individual significance probabilities $q_k$ are computed in markedly less than the time $T_R$ potentially required by the recursive algorithm, even for modest sample sizes. Harding's method must allow for the possibility of having to store $\lceil \bar{U} \rceil$ numbers, with $\bar{U}$ given in (14.27); the integration method occupies only a small, fixed amount of computer storage.

Table 14.5

Jonckheere Statistic

| k | $N_{st}$ | $T_I$(sec.) | $q_k$ | Relative error |
|---|---|---|---|---|
| | $s = 3, M_1 = 5, M_2 = 10, M_3 = 15, T_R = 127.9$ sec. | | | |
| 56 | 7 | 60.5 | 4.89313(-4) | 2.59(-7) |
| 78 | 6 | 48.6 | 9.55420(-3) | 1.00(-6) |
| 115 | 6 | 48.8 | 1.96011(-1) | 6.78(-5) |
| | $s = 3, M_1 = M_2 = M_3 = 10, T_R = 189.1$ sec. | | | |
| 65 | 7 | 56.6 | 4.53680(-4) | 2.29(-7) |
| 88 | 6 | 45.6 | 9.07913(-3) | 1.18(-6) |
| 127 | 6 | 45.5 | 1.98204(-1) | 6.95(-5) |
| | $s = 4, M_1 = M_2 = M_3 = M_4 = 10, T_R = 591.2$ sec. | | | |
| 165 | 6 | 62.2 | 4.56798(-4) | 2.42(-8) |
| 203 | 6 | 58.9 | 9.52746(-3) | 1.32(-6) |
| 264 | 6 | 58.7 | 1.97177(-1) | 6.46(-5) |
| | $s = 4, M_1 = M_2 = 5, M_3 = M_4 = 15, T_R = 446.5$ sec. | | | |
| 144 | 7 | 71.5 | 4.67654(-4) | 7.14(-8) |
| 181 | 6 | 60.5 | 9.82626(-3) | 1.25(-6) |
| 240 | 6 | 60.3 | 1.98789(-1) | 6.46(-5) |
| | $s = 6, M_1 = M_2 = M_3 = M_4 = M_5 = M_6 = 5, T_R = 305.9$ sec. | | | |
| 98 | 6 | 48.6 | 4.59736(-4) | 7.76(-8) |
| 123 | 6 | 43.6 | 9.64348(-3) | 1.58(-6) |
| 163 | 6 | 45.9 | 1.93787(-1) | 6.73(-5) |

References


1. G. F. Carrier, M. Krook, and C. E. Pearson, Functions of a Complex Variable, (McGraw-Hill, New York, 1966). See pp. 257ff.
2. H. A. Spang, III, SIAM Review 4, 343-365 (1962).
3. S. O. Rice, Bell System Tech. J. 52, 707-722 (1973).
4. S. O. Rice, Bell System Tech. J. 54, 155-164 (1975).
5. C. W. Helstrom, Trans. IEEE AES-19, 428-437 (1983).
6. C. Schwartz, J. Comput. Phys. 4, 19-29 (1969).
7. G. Birkhoff and D. Young, J. Math. & Phys. 29, 217-221 (1950).
8. C. W. Helstrom, Trans. IEEE AES-14, 630-640 (1978).
9. C. W. Helstrom, Statistical Theory of Signal Detection, 2nd ed. (Pergamon Press, Oxford, 1968).
10. P. Swerling, Trans. IRE IT-6, 269-308 (1960).
11. J. V. DiFranco and W. L. Rubin, Radar Detection (Prentice-Hall, Englewood Cliffs, N.J., 1968).
12. C. W. Helstrom and J. A. Ritcey, Trans. IEEE AES-20, 624-634 (1984).
13. C. W. Helstrom and J. A. Ritcey, SIAM J. Sci. Stat. Comput. 6, 505-514 (1985).
14. J. T. Rickard and G. W. Dillard, Trans. IEEE AES-13, 338-343 (1977).
15. H. Rohling, Trans. IEEE AES-19, 608-621 (1983).
16. J. A. Ritcey, "Exact performance analysis of the censored mean-level detector in a multiple-target environment," to appear in IEEE Trans. on Aerospace & Electronic Systems.
17. J. A. Ritcey, "Calculating Radar Detection Probabilities by Contour Integration," Ph.D. thesis, Dep't of Electrical Engineering & Computer Sciences, University of California, San Diego; June, 1985.
18. J. I. Marcum, Trans. IRE IT-6, 59-267 (1960).

19. S. O. Rice, Bell System Tech. J. 23, 282-332 (1944); 24, 46-156 (1945).

20. M. Abramowitz and I. Stegun, Handbook of Mathematical Functions, NBS Appl. Math. Series, #55, U.S. Gov't Printing Office, Washington, D.C. (1964).

21. M. Kac and A. J. F. Siegert, J. Appl. Phys. 18, 383-397 (1947).

22. D. Slepian, Bell System Tech. J. 37, 163-184 (1958).

23. C. W. Helstrom, "Distribution of the filtered output of a quadratic rectifier computed by numerical contour integration," to appear in IEEE Trans. on Information Theory.

24. A. J. F. Siegert, Trans. IRE IT-3, 38-43 (1957).

25. C. W. Helstrom, J. Opt. Soc. Am. A2, 674-682 (1985).

26. D. Slepian and E. Sonnenblick, Bell System Tech. J. 44, 1745-1760 (1965).

27. C. W. Helstrom, "Calculating error probabilities for intersymbol and co-channel interference," to appear in IEEE Trans. on Communications.

28. E. N. Gilbert and H. O. Pollak, Bell System Tech. J. 39, 333-350 (1960).

29. R. Lugannani and S. O. Rice, Proc. Eighth Princeton Conf. on Information Sciences and Systems, March, 1974, 47-51.

30. O. C. Yue, R. Lugannani, S. O. Rice, Trans. IEEE COM-26, 45-54 (1978).

31. R. Lugannani, S. O. Rice, O. Yue, "Tables of the Probability Distribution and Density for Selected Shot Processes," Dep't of Applied Physics & Information Science, University of California, San Diego (n.d.).

32. D. Snyder, Random Point Processes (Wiley, New York, 1966). See pp. 168-171.

33. C. W. Helstrom, SIAM J. Sci. Stat. Comput. 4, 353-356 (1983).

34. C. W. Helstrom and S. O. Rice, J. Comput. Phys. 54, 289-324 (1984).

35. G. Bédard, Phys. Rev. 151, 1038-1039 (1966).

36. S. O. Rice, Bell System Tech. J. 47, 1971-2013 (1968).

37. R. Lugannani and S. O. Rice, Adv. Appl. Prob. 12, 475-490 (1980).

38. J. R. Prescott, Nucl. Instr. & Meth. 39, 173-179 (1966).

39. C. W. Helstrom, J. Appl. Phys. 55, 2786-2792 (1984).

40. K. S. Fahady, M. P. Quine, D. Vere-Jones, Adv. Appl. Prob. 3, 282-300 (1971).

41. R. J. McIntyre, Trans. IEEE ED-19, 703-712 (1972).

42. S. D. Personick, Bell System Tech. J. 50, 3075-3095 (1971).

43. C. W. Helstrom, Trans. IEEE ED-31, 955-958 (1984).

44. S. D. Personick, P. Balaban, J. H. Bobsin, P. R. Kumar, Trans. IEEE COM-25, 541-548 (1977).

45. C. W. Helstrom, "Computing the performance of optical receivers with avalanche diode detectors," submitted to IEEE Trans. on Communications.

46. C. W. Helstrom, Trans. IEEE COM-27, 186-191 (1979).

47. S. Karp and J. R. Clark, Trans. IEEE IT-16, 672-680 (1970).

48. S. R. Laxpati and G. Lachs, J. Appl. Phys. 43, 4773-4776 (1972).

49. F. Wilkinson, S. K. Katti, R. A. Wilcox, in H. L. Harter and D. B. Owen, Selected Tables in Mathematical Statistics (Amer. Math. Soc., Providence, R. I., 1973) vol. I, 171-259.

50. A. R. Jonckheere, Biometrika 41, 133-145 (1954).

51. H. B. Mann and D. R. Whitney, Ann. Math. Stat. 18, 50-60 (1947).

52. E. F. Harding, Appl. Statist. 33, 1-6 (1984).

Papers written under Grant AFOSR 82-0343


C. W. Helstrom: 'Evaluating the detectability of Gaussian stochastic signals by steepest-descent integration', IEEE Trans. Aerospace & Electronic Systems AES-19:428-437. 1983.

C. W. Helstrom and S.O. Rice: 'Computation of counting distributions arising from a single-stage multiplicative process', J. Computational Physics 54:289-324. 1984.

C. W. Helstrom: 'Output distributions of electrons in a photomultiplier', J. Appl. Phys. 55: 2786-2792. 1984.

C. W. Helstrom: 'Computation of output distributions of electrons in an avalanche photodiode', IEEE Trans. on Electron Devices ED-31:955-958. 1984.

C. W. Helstrom and J. A. Ritcey: 'Evaluating radar detection probabilities by steepest descent integration', IEEE Trans. on Aerospace & Electronic Systems AES-20:624-634. 1984.

C. W. Helstrom: 'Computation of photoelectron counting distributions by numerical contour integration', J. Opt. Soc. Am. A2:674-682. 1985.

C. W. Helstrom and J. A. Ritcey: 'Evaluation of the non-central F-distribution by numerical contour integration', SIAM J. Sci. Stat. Comput. 6:505-514. 1985.

J. A. Ritcey, "Exact performance analysis of the censored mean-level detector in a multiple-target environment," to appear in IEEE Trans. on Aerospace & Electronic Systems.

J. A. Ritcey, "Calculating Radar Detection Probabilities by Contour Integration," Ph.D. thesis, Dep't of Electrical Engineering & Computer Sciences, University of California, San Diego; June, 1985.

C. W. Helstrom, "Distribution of the filtered output of a quadratic rectifier computed by numerical contour integration," to appear in IEEE Trans. on Information Theory.

C. W. Helstrom, "Calculating error probabilities for intersymbol and co-channel interference," to appear in IEEE Trans. on Communications.

C. W. Helstrom, "Computing the performance of optical receivers with avalanche diode detectors," submitted to IEEE Trans. on Communications.

Persons employed on AFOSR Grant 82-0343

C. W. Helstrom, principal investigator

S. O. Rice, consultant (unsalaried)

J. A. Ritcey, graduate research assistant.
Mr. Ritcey received the Ph.D. in June, 1985, with a thesis entitled "Calculating Radar Detection Probabilities by Contour Integration."

Chia-Lu Ho, graduate research assistant

Victor E. Staggs, graduate research assistant

AIR FORCE OFFICE OF SCIENTIFIC RESEARCH (AFSC)
NOTICE OF TRANSMITTAL TO DTIC
This technical report has been reviewed and is approved for public release IAW AFR 190-12.
Distribution is unlimited.
MATTHEW J. KEMPER
Chief, Technical Information Division

Approved for public release;
distribution unlimited.

SECURITY CLASSIFICATION OF THIS PAGE

# REPORT DOCUMENTATION PAGE

| | |
|---|---|
| 1a REPORT SECURITY CLASSIFICATION<br>UNCLASSIFIED | 1b RESTRICTIVE MARKINGS |
| 2a SECURITY CLASSIFICATION AUTHORITY | 3 DISTRIBUTION/AVAILABILITY OF REPORT<br>Approved for public release; distribution unlimited. |
| 2b DECLASSIFICATION/DOWNGRADING SCHEDULE | |
| 4 PERFORMING ORGANIZATION REPORT NUMBER(S) | 5. MONITORING ORGANIZATION REPORT NUMBER(S)<br>**AFOSR-TR- 86-2183** |
| 6a NAME OF PERFORMING ORGANIZATION<br>University of California<br>San Diego<br>6b OFFICE SYMBOL (If applicable) | 7a. NAME OF MONITORING ORGANIZATION<br>Air Force Office of Scientific Research |
| 6c. ADDRESS (City, State and ZIP Code)<br>Dept. of EE&CS, C-014<br>U.C.S.D., La Jolla, Calif. 92093 | 7b. ADDRESS (City, State and ZIP Code)<br>Directorate of Mathematical & Information Sciences, Bolling AFB DC 20332-6448 |
| 8a NAME OF FUNDING/SPONSORING ORGANIZATION<br>AFOSR<br>8b OFFICE SYMBOL (If applicable)<br>NM | 9. PROCUREMENT INSTRUMENT IDENTIFICATION NUMBER<br>Grant 82-0343 |
| 8c ADDRESS (City, State and ZIP Code)<br>Bld 410<br>Bolling AFB DC 20332-6448 | 10 SOURCE OF FUNDING NOS<br>PROGRAM ELEMENT NO. 61102F; PROJECT NO 2304; TASK NO A5; WORK UNIT NO |
| 11 TITLE (Include Security Classification)<br>Calculation of cumulative distributions and detection probabilities in communications and | |
| 12 PERSONAL AUTHOR(S)<br>Carl W. Helstrom | |
| 13a TYPE OF REPORT<br>Final | 13b TIME COVERED<br>FROM 1982 TO 1986 |
| 14 DATE OF REPORT (Yr., Mo., Day)<br>1986, March 31 | 15 PAGE COUNT<br>ii + 129 |
| 16 SUPPLEMENTARY NOTATION | |
| 17 COSATI CODES<br>FIELD / GROUP / SUB GR | 18 SUBJECT TERMS (Continue on reverse if necessary and identify by block number)<br>probability distributions, detection, radar, communications, photoelectric counting, numerical integration |


19 ABSTRACT (Continue on reverse if necessary and identify by block number) This report treats the numerical computation of cumulative distributions of random variables occurring primarily in communications, radar, and optics when their moment-generating or probability-generating functions are known. The cumulative distribution of a continuous random variable is expressed as a Laplace inversion integral of its moment-generation function, that of an integer-valued random variable as a contour integral that arises from Cauchy's theorem and whose integrand involves the probability-generating function. These integrals are evaluated by numerical quadrature along contours in the complex plane chosen for efficiency and convenience. Applications include radar detection probabilities with fading and unfading signals and fixed-threshold and constant-false-alarm rate receivers; the distributions of the integrated output of a linear rectifier and of the filtered output of a quadratic rectifier; the error probability in a binary symmetric communication channel with intersymbol and cochannel interference; the distribution of shot noise; the distributions of the numbers of electrons emerging from photoelectric detectors, photomultipliers, and avalanche diodes; and significance probabilities in statistical rank tests.


| | |
|---|---|
| 20 DISTRIBUTION AVAILABILITY OF ABSTRACT<br>UNCLASSIFIED UNLIMITED ☒ SAME AS RPT ☐ DTIC USERS ☐ | 21 ABSTRACT SECURITY CLASSIFICATION<br>UNCLASSIFIED |
| 22a NAME OF RESPONSIBLE INDIVIDUAL<br>Major Brian Woodruff | 22b TELEPHONE NUMBER (Include Area Code)<br>(202) 767- |
| | 22c OFFICE SYMBOL<br>NM |

DD FORM 1473, 83 APR EDITION OF 1 JAN 73 IS OBSOLETE

UNCLASSIFIED

SECURITY CLASSIFICATION OF THIS PAGE

END

1-87

DTIC